

UNIVERSITY OF OKLAHOMA

GRADUATE COLLEGE

**CHARACTERIZATION OF CRYSTALLINE AND AMORPHOUS PHASES IN  
POLY(N-METHYLETHYLENIMINE) POLYMER ELECTROLYTES  
AND MODEL SYSTEMS**

A Dissertation

SUBMITTED TO THE GRADUATE FACULTY

in partial fulfillment of the requirements for the

degree of

Doctor of Philosophy

By

Rebecca Anne Sanders

Norman, Oklahoma

2003

UMI Number: 3102430

Copyright 2003 by  
Sanders, Rebecca Anne

All rights reserved.

UMI<sup>®</sup>

---

UMI Microform 3102430

Copyright 2003 by ProQuest Information and Learning Company.  
All rights reserved. This microform edition is protected against  
unauthorized copying under Title 17, United States Code.

ProQuest Information and Learning Company  
300 North Zeeb Road  
P.O. Box 1346  
Ann Arbor, MI 48106-1346

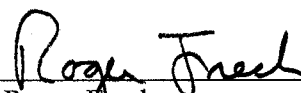
© Copyright by Rebecca A. Sanders 2003

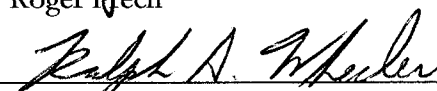
All Rights Reserved

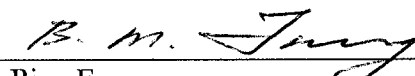
CHARACTERIZATION OF CRYSTALLINE AND AMORPHOUS PHASES IN  
POLY(N-METHYLETHYLENIMINE) POLYMER ELECTROLYTES  
AND MODEL SYSTEMS

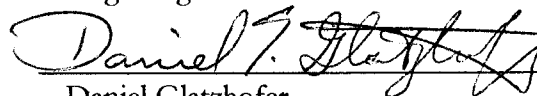
A Dissertation APPROVED FOR  
THE DEPARTMENT OF CHEMISTRY AND BIOCHEMISTRY

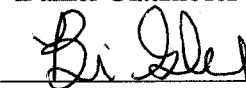
BY

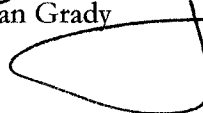
  
\_\_\_\_\_  
Roger Frech

  
\_\_\_\_\_  
Ralph Wheeler

  
\_\_\_\_\_  
Bing Fung

  
\_\_\_\_\_  
Daniel Glatzhofer

  
\_\_\_\_\_  
Brian Grady



## **ACKNOWLEDGEMENTS**

---

Roger Frech, I want to thank you for your patience, encouragement, and wisdom, which made graduate school a pleasurable experience. I will never forget all the potluck parties that we had at your house when you were in Scotland. I will miss all the fun we had in your lab and at scientific meetings.

I appreciate my committee members for enduring my long presentations: Ralph Wheeler, Bing Fung, Daniel Glatzhofer, and Brian Grady. John Furneaux, thanks for helping us with our nitrogen adsorption project for Colloids/Surface Science class. I also want to thank Jean Keil for keeping on top of all the travel reimbursement paperwork.

I have enjoyed collaborating with Scott Boesch, Albert Snow, Richard Hu, and Masood Kahn. Scott Boesch, thanks for your hard work, dedication, and long hours slaving over a computer in order to finish the computations necessary for my dissertation and our manuscript. Make sure you take sometime off so that you can enjoy life. Albert Snow, I appreciate your listening to me and helping me through the rough times.

Thanks to Shawna York and Chris Rhodes for their guidance and encouragement in the Lab. Jeff Thamer, I want to thank you for preparing me to teach Physical Chemistry Labs. Varuni Seneviratne, I enjoyed discussing research and personal topics with you. Thank you, Fred McKenna for tolerating all my questions about complex impedance and other research topics. Chris Burba, I appreciate the time you took to run all of my powder X-ray diffraction samples. Matt Petrowsky, thank you for being a good sport when we picked on you. Nathalie Rocher, I want to thank you for bringing culture to my life, helping me keep the lab clean, and working out with me at the gym. Thank you, Rachel Mason for your advice and wisdom in the preparation for an industrial position.

For financial support, I thank the Department of Chemistry and Biochemistry and National Science Foundation for a monthly paycheck and travel funds. I am grateful to the Graduate Student Senate and Graduate College for additional travel funds.

Last but not least, I would like to thank my husband, friends, and family. Greg Sanders (my husband), I appreciate your support and patience during this long journey. I could not have done it without you. Also, I want to thank my husband for keeping me company through all those overnight conductivity runs. Thank you to Margaret Springer (mother), Al Springer (stepfather), and Suzanne Crumbacher (sister) for your support and words of encouragement throughout my college years. Thanks to my dad (David Dunning), for supporting me and sharing with me your love for chemistry. Linda Sanders (mother-in-law) and Everett Sanders (father-in-law), thanks for your support and for patiently waiting for grandchildren. Thanks to all my extended family and friends (Jennifer Bartlett & Evon Hromy). I appreciate everything that God has provided for me and for leading me down this path.

## TABLE OF CONTENT

ACKNOWLEDGEMENTS.....	iv
ABSTRACT.....	viii
PREFACE.....	x
1 INTRODUCTION.....	1
1.1 Battery Technology.....	1
1.2 Polymer Electrolytes.....	3
1.2.1 Hard/Soft Acid/Base Principle.....	4
1.2.2 Contribution of the Cation and Anions.....	5
1.2.3 Thermodynamics of Dissolution.....	6
1.3 Poly(ethylene oxide).....	7
1.3.1 PEO-Salt Complexes.....	8
1.3.2 Ionic Conductivity.....	10
▪ <i>Model for Conductivity</i> .....	12
▪ <i>Transport and Transference Numbers</i> .....	15
▪ <i>Ionic Association</i> .....	17
1.4 Linear Poly(ethylenimine) .....	18
1.4.1 LPEI Crystalline Structure.....	19
1.4.2 LPEI Hydrates.....	20
1.4.3 LPEI-Salt Complexes.....	20
1.4.4 Model Compounds.....	22
1.4.5 LPEI as Crosslinked Polymer Electrolytes and Proton Conductors....	23
1.5 Linear Poly(N-methylethylenimine) .....	23
2 EXPERIMENTAL.....	25
2.1 Sample Preparation.....	25
2.1.1 Model Salt Complexes.....	25
2.1.2 Polymer Electrolytes.....	26
2.2 Spectroscopy .....	26
2.2.1 Fourier Transform Infrared Spectroscopy.....	26
▪ <i>Model Compounds</i> .....	27
▪ <i>Polymer Electrolytes</i> .....	27
2.2.2 Raman Spectroscopy.....	27
2.3 Quantum Chemical Calculations.....	28
2.4 X-ray.....	28
2.4.1 X-ray Diffraction.....	28
2.4.2 X-ray Powder Diffraction.....	29
2.5 Differential Scanning Calorimetry.....	30
2.5.1 Model Compounds.....	30
2.5.2 Polymer Electrolytes.....	30
2.6 AC Complex Impedance.....	31
3 MODEL COMPOUNDS.....	32
3.1 DMEDA Complexed with NaTf.....	32
3.1.1 Crystal Structure.....	33
3.1.2 Thermal Analysis.....	34
3.1.3 Vibrational Spectroscopy.....	35
▪ <i>Ionic Association Regions</i> .....	35
▪ <i>Conformation Region</i> .....	38

	▪ <i>NH Stretching Region</i> .....	39
3.2	TMEDA Complexed with LiTf and NaTf.....	39
	3.2.1 Crystal Structure.....	39
	3.2.2 Thermal Analysis.....	40
	3.2.3 Quantum Chemical Calculations.....	41
	3.2.4 Band Assignments.....	45
	▪ <i>Conformation Region</i> .....	45
	▪ <i>Ionic Association Regions</i> .....	46
3.3	PMDETA Complexed with LiTf and NaTf.....	47
	3.3.1 Crystal Structure.....	47
	3.3.2 Thermal Analysis.....	48
	3.3.3 Quantum Chemical Calculations.....	48
	3.3.4 Experimental Results.....	50
	▪ <i>Ionic Association Region</i> .....	51
	▪ <i>Conformation Region</i> .....	52
	3.3.5 Band Assignments.....	54
4	LINEAR POLY(N-METHYLETHYLENIMINE) .....	56
4.1	LPMEI Complexed with LiTf and NaTf.....	56
	4.1.1 Spectroscopic Analysis.....	56
	▪ <i>Conformation Region</i> .....	56
	▪ <i>Ionic Association Regions</i> .....	58
	4.1.2 Thermal Analysis.....	60
	4.1.3 Powder X-Ray Diffraction Analysis.....	61
	4.1.4 Ionic Conductivity Analysis.....	62
4.2	LPMEI Characterized by Modeled Compounds.....	64
	4.2.1 LPMEI Modeled by TMEDA.....	64
	4.2.2 LPMEI Modeled by PMDETA.....	66
	▪ <i>PMDETA:LiTf</i> .....	68
	▪ <i>PMDETA:NaTf</i> .....	70
5	CONCLUDING REMARKS.....	71
6	REFERENCES.....	73
	APPENDIX A – Included manuscripts.....	77
	I. DMEDA complexed with LiTf and NaTf.....	77
	II. TMEDA complexed with LiTf and NaTf.....	86
	III. PMDETA complexed with LiTf and NaTf.....	97
	IV. LPMEI complexed with LiTf and NaTf.....	107
	V. LPMEI modeled by PMDETA.....	115
	APPENDIX B – Manuscripts not included.....	119



## ***ABSTRACT***

---

Polymer electrolytes have been investigated as ionic conductors in rechargeable lithium batteries. Poly(ethylene oxide):salt systems are the most widely investigated polymer electrolytes. However, the conductivity values for these system are not sufficiently high to be useful for practical lithium batteries. Therefore, other polymer electrolytes are being explored such as linear poly(ethylenimine), LPEI, and linear poly(N-methylethylenimine), LPMEI.

LPEI is analogous to PEO, except LPEI has a heteroatom that is synthetically versatile because different side groups can be readily attached. LPEI:salt systems are not well understood as polymer electrolytes. Therefore, N,N'-dimethylethylenediamine (DMEDA) complexed with  $\text{NaCF}_3\text{SO}_3$  (NaTf) was investigated in this dissertation as a model compound for LPEI, in order to gain further insight into hydrogen bonding in amine systems. While studying DMEDA:NaTf, single crystals were discovered and characterized with infrared and Raman spectroscopy, X-ray diffraction, and differential scanning calorimetry (DSC). In DMEDA:NaTf solutions, there is evidence of local structures similar to that in crystalline DMEDA:NaTf based on infrared and Raman spectroscopy data.

LPMEI is a derivative of LPEI. LPMEI is amorphous at room temperature unlike LPEI, which melts at 58°C. Because there is a limited amount of information reported about LPMEI as polymer electrolytes, this dissertation characterizes LPMEI complexed with LiTf and NaTf utilizing IR, differential scanning calorimetry (DSC), powder X-ray diffraction, and complex impedance. To gain further insight into LPMEI systems, model systems were investigated such as N,N,N',N'-tetramethylethylenediamine (TMEDA) and N,N,N',N',N''-pentamethyldiethylenetriamine (PMDETA) complexed with LiTf and NaTf. When studying these model systems, crystalline compounds were discovered and

characterized utilizing X-ray diffraction, DSC, IR, and Raman spectroscopy. The local structures in crystalline TMEDA:LiTf, TMEDA:NaTf, and PMDETA:NaTf can be correlated to these samples in solution, which provides greater insight into the local environment of the LPMEI:salt systems.

## **PREFACE**

---

This thesis contains a summary from the work accomplished in the following publications. These publications are included in Appendix A and will be referred to in the text by its Roman numerals.

- I. Rebecca A. Sanders, Roger Frech, and Masood A. Khan. "Characterization of the Crystalline and Solution Phases in N,N',-Dimethylethylenediamine (DMEDA) with Sodium Triflate (NaCF<sub>3</sub>SO<sub>3</sub>)."  
*J. Phys. Chem. B*, submitted.
- II. Rebecca A. Sanders, Roger Frech, and Masood A. Khan. "Structural Investigation of Crystalline and Solution Phases in N,N,N',N'-Tetramethylethylenediamine (TMEDA) with Lithium Triflate (LiCF<sub>3</sub>SO<sub>3</sub>) and Sodium Triflate (NaCF<sub>3</sub>SO<sub>3</sub>)."  
*J. Phys. Chem. B* 107 (33) 2003, *in press*.
- III. Rebecca A. Sanders, Roger Frech, and Masood A. Khan. "Characterization of the Crystalline and Solution Phases in N,N,N',N',N"-Pentamethyldiethylenetriamine (PMDETA) with Lithium Triflate (LiCF<sub>3</sub>SO<sub>3</sub>) and Sodium Triflate (NaCF<sub>3</sub>SO<sub>3</sub>)."  
*Manuscript in progress*.
- IV. Rebecca A. Sanders, Albert G. Snow, Roger Frech, and Daniel T. Glatzhofer. "A Spectroscopic and Conductivity Comparison Study of Linear Poly(N-methylethylenimine) with Lithium Triflate and Sodium Triflate."  
*Electrochimica Acta* 48 (14-16) 2003, 2247-2253.
- V. Rebecca A. Sanders, Scott E. Boesch, Albert G. Snow, Lieyu (Richard) Hu, Roger Frech, Ralph A. Wheeler, and Daniel T. Glatzhofer. "N,N,N',N',N"-Pentamethyldiethylenetriamine (PMDETA) as a Model Compound for Linear Poly(N-methylethylenimine), LPMEI".  
*Polym. Prepr.* 44 (1) 2003, 966-967.

## Chapter 1: INTRODUCTION

### 1.1 Battery Technology

The major goal of battery technology is to engineer a “high energy density battery” that is rechargeable, long lasting, energy efficient, cost efficient, and easily produced (1). Some of the different battery technologies include lead-acid, Ni-Cd, Ni-MH (nickel metal hydride), Li-ion, Li-ion hybrid polymer electrolyte (PLiON), and lithium metal batteries. Lead-acid batteries are used in automobiles for lighting and ignition purposes only (2). Ni-Cd batteries are widely used for high power applications and portable devices. These batteries make up 23% of the entire world sales of portable batteries (2). By comparison, Ni-MH and Li-ion batteries account for 14% and 63% of the worldwide sales of portable batteries (2). The PLiON batteries utilize a solid polymer swelled with a liquid Li-ion system; these batteries are sometimes used in portable devices (2). In contrast, the lithium metal batteries are not currently commercially used, because these batteries are unsafe. In terms of volumetric and gravimetric energy densities (Figure 1.1), Li-ion and PLiON batteries have

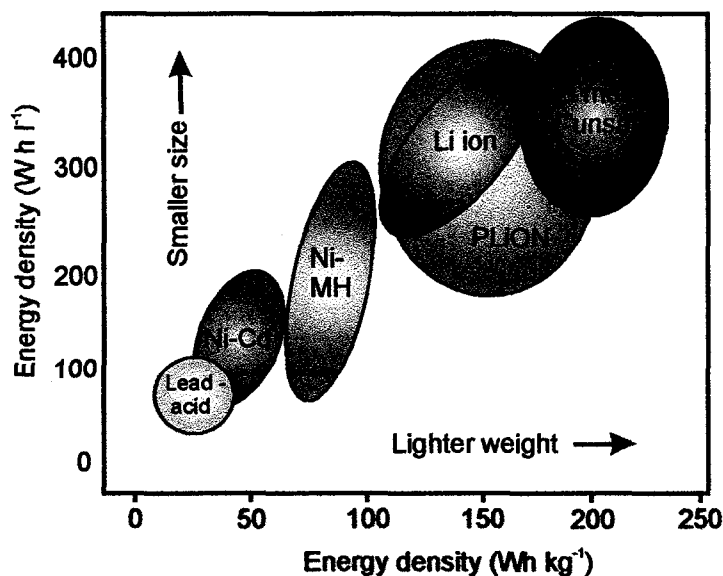
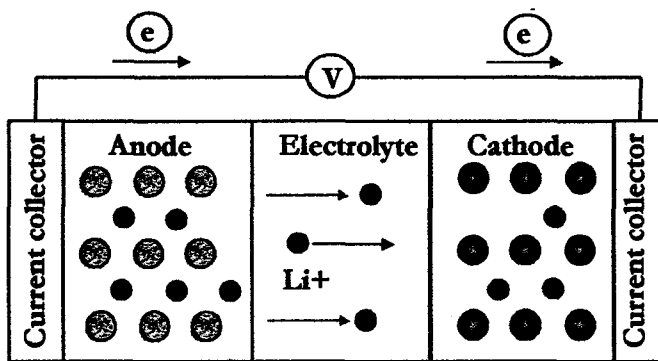


Figure 1.1: A comparison of different types of batteries (2).

higher energy densities than Ni-MH, Ni-Cd, and Pb-acid batteries (2). Lithium is a useful battery material, because it is a lightweight element and has a high oxidation potential (1). The progress in battery technology is very slow, but there have been some advances in Ni-MH and Li-ion batteries (2).

In early 1970s, lithium rechargeable batteries were investigated (3,4). These batteries were comprised of lithium metal (anode), a nonaqueous electrolyte, and a transition metal oxide host (cathode) (2). The oxides in the cathodes provide a framework that gives the lithium ion more mobility in the electrode (2). On the down side, the lithium metal anodes can be extremely dangerous when in contact with the liquid electrolytes (1). Therefore, other materials have been explored for lithium rechargeable batteries. In late 1970, the concept of the lithium ion battery or rocking chair battery (Figure 1.2) was first demonstrated by Murphy *et al.* (5). These batteries contain carbon (anode), a liquid electrolyte, and  $\text{Li}_n\text{XO}_n$  (cathode) materials (2); in addition, other anode materials are currently being investigated, such as  $\text{Li}_{3-x}\text{Co}_x\text{N}_x$  and  $\text{LiSnO}$  (2). In the rocking chair batteries, the lithium ions intercalate in and out of the anode and cathode materials upon charging and discharging. The rocking chair battery is not as hazardous as lithium metal batteries. However, the liquid electrolytes have a tendency to decompose at the metal oxide cathodes due to the high oxidation



**Figure 1.2:** Rocking chair battery with a lithium polymer electrolyte and current collectors.

potential of the cathodes (1). Furthermore, the liquid electrolytes are unsafe to the environment. Therefore, polymer electrolytes are being explored as potentially usable, safer materials for lithium ion batteries (3,6).

In 1973, Wright discovered the conductive properties of polymer electrolytes (7). By 1978, polymer electrolytes were recognized by Armand *et al.* as being applicable for use in batteries (3). The major advantages of using polymer electrolytes over liquid electrolytes are the ease of processing and manipulating the films (6). In addition, they are also electrochemically stable (6). In order to be useful for electronic devices, lithium ion batteries using solid polymer electrolytes should exhibit energy densities between 100–120 Wh/kg, power densities greater than 100 W/kg (peaks at 1kW/kg), cycle life greater than 500 deep cycles (>50% original capacity), low self-discharge of less than 5% per year, and no scale-up effect from 1 to > 1000 cm<sup>2</sup> (6). In addition, the polymer electrolytes must be stable between -20 to 60°C, which is the usual operational temperature range of portable devices and electrically powered vehicles (8).

## 1.2 Polymer Electrolytes

Polymer electrolytes are formed when a salt is dissolved into a polymer matrix, which is accomplished using a solvent. The polymer matrix must have heteroatoms that can coordinate to cations and be reasonably spaced to facilitate “multiple intrapolymer-ion bonds” (9). In addition, the backbone of the polymer must be flexible enough to exhibit significant segmental motion, which is a major contributor to ionic conduction (9). Polymer electrolytes can be formed from comb-like, coblock, linear, or branched polymers.

Some of the polymer hosts studied include poly(ethylene oxide) (PEO), poly(ethylenimine) (PEI), and poly(bis-(methoxyethoxyethoxy)phosphazine (MEEP). When

the latter polymer host contains  $\text{LiCF}_3\text{SO}_3$  at a 24:1 (lithium:ether oxygen, molar ratio) composition, it has one of the highest room temperature conductivity values ( $10^{-5} \text{ Scm}^{-1}$ ) reported for a single phase, polymer electrolyte-based system without plasticizers (10). Nishimoto *et al.* reported a conductivity of  $10^{-4} \text{ Scm}^{-1}$  at  $30^\circ\text{C}$  for poly[ethylene oxide-*co*-2-(2-methoxyethoxy)ethyl glycidyl ether] [P(EO/MEEGE)] complexed with  $\text{LiN}(\text{CF}_3\text{SO}_2)_2$  (11). However, a majority of the research in polymer electrolytes has been focused on PEO materials. In polymer electrolytes, the most commonly studied salts are  $\text{LiCF}_3\text{SO}_3$ ,  $\text{LiBF}_4$ ,  $\text{LiN}(\text{CF}_3\text{SO}_2)_2$ , and  $\text{LiPF}_6$ . The salts used in polymer electrolytes depend on several factors, such as the nature of the cation and anion, hardness and softness properties, lattice energies, charge density, and polarizability. Some of these factors will be discussed in sections 1.2.1 and 1.2.2. The types of solvent used to prepare polymer electrolytes must also be considered.

Polar and nonpolar solvents (Lewis Bases) can be used for preparing polymer electrolytes (9). However, these solvents influence the interaction of the salt with the polymer host due to the “short-range interactions” between the solvent and the ions (9). If these “short-range interactions” are weak enough, the cations can coordinate to the polymer host and allow the anion to dissolve into the polymer matrix (9). In aprotic solvents, most of the anions can be dissolved into the polymer matrix; therefore, these solvents are favored for the preparation of polymer electrolytes (9). However, protic solvents are not preferred, because of their strong interactions with the salt and polymer due to hydrogen bonding (6).

**1.2.1 Hard/Soft Acid/Base Principle.** An acid and base are considered hard or soft on the basis of their polarizability, electronegativity, and ability to oxidize. Acids and bases that have high electronegativity (12) and low polarizability (12,13) are difficult to oxidize, because

their electrons are not easily removed (14). Therefore, these acids and bases are considered to be hard. However, acids and bases are considered to be soft if they have low electronegativity (12) and high polarizability (12,13). This is due to their ability to be easily oxidized because their electrons are readily removed from the valence shell (14). Typically, hard acids have favorable complexation to hard bases and soft acids to soft bases (12). Bonding of acids to bases is the strongest when their size and electronegativity are similar (12). Hard acids and bases are associated with ionic bonding due to their small size and highly positive and negative charges (15). Covalent bonding occurs mostly in soft acids and bases (15). Generally, PEO- and PEI-type polymers are considered to be hard bases. Therefore, they form polymer:salt complexes with hard acids such as  $\text{Li}^+$ ,  $\text{Na}^+$ , and  $\text{K}^+$  (14). However, the acid-base interactions are only one factor that contributes to the formation of polymer electrolytes.

**1.2.2 Contribution of the Cation and Anion.** As mentioned above, the hard acid cations are favored when forming polymer electrolytes with PEO- and PEI-type polymers. Cations can either be monovalent, divalent, or trivalent. However, only some of the divalent and trivalent cations are mobile, which is necessary for ionic conduction (16). The mobility of the cation depends on the strength of the cation-polymer interactions (16). If these interactions are strong, the likelihood for the cation to move is small compared with systems in which cation-polymer interactions that are weak (16). The mobility of the cation is also dependent on its radius. The strength of the cation-polymer interactions diminishes for cations with larger ionic radii; therefore, the larger cations are more mobile. However, the mobility of the cations will be hindered for ionic radii that are too large (9).



Bulkier anions ( $\text{ClO}_4^- > \text{CF}_3\text{SO}_3^- > \text{BF}_4^- > \text{AsF}_6^-$ ) with low charge density and basicity work best in aprotic, dipolar polymer hosts with low-dielectric constants. This is true because their salts are able to dissociate into cations and anions in the solvent and form polymer electrolytes (14). The bulkier monovalent anions dissolve better in polymers, because their low lattice energies and charge delocalization enable the anions to easily solvate in the solvent (6,14,16). In addition, anions that are polarizable dissolve more easily in polymers (16). However, some smaller anions such as  $\text{I}^-$  can be used (16).

**1.2.3 Thermodynamics of Dissolution.** The thermodynamics for dissolution of a salt into a polymer can be described by the free energy of dissolution,  $\Delta G$ , (Eqn. 1.1). This equation consists of three components: entropy of dissolution ( $\Delta S$ ), enthalpy of dissolution ( $\Delta H$ ), and temperature ( $T$ ).

$$\Delta G = \Delta H - T\Delta S \quad \text{Eqn. 1.1}$$

For a salt to dissolve into a polymer matrix,  $\Delta G$  has to be negative. For this to be true,  $\Delta H$  must also be negative and larger than  $T\Delta S$ , because polymer electrolytes typically have a net negative  $\Delta S$ . In polymer electrolytes, the entropy is increased (positive  $\Delta S$ ) due to the dissolution of ions in the polymer matrix. However, the entropy is decreased (negative  $\Delta S$ ) to a greater extent by the confinement of ions to the polymer chain. The overall change in entropy is insignificant compared to the amount of change in the enthalpy (9,17). In addition, there is less variation in  $\Delta S$  compared to  $\Delta H$  among different systems (9).

Dissolving a salt into a polymer matrix can only be feasible if the salt has a greater attraction for the polymer than for the solvent, resulting in a negative  $\Delta H$  under the assumption that anion solvation is not important. There are many factors affecting the

overall  $\Delta H$ . For instance, the rearrangement of the polymer matrix to facilitate coordination of the salt contributes to a positive  $\Delta H$ . From the salt aspect, one must consider the positive enthalpy contribution from the lattice energy. However, the coordination of the cations to the polymer sites results in a negative contribution for  $\Delta H$  (16). In order to achieve the necessary negative enthalpy to dissolve the salt into the polymer matrix, the contribution from the coordination of the cation to the heteroatom must be larger than the other enthalpic contributions (16).

### 1.3 Poly(ethylene oxide).

The most widely studied polymer electrolyte is poly(ethylene oxide), PEO, which was first synthesized at low molecular weights by Lourenco (18) and Wurtz (19) in the late 1920s. However, high molecular weight PEO was not made commercially available until the late 1950s (9). In its crystalline form, PEO consists of single stranded helices and has a melting point at  $\sim 65^\circ\text{C}$  (20). However, PEO has crystalline and amorphous phases when it is above the glass transition temperature ( $-67^\circ\text{C}$ ) (21),  $T_g$  (temperature at which segmental motions can occur).

Model compounds have been extensively investigated in order to better understand the complex nature of PEO. Some of the model compounds studied include the dimethyl ethers of ethylene oxides  $\text{CH}_3(\text{OCH}_2\text{CH}_2)_n\text{OCH}_3$  ( $n = 1-4$ ) complexed with various salts (22-28). These model compounds are referred to as glymes (mono-, di-, tri-, etc.). The glymes and glymes:salt complexes are used to increase understanding of the local structure (ionically associated species and local backbone conformation) of the complicated PEO and PEO:salt systems. The ionically associated species (29) are due to cation-anion interactions (30), while changes in the polymer backbone conformation (30,31) are attributed to cation-polymer

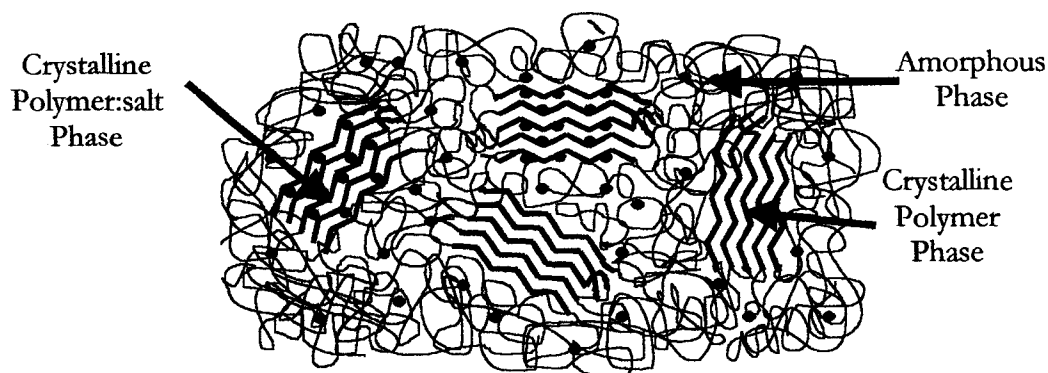


**Figure 1.3:** A schematic of a PEO-based polymer electrolyte.

interactions (4). Single crystals have been obtained from the glyme:salt systems (23,24,28), which have made it easier to understand the local structures of these systems in solution and analogous local structures of high molecular weight PEO:salt systems in the amorphous phase.

**1.3.1 PEO-Salt Complexes.** Most metal cations can dissolve into PEO because its “solvating properties” parallel that of water (6). This is due to their similar donicities of the oxygen atoms (6). The main difference between PEO and water is the inability of PEO to solvate the anions efficiently (6).

When salt is added to PEO, its helical structure is altered. Depending on the salt composition, the PEO-salt complexes can contain varying amounts of both amorphous and crystalline phases as illustrated in **Figure 1.3**. Both the crystalline and amorphous phases result from either pure PEO domains, PEO:salt domains, or a combination of the two. In the pure crystalline phase, PEO-based electrolytes take on a “spherulitic morphology” ranging from micrometers to centimeters (32). These spherulites exhibit a lamellar structure, which is also present in the PEO:salt complexes containing both crystalline and amorphous phases (33).

Some of the crystalline salt complexes that form with PEO include PEO:KSCN,

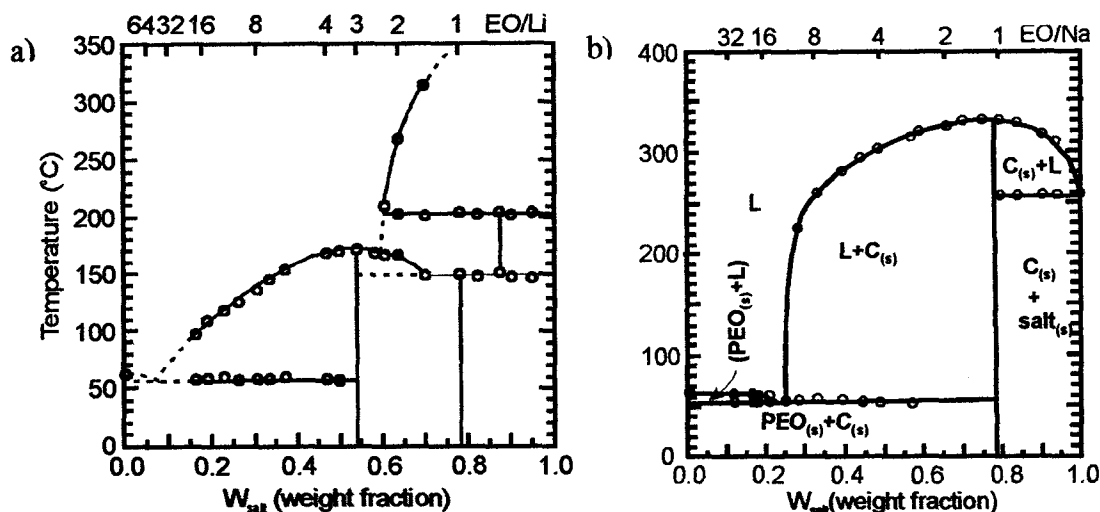


**Figure 1.4:** Phase diagram of PEO with **a)** (36)  $\text{LiCF}_3\text{SO}_3$  and **b)** (37)  $\text{NaCF}_3\text{SO}_3$ . Data were collected from NMR, DTA, DSC, X-ray, and optical microscopy (36,37).

PEO: $\text{NH}_4\text{SCN}$ , PEO: $\text{RbSCN}$ , PEO: $\text{LiCF}_3\text{SO}_3$ , PEO: $\text{NaSCN}$ , PEO: $\text{NaClO}_4$ , and PEO: $\text{NaI}$  (32). The amount of crystallinity in the PEO-salt complexes varies with composition (34), time (35), molecular weight, and temperature (34). The growth of crystallization is dependent on multiple factors, such as the rate of solvent removal (9,32), type of solvent used (9,32), salt composition (32), molecular weight of the polymer (32), temperature (32), and time (38). Phase diagrams of polymer-based electrolytes have been constructed in order to better understand conduction in these systems. There are many reported phase diagrams of PEO-salt complexes, such as  $\text{PEO}_4:\text{NH}_4\text{CF}_3\text{SO}_3$  (39),  $\text{PEO}_4:\text{NH}_4\text{SCN}$  (39),  $\text{PEO}_3:\text{LiCF}_3\text{SO}_3$  (36,40),  $\text{PEO}_3:\text{LiN}(\text{CF}_3\text{SO}_2)_2$  (36),  $\text{PEO}_3:\text{NaCF}_3\text{SO}_3$  (37),  $\text{PEO}_4:\text{LiAsF}_6$  (40),  $\text{PEO}_3:\text{LiClO}_4$  (36,40), and  $\text{PEO}_3:\text{NaI}$  (34,41). These phase diagrams are constructed using differential scanning calorimetry, X-ray diffraction, and optical microscopy (36,37). **Figures 1.4a and b** represent the phase diagrams of PEO: $\text{LiCF}_3\text{SO}_3$  (PEO: $\text{LiTf}$ ) and PEO: $\text{NaCF}_3\text{SO}_3$ ,

(PEO:NaTf). As seen in **Figures 1.4a and b**, both systems have a number of phases, depending on the weight fraction of salt.

**1.3.2 Ionic Conductivity.** For dilute solutions, ionic conductivity can be expressed by the Kohlrausch summation.

$$\sigma = \sum_i \mu_i q_i n_i \quad \text{Eqn. 1.2}$$

in which  $\sigma$  is the conductivity,  $n_i$  is the concentration of the  $i$ th ion,  $q$  is the charge,  $\mu$  is the ion mobility. Therefore, high conductivity values can only be obtained with large concentrations of charge carriers with high ionic mobilities (1). The mobility of the lithium ion in polymer electrolytes has been attributed to either coupling with segmental motion or ion hopping, depending on the models used. Angell proposed a coupling between the ionic motion and structural relaxation, such that faster relaxation processes in the polymer host yields higher ionic conductivities (42). Angell rationalized this behavior using the following equation (42),

$$R = \frac{\tau_s}{\tau_\sigma} \quad \text{Eqn. 1.3}$$

where  $R$ ,  $\tau_s$  and  $\tau_\sigma$  represent the decoupling ratio, segmental relaxation time, and conductivity relaxation time, respectively. Above  $T_g$ , the decoupling ratios for polymer:salt complexes are slightly below one (43,44). This suggests that ionic mobility is “fully coupled” to the segmental relaxation process. Therefore, ionic mobility can only occur if the segmental relaxation process has been initiated.

The ionic conductivity can also be expressed in terms of diffusion coefficient ( $D$ ) using the Nernst-Einstein relationship (Eqn.1.4).

$$\sigma = \frac{nq^2D}{k_bT} \quad \text{Eqn. 1.4}$$

in which  $\sigma$  is the conductivity,  $n$  is the concentration,  $q$  is the charge,  $k_b$  is the Boltzmann's constant, and  $T$  is the temperature in Kelvin (1,43).

Ionic conductivity of polymer electrolytes can be measured using either direct current (d.c.) or alternating current (a.c.) methods. Direct current measurements are a direct way to obtain the ionic conductivity of polymer electrolytes (45). However, there are several disadvantages of using this method, particularly in the difficulty of constructing a cell (four electrode cell), complications due to concentration polarization, and instability of the reversible electrode materials over a broad temperature range (45). By comparison, a.c. measurements are the most common method of determining ionic conductivity in polymer electrolytes (45). In addition to a simplistic cell design (two electrode cell), the a.c. method is

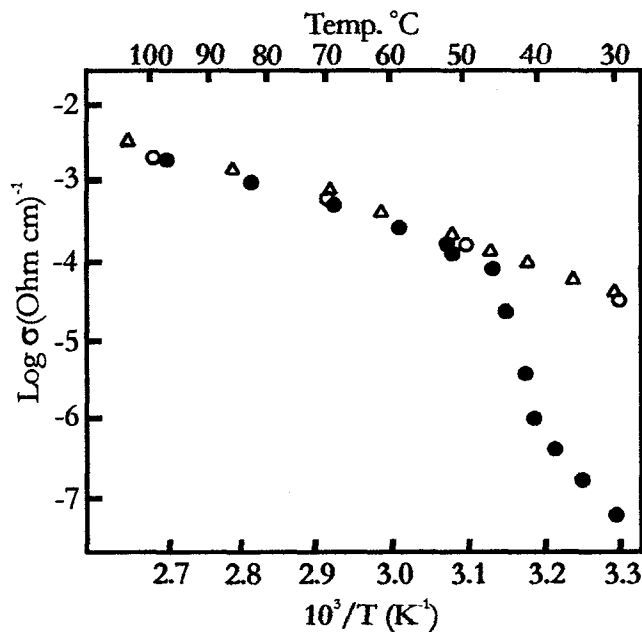


**Figure 1.5:** Conductivity plots of  $(\text{PEO})_8:\text{NH}_4\text{SCN}$  at a 8:1 (salt:oxygen) composition represents the heating (●) of the crystalline phase into the amorphous phase. This amorphous phase is then cooled (Δ) and heated (○) (39,46,47).

preferred because this method can utilize blocking electrodes, which are stable over a broad

In PEO:salt systems, conductivities range between  $10^{-6}$  to  $10^{-8}$   $\text{Scm}^{-1}$  at room temperature(6,36,48,49). For the 8:1 (salt:oxygen molar ratio)  $(\text{PEO})_8:\text{NH}_4\text{SCN}$  (**Figure 1.5**), the ionic conductivity is greater in the amorphous phase than in the crystalline phases below  $T_g$  (39,46,47). Above  $T_g$ , the crystalline phases become mostly amorphous, thus exhibiting similar ionic conductivity values (**Figure 1.5**) (20,39,46,47,50). However, Gadjourova *et al.* have published data showing that the crystalline phase is more conductive than the amorphous phase in the  $(\text{PEO})_6:\text{LiSbF}_6$  complex (51).

There is evidence that the maximum ionic conduction of polymer electrolytes is achieved at the eutectic composition (6). In addition, heavier alkali ions yield the highest conductivities in PEO-based electrolytes such that  $\text{Li} < \text{Na}$  and  $\text{K} < \text{Rb}, \text{Cs}$  (6). Ionic conductivities in polymer electrolytes are dependent upon concentration (9), pressure (52), and temperature. Modeling techniques are often used to attempt to understand the ionic transport mechanism, which will be discussed in the next section.

*Models for Conductivity.* The temperature dependence of the conductivity in polymer electrolytes is commonly described by Arrhenius (Eqn. 1.5) or Vogel-Tamman-Fulcher, VTF, behavior (Eqn. 1.6).

$$\sigma = \sigma_o \exp\left[\frac{-E_a}{kT}\right] \quad \text{Eqn.1.5}$$

$$\sigma = \sigma_o \exp\left[\frac{B}{(T - T_o)}\right] \quad \text{Eqn.1.6}$$

in which  $\sigma$  is the conductivity,  $\sigma_o$  is the prefactor,  $E_a$  is the activation energy,  $k$  is the Boltzmann constant, and  $B$  is a constant, and  $T_o$  is a fitting parameter, typically about 50K below  $T_g$  (52,53). For instance, the conductivity plots in **Figures 1.6a** and **b** illustrates the

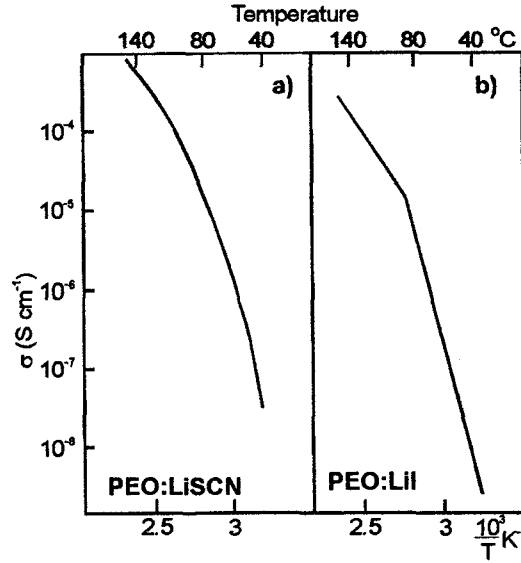


**Figure 1.6:** Conductivity plot of  $\log \sigma$  vs  $T^{-1}$  of PEO with a) LiSCN ( $O/Li = 5$ ) and b) LiI ( $O/Li = 4.5$ ) (52). VTF type behavior is seen in the PEO:LiSCN curve whereas PEO:LiI has a Arrhenius type behavior (52).

VTF and Arrhenius behavior, respectively. In **Figure 1.6b**, the conductivity curve consist of two distinct regimes of Arrhenius behavior, in which activation energies from an Arrhenius curve are typically larger below  $T_g$ . In addition, some conductivity plots exhibit both Arrhenius (at low temperatures) and VTF (at higher temperatures) behaviors (52). In contrast, there are also reports of Arrhenius curves at high temperatures and VTF curves at temperatures slightly above  $T_g$  (4).

The Williams-Landel-Ferry (WLF) equation (Eqn.1.7), a “classical extension” of the VTF equation (9), can also be used to describe the dependence of conductivity on temperature:

$$\log a_T = \frac{-17.44(T - T_g)}{51.6 + T - T_g} \quad \text{Eqn.1.7}$$



In the WLF equation (Eqn.1.7),  $a_T$  is a shift factor correlating to the “ratio of any mechanical relaxation” at temperatures,  $T$ , and the glass transition temperature,  $T_g$ , respectively (52). Eqn. 1.7 is only valid if  $T$  is greater than  $T_g$ . The WLF equation is based on relaxation times of the polymer host, whereas the VTF equation stems from viscosity parameters of super-cooled liquids (52). The VTF and WLF equations only consider the free volume theory for ionic mobility. However, these empirical equations are not derived from the free volume theory. Free volume theory is described by Cohen and Turnbull as a redistribution of free volume to accommodate diffusion (52). This theory is an implicit way of describing segmental motions in the polymer host, but not in polymer:salt complexes (52). Additional factors which are not considered when using the free volume model include sample inhomogeneity, kinetic effects, and significant contribution from ionic interactions (52). Other models studied for ionic conductivity of polymer electrolytes include configurational entropy (52) and dynamic bond percolation theory (16,43,44,54,55).

The configurational entropy model is an attempt to provide a better representation of the ionic conductivity for polymer electrolytes. This model takes into consideration both the number of lattice sites and distorted bonds. This theoretical model is preferred over the free volume method, because it is a better representation of the pressure dependence of the ionic conduction (52). However, like the free volume theory, the configurational entropy model describes the effects of the polymer host, not the polymer:salt complex (52).

Both the free volume and the configurational entropy models employ static methods for describing the polymer host, which is a major drawback to these models. In addition, these models provide macroscopic representations of ionic conduction (52). However, a microscopic representation is necessary to understand the mechanism of ionic conduction (52). The dynamic bond percolation model (DBP), such an approach, utilizes the “actual

motion of the individual ions” to describe the mechanism of ionic conduction (43). In the DBP model, the polymer lattice is continuously rearranging to facilitate ion hopping (54). The DBP model considers the frequency dependence of the properties and the interionic interactions, unlike the free volume and configurational entropy models (43,44). This model assumes [1] the movements of the ions occur among the sites in the polymer host (43); [2] the material is dense; [3] the sites in the dense material consist of charge carriers; [4] the site-to-site motion is regulated by the hopping time and structural relaxation time; and [5] “the experimental time scale is at least as large as” the hopping time (55). The major drawback of the DBP model is its failure to consider the motion of clusters or aggregate species in the system.

There are many extensions of the DBP, such as the Druger-Nitzan-Ratner (DNR), and the Harrison-Zwanzig (HZ) models. The DNR model represents a global dynamic disorder using a random walk method to describe the motions (55). However, the HZ model is based on the theory that one bond fluctuates while the others stay the same (local dynamic disordering) (55).

*Transport and Transference numbers.* Ionic mobility is a major factor governing ionic conductivity. Transport properties, transport numbers and transference numbers are measured to gain insight about ionic mobility. Assuming the Nernst-Einstein relationship, the transport number can be written as

$$t_+ = \frac{I_+}{I_0} \quad \text{Eqn.1.8}$$

in which  $t_+$ ,  $I_+$ , and  $I_0$  are the cation transport number, the steady state value of current carried by the cation, and the initial value of the total current, respectively (29). The

transport number can also be represented in terms of diffusion coefficients,  $D$ , as shown in Eqn. 1.9 (14,29).

$$t_+ = \frac{D_+}{D_{total}} \quad \text{Eqn.1.9}$$

in which  $D_+$  and  $D_{total}$  are the diffusion coefficients of a given cationic charge carrier and of the total charge carriers (29). At one time, single ion transport numbers were the focus for studies of the mechanism of conductivity in polymer electrolytes. However, there were major discrepancies in the transport numbers reported (29,56-59). These discrepancies were a result of not being able to detect the movement of only one type of charge carrier. It soon became clear that transport numbers could not be measured with confidence in polymer electrolytes. Therefore, research efforts have been focused on measuring transference numbers.

The transference number,  $T$ , is defined as the “net number of moles of an ion constituent that crosses a reference plane fixed with respect to the solvent when one Faraday of current is passed through the fixed plane in absence of concentration gradient” (60). For a polymer electrolyte system with multiple ionic species, e.g.  $m^+$ ,  $x^-$ ,  $mx$ ,  $m_2x^+$ , and  $mx_2^-$ , the transference number is defined as (60):

$$Tx^- = t(x^-) + 2t(mx_2^-) - t(m_2x^+) \quad \text{Eqn.1.10}$$

$$Tm^+ = t(m^+) + 2t(m_2x^+) - t(mx_2^-) \quad \text{Eqn.1.11}$$

in which  $t$  is the individual transport number of each ionically charged species present (29). There are several different methods used to measure these numbers, such as pulsed-field gradient nuclear magnetic resonance (61-63), electrophoretic nuclear magnetic resonance (63), potentiostatic polarization (17,56,65,66), and the Hittorf-style technique (57).

In liquids with single cations and anions, the transference numbers of cations and anions can be successfully determined. However, transference numbers in polymer electrolytes are complicated by the presence of charged aggregate species. The presence of multiple charged species makes it difficult to decipher which ions are moving. If the cation is the major contributor to the charge carriers, then the transference number should be close to one (1). By comparison, negative values for cation transference numbers indicate negatively charged aggregate species are the predominant mobile species (60,62,67). The majority of the ambiguities in the transference numbers occur when  $T_m^+$  values are less than one. In addition, there are many discrepancies in the transference numbers reported for a polymer electrolyte system (58,59,64,68,69). There are many other factors that affect the transference numbers, such as the nature of the polymer host and anion along with the salt concentration (50,56,58,60,64,67-70).

*Ionic Association.* The ionic species present in a polymer electrolyte system sometimes can be determined by studying the cation-anion interactions. Ionic association refers to the interactions between the cation and anion, which can lead to “free” ions, contact ion pairs, or aggregate species. The degree of ionic association of the cation to the anion has been extensively studied in certain polymer:salt systems (71-79) where these species can be identified using infrared and Raman spectroscopy. This is accomplished by curve-fitting the bands associated with the ionic association regions such as the  $\text{CF}_3$  deformation mode,  $\delta(\text{CF}_3)$ , and the  $\text{SO}_3$  stretching mode,  $\nu(\text{SO}_3)$  in  $\text{CF}_3\text{SO}_3^-$  containing polymer electrolytes. Once the ionically-associated species in a particular polymer electrolyte are known, this information can be correlated to the ionic conductivity values. For instance, in the 24:1 ( $\text{Li}^+$ :ether oxygen, molar ratio) MEEP:LiTF sample that has one of the best room

temperature conductivities ( $10^{-5} \text{ Scm}^{-1}$ ) reported for a polymer electrolyte, there is convincing evidence that contact ion pairs are the dominant species present (74).

In PEO:LiTf systems, the  $\delta(\text{CF}_3)$  bands and their assignments are: "free" ions at  $752\text{--}753 \text{ cm}^{-1}$ , contact ion pairs [LiTf] at  $756\text{--}758 \text{ cm}^{-1}$ , and aggregate species  $[\text{Li}_2\text{Tf}]^+$  at  $761\text{--}763 \text{ cm}^{-1}$ . For the  $\nu(\text{SO}_3)$  region, these bands occur between  $1032\text{--}1034 \text{ cm}^{-1}$  ("free"),  $1037\text{--}1042 \text{ cm}^{-1}$  (contact ion pairs), and  $1047\text{--}1054 \text{ cm}^{-1}$  (aggregate) (75-78).

For PEO:NaTf systems, the ionically associated species determined from Raman-active  $\delta(\text{CF}_3)$  bands are "free" ions at  $753 \text{ cm}^{-1}$ , contact ion pairs [NaTf] at  $756 \text{ cm}^{-1}$ , an aggregate I species at  $761 \text{ cm}^{-1}$ , and an aggregate II species at  $769 \text{ cm}^{-1}$ . For the  $\nu(\text{SO}_3)$  region, these bands are assigned at  $1032 \text{ cm}^{-1}$  ("free"),  $1037 \text{ cm}^{-1}$  (contact ion pairs),  $1050 \text{ cm}^{-1}$  (aggregate I), and  $1058 \text{ cm}^{-1}$  (aggregate II) (79).

#### 1.4 Poly(ethylenimine)

Compared to PEO, poly(ethylenimine), PEI, is a synthetically versatile polymer host (80-82) in that various groups can be attached to the nitrogen atom. Therefore, PEI can be either branched or linear. Both BPEI (83-85) and LPEI (74,83,86-96) have been investigated as a polymer host for polymer electrolytes. BPEI has a very complex structure consisting of asymmetric branches with primary, secondary, and tertiary amines. However, LPEI is comprised of only secondary amines, resulting in a more simplified structure. Therefore, research efforts have been focused mainly on LPEI systems as a polymer host rather than BPEI. LPEI melts at  $58^\circ\text{C}$  and has a  $T_g$  at  $-23^\circ\text{C}$  (97-99). LPEI is soluble in methanol, ethanol, chloroform (99), and hot water (97).

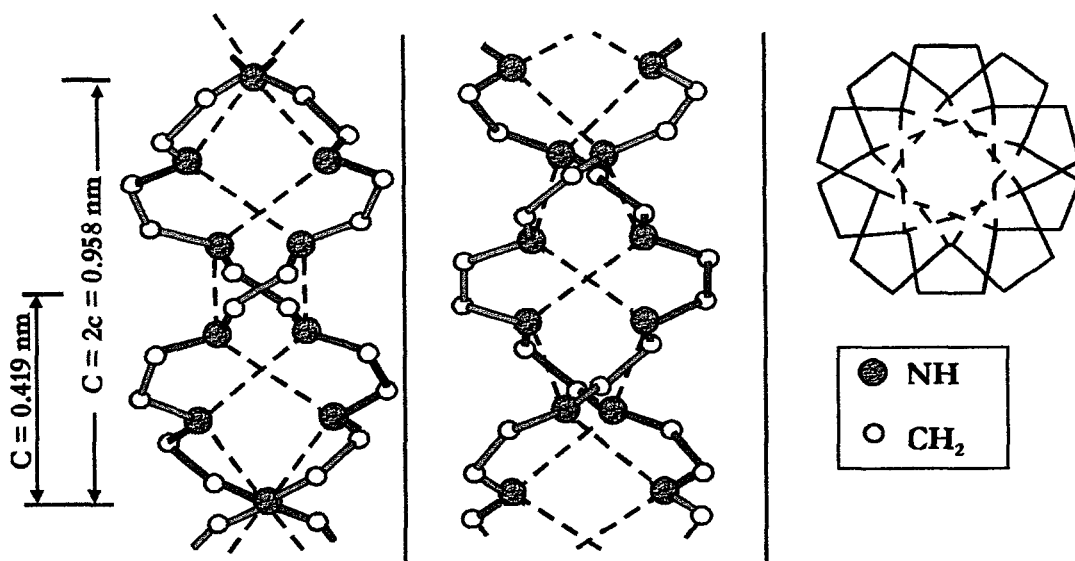


Figure 1.7: Crystalline anhydrous LPEI in three different views (100).

**1.4.1 LPEI Crystalline Structure.** Chatani *et al.* proposed that the crystalline LPEI forms a 5/1 double-stranded helix when it is completely anhydrous (Figure 1.7) based on an X-ray diffraction study (100). However, there is a discrepancy in the proposed structure in that only half the fiber axis of the double-stranded helix is incorporated into the unit cell. In addition, Chatani *et al.* had to make a number of assumptions to solve the structure, such as restricting the values of certain bond lengths and angles. According to Chatani *et al.*, the core of the double-stranded helix is made up of NH groups, in which the helical structure is maintained primarily through intermolecular hydrogen bonding (100). The double-stranded helix is in an Fddd space group, such that the strands are hexagonal-close-packing. Each double strand is packed next to two right-handed and four left-handed strands (100). In crystalline LPEI, each nitrogen atom is covalently bonded to one carbon atom and one hydrogen atom. In addition, there is intermolecular hydrogen bonding to the each nitrogen atom. Other than Chatani *et al.*, there are no reports of the LPEI crystal structure. In a different study of anhydrous LPEI, there are three crystalline peaks in the X-ray powder

diffraction patterns ( $2\theta = 11.8, 20.5, 23.8$ ), which obviously could not be solved to yield a crystal structure (96). Anhydrous LPEI is very hydroscopic and can form three different crystalline hydrates: hemihydrate, sesquihydrate, and dihydrate (101-103).

**1.4.2 LPEI Hydrates.** In all crystalline LPEI hydrates, the polymers align in a planar zigzag geometry forming hydrogen-bonding networks in which the amine hydrogen atoms interact with the water oxygen atoms and the water hydrogen atoms interact with the amine nitrogen atoms. In all crystalline hydrates, there are two water molecules coordinated to each nitrogen atom. However, the local environment of the water molecules is different in each hydrate. In the hemihydrate, there are two NH groups coordinated to each oxygen atom. In the sesquihydrates, there are two different local environments of the water molecules; [1] two water molecules coordinate to two NH groups, and [2] three water molecules coordinate to one NH group. The latter coordination occurs twice as often as the former. In the dihydrate, three water molecules and one NH group coordinate to each water molecule (103).

The LPEI hydrates are not practical for polymer electrolytes, because water promotes corrosion in lithium ion batteries. Therefore, anhydrous LPEI-based polymer electrolytes have been the main focus of polymer electrolyte research.

**1.4.3 LPEI:Salt Complexes.** LPEI as a polymer electrolyte has been investigated using salts such as LiTf (74,96), NaTf (74,96), LiClO<sub>4</sub> (93), and LiSbF<sub>6</sub> (104,105). Lithium salts containing Cl<sup>-</sup>, Br<sup>-</sup>, I<sup>-</sup>, SCN<sup>-</sup>, ClO<sub>4</sub><sup>-</sup>, BF<sub>4</sub><sup>-</sup> (86), and Tf (86,93,96) can be dissolved in LPEI using a co-solvent. Crystalline complexes have been reported for LPEI with NaTf (106), CH<sub>3</sub>COOH (107), and HCl (98). Crystal structures have been solved for only the

LPEI:CH<sub>3</sub>COOH and LPEI:HCl crystalline complexes. Formation of a crystalline compound in the LPEI:NaTf system has been reported to occur at a 4:1 nitrogen to sodium ratio, based on X-ray powder diffraction and differential scanning calorimetry (106). This crystalline complex melts at 160°C (106).

When LiTf or NaTf are added, LPEI becomes very disordered at moderate salt concentrations (>10:1) (96) and at moderate temperatures (above T<sub>g</sub>) (97). This disordering is due to the breaking of intermolecular hydrogen bonding therefore reducing the degree of crystallinity in LPEI (74,96,104,105). This loss of crystallinity is evidenced by an increased bandwidth in infrared spectral bands and a significantly decreased peak intensity in DSC endotherms (melting points) (96). According to Tanaka and Saito, the T<sub>g</sub> of LPEI increases as the LiTf composition increases (93). The disordering also can be detected by monitoring the NH stretching modes using infrared spectroscopy because there are distinct bands due to crystalline and amorphous components. Disordering of LPEI is also evident in samples containing LiSbF<sub>6</sub> (104). This disordering is also attributed to the coordination of lithium ions to nitrogen atoms, although N-H...F interactions may also play a role. The N-H...F interactions are evidenced by the ~70 cm<sup>-1</sup> shift in the SbF<sub>6</sub><sup>-</sup> band at 669 cm<sup>-1</sup> (105), which is an unusually large frequency shift (108) compared to spectra of PEO:LiSbF<sub>6</sub> (109), glymes:LiSbF<sub>6</sub> (110), and linear poly(N-methylethylenimine):LiSbF<sub>6</sub> (111).

In LPEI:LiTf systems, the "free" ions, contact ion pairs, and two aggregate species based on the  $\delta(\text{CF}_3)$  bands occur at 752-3 cm<sup>-1</sup>, 755-757 cm<sup>-1</sup>, 759-762 cm<sup>-1</sup>, and 763 cm<sup>-1</sup>, respectively. In LPEI:NaTf systems, these species appear at 754 cm<sup>-1</sup>, 756-757 cm<sup>-1</sup>, and 762 cm<sup>-1</sup> (96). In addition, the ionic association of LPEI increases with increasing LiTf composition. However, in the LPEI:NaTf systems, aggregate and "free" ions are only evident in samples with high concentrations of NaTf (5:1).



The conductivity of pure LPEI is on the order of  $10^{-9} \text{ Scm}^{-1}$  at room temperature (74,106). LPEI is poorly conducting due to the presence of highly crystalline domains. The highest reported conductivity value for LPEI:LiTf is ca.  $10^{-5} \text{ Scm}^{-1}$  at a 20:1 (N:Li) molar ratio at 70°C(74). Below  $T_g$  ( $\sim 30^\circ\text{C}$ ), the highest conductivity value is achieved at a 5:1 composition ( $10^{-7} \text{ Scm}^{-1}$ ) (74). By attaching various side chains [e.g.,  $-\text{CH}_3$  (93,99,112-120),  $-\text{CH}_2\text{CH}_3$ ,  $-\text{CH}_2\text{CH}_2\text{CN}$  (121),  $-(\text{CH}_2\text{CH}_2\text{O})_n\text{CH}_3$  (122)] to LPEI, the crystallinity is decreased, therefore the conductivity of these systems should improve. Snow *et al.* tethered diglyme to LPEI, linear poly(methyldiethylene oxide ethylenimine) or  $[\text{CH}_2\text{CH}_2\text{N}(\text{CH}_2\text{CH}_2\text{O})_2\text{CH}_3]_n$ , and were able to achieve a room temperature conductivity of  $5 \times 10^{-6} \text{ Scm}^{-1}$  at a 20:1 (N:Li<sup>+</sup>, molar ratio) composition (122).

**1.4.4 Model Compounds.** To acquire a better understanding of the local structures of LPEI, N,N'-dimethylethylenediamine (DMEDA) has been investigated as a model compound for LPEI by York *et al.* (74,123) and Boesch *et al.* (124). Vibrational mode assignments of LPEI were aided by computational studies of DMEDA and a tetrameric unit of LPEI,  $(\text{CH}_3)_2\text{NH}(\text{CH}_2\text{CH}_2\text{NH})_4$  (125). York *et al.* have reported that the  $\delta(\text{CF}_3)$  bands in DMEDA:LiTf are assigned to “free” ions at  $755 \text{ cm}^{-1}$ , contact ion pairs at  $758\text{--}760 \text{ cm}^{-1}$ , and aggregate species at  $763 \text{ cm}^{-1}$  based on Raman spectra (123). In addition, the  $\nu_s(\text{SO}_3)$  bands in the Raman data are reported at  $1034\text{--}1036 \text{ cm}^{-1}$  (“free” ions),  $1040\text{--}1044 \text{ cm}^{-1}$  (contact ion pairs), and  $1054 \text{ cm}^{-1}$  (aggregate species) (123). To further understand the polymer-cation and cation-anion interactions in LPEI, single crystals of DMEDA complexed with NaTf were grown and investigated by IR, Raman, DSC, and X-ray diffraction. These data along with the correlation between crystalline and solutions DMEDA:NaTf will be discussed in Chapter 3 section 1.

**1.4.5 LPEI as Crosslinked Polymer Electrolytes and Proton Conductors.** BPEI and LPEI have also been used in crosslinked polymer electrolytes (88,89,92) and as proton conductors (94,126). As yet, these areas have not been vigorously explored. PEI can be easily crosslinked through the nitrogen atoms, which makes it useful for preparing elastomeric polymer electrolytes. Most of the crosslinked systems reported are made from crosslinking LPEI with alkyl sulfate surfactants (88,89,92). When these PEI crosslinked systems are swelled with a diluent, the PEI becomes sensitive to changes in the pH of the diluent. For examples, the crosslinked PEI will shrink and expand as a result of changing the pH from 11 to 3 (88,89,92).

Daniel *et al.* and Tanaka *et al.* were successful in utilizing BPEI as a host for proton conductors, using  $\text{H}_3\text{PO}_4$  and  $\text{H}_2\text{SO}_4$  (94,126). Tanaka *et al.* have also reported results on LPEI utilizing the same acids (94). For both the LPEI and BPEI proton conductors, the conductivities are dependent on the composition of the system. However, BPEI is less dependent on the composition than the LPEI systems (94). Tanaka *et al.* reported conductivities at 60°C on the order of  $10^{-5} \text{ Scm}^{-1}$  for a 0.8 moles of  $\text{H}_3\text{PO}_4$  per PEI repeat unit (94). According to Daniel *et al.*, BPEI: $\text{H}_2\text{SO}_4$  conducts better than the BPEI: $\text{H}_3\text{PO}_4$  proton conductors (126).

**1.5 Linear Poly(N-methylethylenimine).** Linear poly(N-methylethylenimine), LPMEI, is a methyl-substituted derivative of LPEI and is completely amorphous at room temperature with a  $T_g$  reported at -90°C (93,116). The polymer exhibits poor mechanical properties even at high molecular weights (ca. 115,000 MW.). LPMEI is soluble in methanol, ethanol, chloroform, acetonitrile, dimethylformamide, tetrahydrofuran, and benzene (99,116). LPMEI is a very hygroscopic, viscous oil. When hydrated, it has a well-defined melting

point at 56°C (99). There has been a limited amount of research reported for LPMEI as a polymer electrolyte (93,114,116,117). Tanaka and Saito investigated LPMEI with LiTf and LiClO<sub>4</sub>, in which the effects of these salts were evident in the value of T<sub>g</sub> (93). The T<sub>g</sub> increases with salt concentration and is more drastic in the LiClO<sub>4</sub> system (93). In addition, Tanaka and Saito reported that LPMEI:LiTf is more conductive than LPMEI:LiClO<sub>4</sub> by about an order of magnitude at temperatures ranging from 20°C to 120°C (93). Tanaka and Saito also reported conductivity values of LPEI:LiTf with low LiTf compositions (15:1) to be higher than those in LPMEI:LiTf (16:1) at temperatures below 60°C (93).

My research objective is to gain further insight into polymer-cation interactions, cation-anion interactions, and ionic conduction in LPMEI:salt complexes. One strategy is to characterize LPMEI complexed with LiTf and NaTf utilizing infrared spectroscopy, complex impedance, powder X-ray diffraction, and differential scanning calorimetry. A second strategy is to investigate model systems utilizing the same techniques augmented with computational studies in order to assign vibrational modes and to understand the polymer-cation and cation-anion interactions of LiTf and NaTf in LPMEI. The model compounds examined for LPMEI include N,N,N',N'-tetramethylethylenediamine (TMEDA) (127) and N,N,N',N',N''-pentamethyldiethylenetriamine (PMDETA) (114,117,128).

While studying these models complexed with LiTf and NaTf, crystalline complexes were discovered in TMEDA:LiTf, TMEDA:NaTf, PMDETA:LiTf, and PMDETA:NaTf. Crystal structures were solved for crystalline TMEDA:LiTf, TMEDA:NaTf, and PMDETA:NaTf. Knowledge of the unambiguous local structures in these crystal provides further insight into the local environment of TMEDA:LiTf, TMEDA:NaTf, and PMDETA:NaTf in solution, which in turn may be correlated to the LPMEI systems.

## ***Chapter 2: EXPERIMENTAL***

---

### **2.1 Sample Preparation.**

N,N'-dimethylethylenediamine (DMEDA), N,N,N',N'-tetramethylethylenediamine (TMEDA), N,N,N',N',N''-pentamethylethylenediamine (PMDETA), anhydrous acetonitrile, NaCF<sub>3</sub>SO<sub>3</sub> (NaTf), LiCF<sub>3</sub>SO<sub>3</sub> (LiTf), and LiSbF<sub>6</sub> were obtained from Aldrich. Both TMEDA and PMDETA were distilled over sodium metal. The anhydrous acetonitrile was used as received. LiTf and NaTf were heated under vacuum at 120°C for 48 hours. Low (~550 MW) and high molecular weight (~115,000 MW) LPMEI were synthesized by Lieyu (Richard) Hu and Albert G. Snow using previously reported methods (116, 117). All of the chemicals were stored and used in a dry nitrogen glovebox (VAC<sub>2</sub> 1ppm H<sub>2</sub>O) at room temperature.

**2.1.1 Model:Salt Complexes.** To prepare the TMEDA:LiTf solutions, LiTf was dissolved into TMEDA at various concentrations and stirred for at least 24 hours. Similar sample preparation was used for the DMEDA:NaTf, TMEDA:NaTf, and PMDETA:LiTf samples, except the samples were stirred only for 4 – 6 hours before collecting the data. Samples of PMDETA:NaTf had to be heated slightly to dissolve the salts, then cooled and stirred for about 24 hours. The compositions of the solutions are reported as a nitrogen to cation molar ratio (N:M<sup>+</sup>, M<sup>+</sup>=cation). The model:salt compounds were prepared with compositions ranging between 20:1 and 3:1.

At higher triflate compositions, the solutions contained both a liquid and a gel-like phase that formed instantly or, in certain cases, within 24 hours of preparing the sample. Over time, all the samples become phase-separated. Several months later, a fine-grained, gritty textured material had formed at the gel-liquid interface and on the glass surface just above the sample. However, in 10:1 PMDETA:LiTf, the gritty textured material appeared

throughout the entire sample. After about 6 months, the entire sample was composed of crystals with only a small amount of residual solvent in the vial. However, in the DMEDA:NaTf samples, there was no evidence of a gritty textured material. Instead, a thin layer of needle-like crystals formed at the liquid-air interface after ~6 months. All of the crystals were allowed to completely dry in a nitrogen atmosphere. The formation of crystals was evident in all samples of DMEDA:NaTf, TMEDA:LiTf, TMEDA:NaTf, PMDETA:LiTf, and PMDETA:NaTf. However, single crystals could be isolated only from the DMEDA:NaTf, TMEDA:NaTf, TMEDA:LiTf, and PMDETA:NaTf samples.

**2.1.2 Polymer Electrolytes.** To prepare the LPMEI:LiTf solutions of a desired composition, the appropriate amount of LiTf was added to high and low molecular weight LPMEI. The high and low molecular weight LPMEI, LPMEI:LiTf, and LPMEI:NaTf samples were dissolved in anhydrous acetonitrile to prepare a homogeneous solution. All of the LPMEI:LiTf solutions were stirred for approximately 2 hours before they were cast into thin films. The compositions of the solutions are reported as a nitrogen to cation molar ratio ( $N:M^+$ ,  $M^+=\text{cation}$ ). The compositions of the low and high molecular weight LPMEI:LiTf and LPMEI:NaTf samples ranged between 20:1 and 5:1.

## 2.2 Spectroscopy

**2.2.1 Fourier Transform Infrared Spectroscopy.** IR data were recorded using a Bruker IFS66V spectrometer with a KBr beam splitter over a range of 500–4000  $\text{cm}^{-1}$  and a 1  $\text{cm}^{-1}$  resolution. The sample preparation and data collection of all the samples were specific to the physical state and type of sample used.

*Model Compounds.* The DMEDA, TMEDA, PMDETA, DMEDA:NaTf, TMEDA:LiTf, TMEDA:NaTf, PMDETA:LiTf, and PMDETA:NaTf solutions were placed between zinc selenide windows in a sealed sample holder. The spectra of the DMEDA, TMEDA and PMDETA solutions were measured under a dry air purge. All crystalline samples were finely ground and made into KBr pellets. In addition, the crystalline DMEDA:NaTf sample was prepared as a Nujol mull.

*Polymer Electrolytes.* The LPMEI, LPMEI:NaTf, and LPMEI:LiTf solutions were cast into a thin film on zinc selenide windows. The thin films were dried under a nitrogen purge for 24 hours and placed under vacuum for 24 hours. The LPMEI data were collected under vacuum (8 mbar). As part of the spectroscopic studies, the bands in the 735 – 840  $\text{cm}^{-1}$  region were resolved using curve-fitting analysis from commercially available software (Thermo Galactic, Grams/AI 7.00). These spectral bands were fitted using a mixed Gaussian-Lorentzian product function and a straight baseline.

**2.2.2 Raman Spectroscopy.** Raman spectra were recorded only for the model compounds. There is a significant amount of fluorescent emitted in the LPMEI and LPMEI salt system therefore suitable Raman spectra could not be obtained. The Raman data were collected in a  $180^\circ$  scattering geometry at a laser power of 300 mW measured at the laser head.

The TMEDA and DMEDA solution samples were placed in a solution well and covered with a glass cover plate. The TMEDA:LiTf, TMEDA:NaTf, DMEDA:NaTf, and PMDETA:NaTf crystals were sealed into a quartz cuvette in the glovebox. Raman data were recorded with a Jobin-Yvon T64000 system in the triple subtractive mode with a CCD detector using a diode-pumped Nd:YVO<sub>4</sub> laser with a 532 nm excitation line. However, all of the TMEDA data were acquired using the 514.5 nm excitation line of an argon laser.

Samples of the PMDETA solutions were placed in a round aluminum sample holder and covered with a glass cover plate. Raman data of these solutions were recorded on a Bruker Equinox (FRA 106) FT-Raman with a CCD detector and Nd:YAG laser (1064 nm line).

## 2.3 Quantum Chemical Calculations

Gas phase vibrational frequency calculations were performed by Scott E. Boesch on single molecules of TMEDA, TMEDA:LiTf, TMEDA:NaTf, PMDETA, PMDETA:LiTf, PMDETA:LiTf, and PMDETA:NaTf using the B3LYP hybrid Hartree-Fock/density functional method with a 6-31G(d) basis set. The vibrational frequencies of PMDETA and TMEDA were calculated at optimized geometries and assigned based on various conformations of these systems. The calculated frequencies above 1000  $\text{cm}^{-1}$  are scaled by a multiplicative factor of 0.9614, and below 1000  $\text{cm}^{-1}$  are scaled by a multiplicative factor of 1.0013 (129).

## 2.4 X-ray

**2.4.1 X-ray Diffraction.** X-ray data were collected at 173 (2) K on a Bruker P4 diffractometer using MoK $\alpha$  radiation ( $\lambda = 0.71073 \text{ \AA}$ ) by Masood A. Khan. The data were corrected for Lorentz and polarization effects; an absorption correction was not applied since it was judged to be insignificant. The structures were solved by the direct method using the SHELXTL system and refined by full-matrix least squares on  $F^2$  using all reflections. All nonhydrogen atoms were refined anisotropically, and all hydrogen atoms were included with idealized parameters.

In DMEDA:NaTf, single crystals for X-ray analysis were grown and isolated from a 3:1 DMEDA:NaTf solution. The final  $R1 = 0.053$  is based on 5863 “observed reflections” [ $I > 2\sigma(I)$ ], and  $wR^2 = 0.156$  is based on all reflections (6999 unique data). Because the Na(5) and Na(6) atoms are situated at the inversion center, each component has a fifty percent occupancy.

In TMEDA:LiTf and TMEDA:NaTf, single crystals for X-ray analysis were grown and isolated from a 38:1 TMEDA:LiTf solution and a 20:1 TMEDA:NaTf solution. For the TMEDA:LiTf crystal, the final  $R1 = 0.068$  is based on 1541 “observed reflections” [ $I > 2\sigma(I)$ ], and  $wR^2 = 0.201$  is based on all reflections (2406 unique data). For the TMEDA:NaTf crystal, the final  $R1 = 0.056$  is based on 6277 “observed reflections” [ $I > 2\sigma(I)$ ], and  $wR^2 = 0.153$  is based on all reflections (9715 unique data). In the TMEDA:NaTf crystal, some parts of the TMEDA are disordered as evident by the large thermal parameters of these atoms. In addition, the positions of the C17 and C18 atoms are not well defined; therefore, these atoms were resolved in two components with a fifty percent occupancy for each component.

In PMDETA:NaTf, single crystals for X-ray analysis were grown and isolated from a 10:1 PMDETA:NaTf solution. The final  $R1 = 0.0420$  is based on 7629 “observed reflections” [ $I > 2\sigma(I)$ ], and  $wR^2 = 0.107$  is based on all reflections (10798 unique reflections).

**2.4.2 X-ray Powder Diffraction.** The NaTf and 5:1 LPMEI:NaTf (brittle film) were ground into a fine powder-like material and pressed on to a microscope slide. The LPMEI, 20:1, 15:1, and 10:1 LPMEI:NaTf samples were cast as films from acetonitrile onto a microscope slide and then dried under nitrogen (24 hr) and vacuum (24 hr). Powder X-ray diffractograms were recorded using a Scintag XTRA diffractometer with  $\text{CuK}\alpha$  radiation



over the range  $8^{\circ} \leq 2\theta \leq 50^{\circ}$  in  $2\theta$  steps of  $0.100^{\circ}$  with a scan rate of  $2.5^{\circ}/\text{min}$ . All X-ray data were recorded at room temperature.

## 2.5 Differential Scanning Calorimetry

DSC data were collected using a Mettler DSC 820 calorimeter with Star<sup>c</sup> software (v.6.10) under a dry nitrogen purge. All samples were sealed in 40  $\mu\text{L}$  aluminum pans. The data were collected at a heating and cooling rate of  $5^{\circ}\text{C}/\text{min}$ .

**2.5.1 Model Compounds.** For crystalline DMEDA:NaTf, a sample weighing about 2 mg was utilized. Data were collected during two heating and cooling cycles between  $0^{\circ}\text{C}$  and  $280^{\circ}\text{C}$ . For TMEDA:LiTf and TMEDA:NaTf, a single crystal weighing approximately 3.5 mg was used. The TMEDA:LiTf crystal data were collected during two heating and cooling cycles between  $0^{\circ}\text{C}$  and  $250^{\circ}\text{C}$ . However, the TMEDA:NaTf crystals were cycled between  $0^{\circ}\text{C}$  and  $300^{\circ}\text{C}$ . For PMDETA:NaTf, data were acquired utilizing an approximately 1.0 mg sample. Data were collected during two heating and cooling cycles between  $25^{\circ}\text{C}$  and  $300^{\circ}\text{C}$ .

**2.5.2 Polymer Electrolytes.** All LPMEI:LiTf and LPMEI:NaTf samples were cast from acetonitrile solutions onto Teflon, dried in a nitrogen environment for 24 hours, and placed under vacuum for 24 hours. As the salt content was increased, the LPMEI:LiTf and LPMEI:NaTf samples became more rigid. In the 10:1 and 5:1 LPMEI:NaTf samples, solid domains were observed, and in the latter composition, the solid domains were very brittle. After drying, data were collected using 10-15 mg samples. The samples were heated to  $60^{\circ}\text{C}$  for thirty minutes followed by two cooling and heating cycles between  $60^{\circ}\text{C}$  and  $-140^{\circ}\text{C}$ .

Additionally, new LPMEI:NaTf samples were cycled between 25°C and 150°C in order to acquire their melting points.

## 2.6 AC Complex Impedance

Each LPMEI:LiTf sample was cast from a acetonitrile solution directly onto a 12.5 mm stainless steel electrode in a nitrogen atmosphere. The solvent was allowed to evaporate for 24 hours in the glove box and 24 hours under vacuum. A micrometer built into the conductivity cell was used to measure the film thickness. Conductivity measurements were made over the frequency range 0.005 to 10,000 kHz using a Hewlett-Packard 4192A LF impedance analyzer with Labview<sup>TM</sup> 5.1 software (National Instruments). Conductivity data for the LPMEI:NaTf samples were not collected due to experimental difficulties originating in interfacial contact problems between the electrodes and the electrolyte.

The conductivity data for all LPMEI:LiTf compositions were measured using a heating cycle ranging from 25°C to 60°C in 10°C increments. The impedance plots were curve-fitted using commercially available software (Solartron Instruments LTD, LEVM 7.1v).

### ***Chapter 3: MODEL COMPOUNDS***

---

*Studies of model compounds are contained in Papers I, II, and III.*

Model compounds for polymer electrolytes usually consist of small organic molecules complexed with salt, resulting in molecules that are structurally similar and mimic the vibrational signatures of polymer electrolytes. A useful model compound for a particular polymer electrolyte should exhibit host-cation and cation-anion interactions similar to that in the target polymer electrolyte. Sometimes model salt complexes form crystalline compounds whose structures can be determined by X-ray diffraction studies. Knowing the crystal structure allows a precise determination of local structures resulting from host-cation and cation-anion interactions. In many cases, the local environment of the crystalline complexes can be related to that in the solution phase of model and extended to polymer electrolyte systems. I have participated in an investigation of DMEDA with NaTf as a model compound for LPEI. However, my research focuses mainly on TMEDA and PMDETA with LiTf and NaTf as possible model compounds for LPMEI.

#### **3.1 DMEDA Complexed with NaTf (*Paper I*)**

York *et al.* (74,123,125) and Boesch *et al.* (124) have investigated solutions of DMEDA complexed with LiTf as a possible model compound for LPEI. There are two forms of DMEDA as determined from a gas phase computational analysis; one consists of DMEDA with no intramolecular hydrogen bonding and the other has only a single intramolecular hydrogen bond (74, 124). This analysis was based on DMEDA molecules that have the lowest energy structure in the gas phase and the best fit of calculated vibrational intensities and frequencies to the experimental values in the liquid phase (74, 124). When LiTf is added to DMEDA, the intramolecular hydrogen bonding is lost while intermolecular hydrogen bonding is gained. This conclusion is a result of the spectral bands

in the NH stretching region (3000 – 3400 cm<sup>-1</sup>) shifting to higher frequencies when the salt composition increases (74, 124). To further understand the polymer-cation and cation-anion interactions in LPEI, some of my research efforts have emphasized growing crystals of DMEDA with NaTf to gain better understanding of the DMEDA system using X-ray and spectroscopic techniques.

**3.1.1 Crystal Structure.** DMEDA:NaTf crystallizes as a triclinic unit cell in the  $P\bar{1}$  space group. Each unit cell contains two [(DMEDA)<sub>2</sub>:(NaTf)<sub>5</sub>] asymmetric units. These crystals form a polymeric chain-like network. In the DMEDA:NaTf crystal (Figure

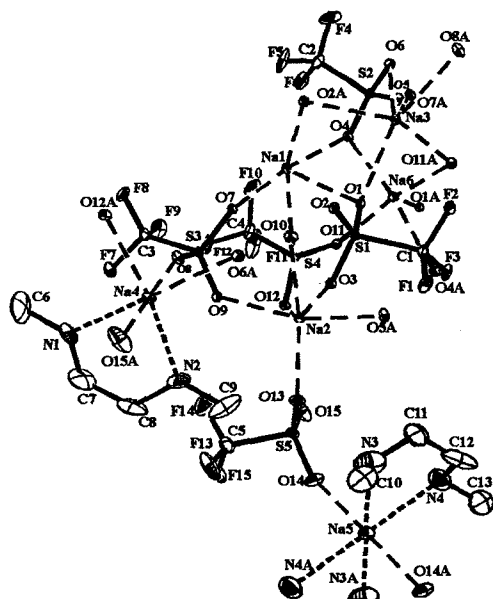


**Figure 3.1:** A complex structure of the DMEDA:NaTf crystal not including the hydrogen atoms. The Na–O bonds are represented as long dashes (---) and the Na–N bonds are represented as short dashes (---).

**Table 3.1:** The bond lengths (Å) of the five symmetrically inequivalent triflate anions (Tf) in the asymmetric unit.

	Bond	Bond length
Tf(1)	O(13)-Na(2)	2.329 (3)
	O(14)-Na(5)	2.427 (3)
Tf(2)	O(3)-Na(2)	2.3297 (18)
	O(1)-Na(3)	2.4050 (18)
	O(1)-Na(1)	2.7499 (19)
Tf(3)	O(7)-Na(1)	2.2587 (19)
	O(9)-Na(2)	2.379 (2)
	O(8)-Na(4)	2.394 (2)
Tf(4)	O(4)-Na(6)	2.316 (3)
	O(4)-Na(1)	2.344 (18)
	O(6)-Na(3)	2.445 (2)
Tf(5)	O(10)-Na(1)	2.307 (2)
	O(11)-Na(6)	2.350 (3)
	O(10)-Na(1)	2.682 (3)
	O(12)-Na(2)	2.785 (2)

3.1), the sodium ions occupy either five- or six-coordinate sites based on a sodium-oxygen (Na–O) and a sodium-nitrogen (Na–N) bond length of 2.80 Å or less. This bond length is typical for glymes complexed to Na<sup>+</sup> of NaTf (23, 79).

All sodium ions coordinated to the DMEDA molecules are six-coordinate. However, one of the these sodium ions is coordinated to two nitrogen atoms and four triflate oxygen atoms while the other sodium ions is coordinated to four nitrogen atoms and only two triflate oxygen atoms. The remaining four sodium ions are coordinated only to the triflate oxygen atoms. Table 3.1 represents the Na–O bond length associated with the five different triflate ions, which will be discussed in greater detail in section 3.1.3. Structural data and selected bond lengths and angles of the DMEDA:NaTf crystal are summarized in Paper I.

The C–N–C–C and N–C–C–N dihedral angles (gauche, *g*,  $60^\circ \pm 30^\circ$ ; gauche minus,  $\bar{g}$ ,  $-60^\circ \pm 30^\circ$ ; skew, *s*,  $120^\circ \pm 30^\circ$ ; skew minus,  $\bar{s}$ ,  $-120^\circ \pm 30^\circ$  trans, *t*,  $\pm 180^\circ \pm 30^\circ$ ) (130) are used to describe the conformational structures of DMEDA oligomers. Because the N–C–C–N dihedral angle is strongly affected by the coordination of the cation to the nitrogen atoms, it receives the most consideration. In the DMEDA:NaTf crystal, DMEDA has two different conformations, *t* $\bar{g}$ *t* and *t**g**s* ( $g = 56.9^\circ$  &  $\bar{g} = -34.5^\circ$ ).

**3.1.2 Thermal Analysis.** The DMEDA:NaTf crystal melts and recrystallizes at 250 °C. This temperature is reproducible upon consecutive heating and melting cycles such that there is no evidence of thermal hysteresis. Therefore this transition appears to be due to congruent melting.

**3.1.3 Vibrational Spectroscopy.** Spectra in the conformation region ( $800 - 1000\text{ cm}^{-1}$ ), ionic association region ( $750 - 765\text{ cm}^{-1}$ ;  $1030 - 1060\text{ cm}^{-1}$ ), and NH stretching region ( $3000 - 3400$ ) will be explored in this section. The conformation and NH stretching regions reflect changes in the host due to host-cation interactions. In the ionic association regions, the  $\delta(\text{CF}_3)$  ( $750 - 765\text{ cm}^{-1}$ ) and  $\nu_s(\text{SO}_3)$  ( $1030 - 1060\text{ cm}^{-1}$ ) bands provide information about the cation-anion interactions.

*Ionic Association Regions.* The  $\delta(\text{CF}_3)$  bands occur between  $755$  and  $763\text{ cm}^{-1}$  in DMEDA:LiTf systems (74, 124). For crystalline DMEDA:NaTf (**Figures 3.2a & b**), the  $\delta(\text{CF}_3)$  bands occur at  $761$ ,  $770$ , and  $772\text{ cm}^{-1}$  in the IR spectra and at  $762$  and  $772\text{ cm}^{-1}$  in the Raman spectra. The existence of three  $\delta_s(\text{CF}_3)$  bands in the IR is due to the different potential energy environments of the triflate ions in an asymmetric unit (see **Table 3.1**). These ions vibrate as either an  $[\text{Na}_2\text{Tf}]^+$  or  $[\text{Na}_3\text{Tf}]^{2+}$  species, assuming to a first approximation that Na-O distances greater than  $2.45\text{ \AA}$  are negligible. Triflate one, Tf(1), is coordinated to two sodium ions and vibrates as an  $[\text{Na}_2\text{Tf}]^+$  species; Tf(2), Tf(3), and Tf(4) are coordinated to three sodium ions and vibrate as  $[\text{Na}_3\text{Tf}]^{2+}$ . However, Tf(2) has one very long Na-O bond length ( $\sim 2.48\text{ \AA}$ ) such that it essentially vibrates as a  $[\text{Na}_2\text{Tf}]^+$  species. In addition, Tf(5) has two short and two very long Na-O bond distances and essentially vibrates as a  $[\text{Na}_2\text{Tf}]^+$  species. The  $[\text{Na}_2\text{Tf}]^+$  vibrations are assigned to the bands at  $761$  (IR) and  $762$  (Raman)  $\text{cm}^{-1}$ , whereas the  $[\text{Na}_3\text{Tf}]^{2+}$  vibrations occur at  $770$  (IR) and  $772$  (Raman)  $\text{cm}^{-1}$ .

In the 15:1 DMEDA:NaTf solution (**Figure 3.2a & b**), the  $\delta(\text{CF}_3)$  bands occur at  $757\text{ cm}^{-1}$  (IR) and  $756\text{ cm}^{-1}$  (Raman), which correspond to contact ion pairs. However, at high compositions of NaTf (3:1), the  $[\text{Na}_2\text{Tf}]^+$  species is also present because of the appearance of the band at  $761\text{ cm}^{-1}$ , a frequency which correlates to one of the triflate

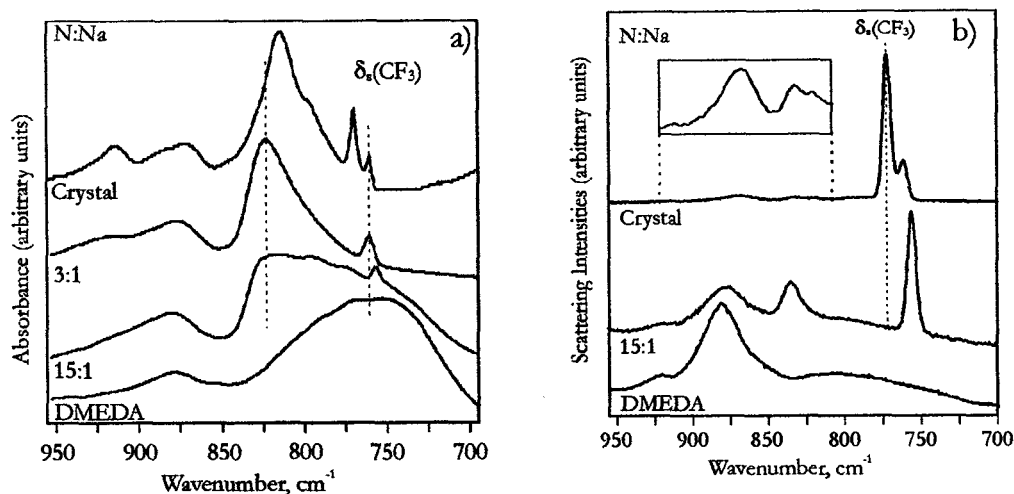


**Figure 3.2:** *a) IR and b) Raman spectra of DMEDA with varying concentrations of NaTf in the  $\delta(\text{CF}_3)$  and conformation regions.*

bands in crystalline DMEDA:NaTf.

The  $\nu_s(\text{SO}_3)$  bands range from 1032 to 1054  $\text{cm}^{-1}$  in DMEDA:LiTf complexes. In crystalline DMEDA:NaTf (Figures 3.3a & b), the  $\nu_s(\text{SO}_3)$  bands occur at 1047, 1042, 1037, and  $\sim 1033 \text{ cm}^{-1}$  in the IR spectrum and at 1057  $\text{cm}^{-1}$  with a weak band at 1045  $\text{cm}^{-1}$  in the Raman spectrum. These bands will be discussed later in this section using a symmetry-based analysis. In the DMEDA:NaTf solutions, the  $\nu_s(\text{SO}_3)$  bands (IR) are centered at 1035  $\text{cm}^{-1}$  in the 15:1 solution and at 1038  $\text{cm}^{-1}$  in the 3:1 solution with two shoulder bands at  $\sim 1035$  and 1042  $\text{cm}^{-1}$  (Figure 3.3b). The latter band probably corresponds to the  $[\text{Na}_2\text{Tf}]^+$  species.

Symmetry-based factor group analysis determines the normal modes that belong to the various irreducible representations of the unit cell group (factor group). An analysis of  $\delta(\text{CF}_3)$  and  $\nu_s(\text{SO}_3)$  results in five Raman active  $A_g$  modes and five IR active  $A_u$  modes (Eqn 3.1).

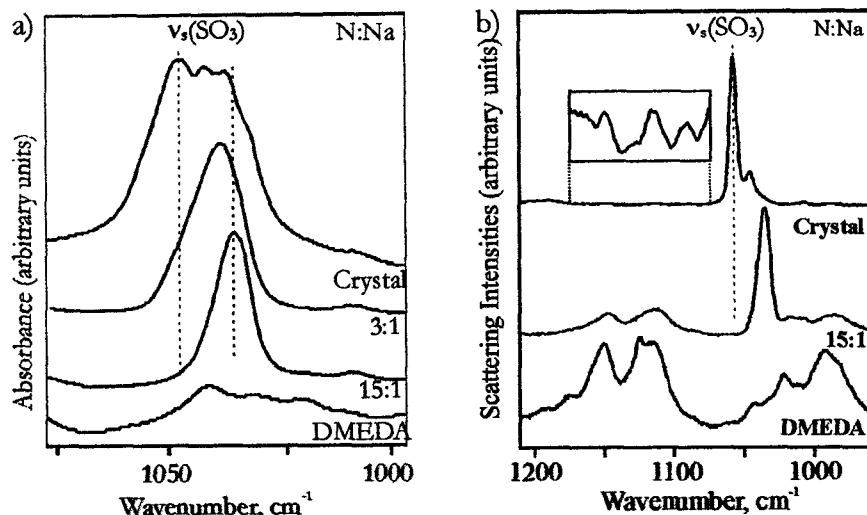


**Figure 3.3:** a) IR and b) Raman spectra of DMEDA with varying concentrations of NaTf in the 1000 to 1075  $\text{cm}^{-1}$  region.

$$\Gamma(\nu_s(\text{SO}_3)) = \Gamma(\delta_s(\text{CF}_3)) = 5A_g + 5A_u \quad \text{Eqn. 3.1}$$

However, only four IR active modes (1033, 1037, 1042, & 1047  $\text{cm}^{-1}$ ) and two Raman active modes (1045 & 1057  $\text{cm}^{-1}$ ) are observed in the  $\nu_s(\text{SO}_3)$  region. Since the DMEDA:NaTf crystal is described by the  $P\bar{1}$  space group, it has a center of symmetry. Therefore, modes should be either Raman active or infrared active, but none should be simultaneously Raman and infrared active except by coincidence. The  $\nu_s(\text{SO}_3)$  vibrations are apparently coupled due to the inversion center because there are no IR bands whose frequencies correspond to Raman bands. However, this is not the case for  $\delta_s(\text{CF}_3)$ , in which there are only three IR-active modes (761, 770, & 772  $\text{cm}^{-1}$ ) and two Raman-active modes (762 & 772  $\text{cm}^{-1}$ ). Because there are two bands that are common to both IR and Raman spectra, the vibrations do not appear to be correlated through the inversion center. This suggests that the molecules are vibrationally decoupled, i.e. the vibrations of the  $\text{CF}_3$  molecules are sufficiently independent such that the role of the inversion center in coupling vibrations is negligible.



*Conformation Region.* The 800 to 1000  $\text{cm}^{-1}$  region reflect changes in backbone conformation (31) due to polymer-cation interactions (25,71,76). There are new bands occurring at 814  $\text{cm}^{-1}$  (IR) and 831  $\text{cm}^{-1}$  (Raman) in the DMEDA:NaTf solutions (Figures 3.2a & b). This band in the IR shifts to 836  $\text{cm}^{-1}$  upon crystallization. In addition, there is a new IR band at 914  $\text{cm}^{-1}$  when NaTf is added to DMEDA. In DMEDA, the broad bands at 880  $\text{cm}^{-1}$  in the IR and Raman spectra shift to 872  $\text{cm}^{-1}$  in the IR spectra and 868  $\text{cm}^{-1}$  in the Raman spectra upon crystallization. In the 15:1 solution spectrum, the new bands centered at 836 and  $\sim 878$   $\text{cm}^{-1}$  are also found in the crystal spectrum. These vibrational patterns reflect the spectroscopic signature of the  $t\bar{g}t$ -sgt conformational sequence seen in the crystal and may be primarily due to the  $\bar{g}g$  sequence of the two N-C-C-N dihedral angles. In addition, when NaTf coordinates to DMEDA even at a 15:1 composition, some of the DMEDA exhibits conformational bands that resembles crystalline DMEDA:NaTf.

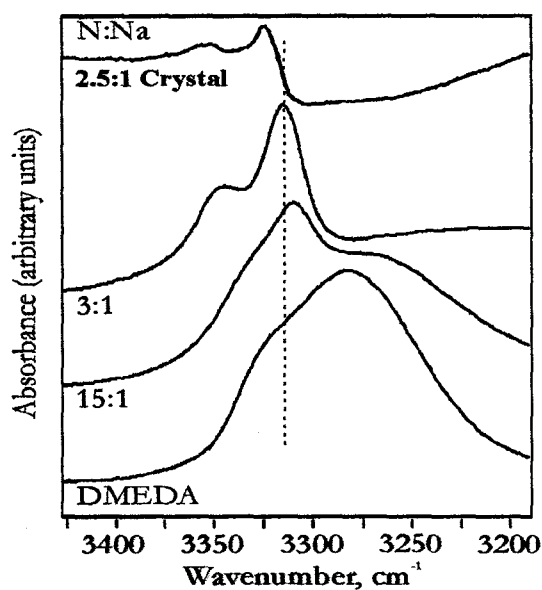


**Figure 3.4:** IR spectra of the NH region of DMEDA with varying concentrations of NaTf. NH Stretching Region.

*NH Stretching Region.* The NH stretching region (3000 to 3400  $\text{cm}^{-1}$ ) can provide information about intramolecular and intermolecular hydrogen bonding. In **Figure 3.4**, the strong broad feature in DMEDA is centered at 3282  $\text{cm}^{-1}$  with a shoulder at 3330  $\text{cm}^{-1}$ . These bands are attributed to intramolecular hydrogen bonding. Upon addition of NaTf, the shoulder shifts to  $\sim 3335 \text{ cm}^{-1}$  and a new band at 3310  $\text{cm}^{-1}$  rises out of a very broad feature. These two bands shift to 3324 and 3352  $\text{cm}^{-1}$ , respectively, upon crystallization. These shifts in the band frequencies are due to formation of intermolecular hydrogen bonding in the crystal and loss of intramolecular hydrogen bonding, based on computational analysis (74, 124). This phenomenon has also been reported in LPEI:NaTf systems (98).

### 3.2 TMEDA Complexed with LiTf and NaTf (*Paper II*)

Investigating TMEDA, TMEDA:LiTf, and TMEDA:NaTf samples as possible model compound for LPMEI is the first step in understanding the fundamentals of methylated poly(ethylenimine) systems. While studying TMEDA as a model compound, crystals were discovered in TMEDA:LiTf and TMEDA:NaTf samples. Crystal structures of TMEDA:LiTf and TMEDA:NaTf provide essential information about the local structures in TMEDA solutions.

**3.2.1 Crystal Structure.** TMEDA:LiTf forms dimers with a (TMEDA:LiTf)<sub>2</sub> asymmetric unit (**Figure 3.5a**), which crystallize in an orthorhombic unit cell in the Pccn space group. There are eight dimers in the unit cell. The lithium atom is four-coordinate such that there are two lithium-nitrogen and two lithium-oxygen bonds. TMEDA:NaTf forms tetramers with a (TMEDA:NaTf)<sub>4</sub> asymmetric unit (**Figure 3.5b**), which crystallize in a triclinic unit cell in the  $P\bar{1}$  space group. Each sodium atom is five-coordinate with two sodium-nitrogen

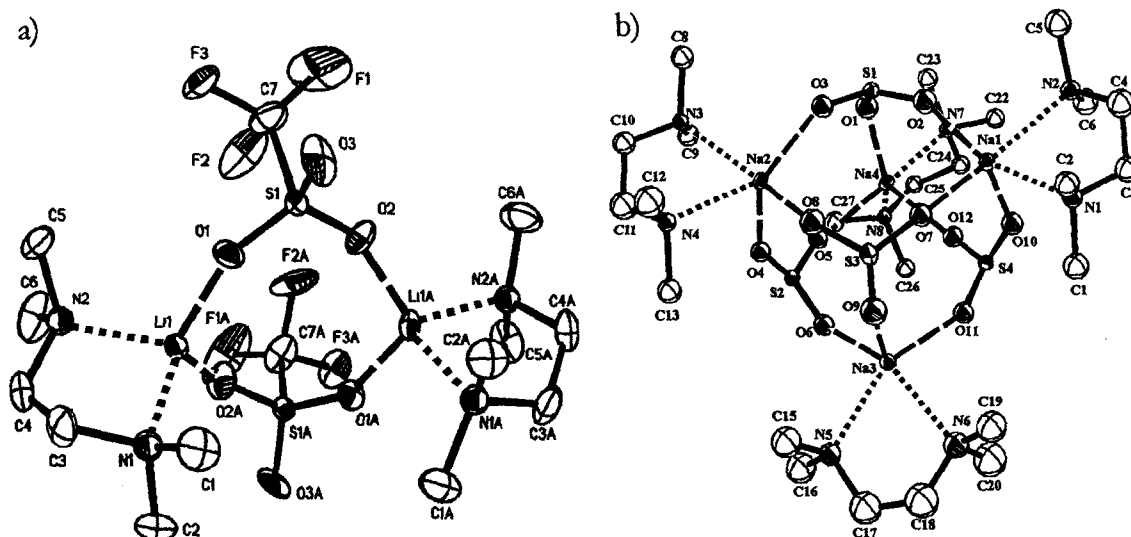


**Figure 3.5:** Structures of **a) TMEDA:LiTf** and **b) TMEDA:NaTf**. The Na-N and Na-O bonds are represented as dotted (---) and dashed (---) lines.

and three sodium-oxygen bonds.

In the TMEDA:LiTf crystal, the conformation of TMEDA is  $x\bar{g}x$  ( $x = t$  or  $\bar{g}$ ) with a  $\bar{g}$  N-C-C-N dihedral angle of  $-54.0^\circ$ . The different C-C-N-C dihedral angles in TMEDA result from the two methyl groups attached to each nitrogen atom. In the TMEDA:NaTf crystal, two TMEDA molecules have a  $x_1\bar{g}x_1$  ( $x_1 = t$  or  $\bar{g}$ ) conformation, one TMEDA molecule has a  $x_2gx_2$  ( $x_2 = t$  or  $g$ ) conformation, and one TMEDA molecule with either  $x_3gx_3$  ( $x_3 = \bar{s}$  or  $s$ ) or  $x_1\bar{g}x_1$  conformations such that the N-C-C-N dihedral angles are  $-53.1$ ,  $-60.3$ ,  $55.4$ , and  $42.3^\circ$ . There are two possibilities for the latter conformation, because there is disorder in the atoms in the C17 and C18 bond.

**3.2.2 Thermal Analysis.** Crystalline TMEDA:LiTf melts at  $154^\circ\text{C}$  and recrystallizes at  $110^\circ\text{C}$ . However, these temperatures decrease to  $128^\circ\text{C}$  and  $107^\circ\text{C}$  during the second thermal cycle, indicating some degree of thermal hysteresis and/or incongruent

melting/recrystallization. In addition, the melting peak (154°C) becomes smaller and broader, indicating a loss of crystallinity of the sample.

Crystalline TMEDA:NaTf has four endothermic phase transitions occurring at 128, 193, 199, and 237°C in the first heating cycle. TMEDA:NaTf recrystallizes at 110 and 238°C. There are only two transitions occurring at 118 and 238°C during the second heating cycle. In addition, the peak at ~118°C becomes broader and smaller, indicating a decrease in the crystallinity of the sample.

**3.2.3 Quantum Chemical Computational Analysis.** Computational analysis is a useful tool for determining vibrational frequencies and modes of small molecules and small molecules complexed with salt, which is an additional advantage of using model compounds. The calculated vibrational frequencies are assigned to experimentally observed bands based on both the agreement of the vibrational frequencies and calculated band intensities. Computational analysis of the vibrational frequencies will be focused on the 750 to 1000 cm<sup>-1</sup> region.

The vibrational modes and frequencies were calculated utilizing TMEDA molecules with a gauche minus (-45.3°) and a trans (-166.8°) N-C-C-N dihedral angle. In addition, the calculations of both TMEDA:LiTf and TMEDA:NaTf complexes resulted in a gauche minus N-C-C-N dihedral angle (-55.6° & -61.8°), respectively. The N-C-C-N dihedral angle for these systems is about 10-15° larger than in TMEDA. The calculated N-C-C-N dihedral angle in TMEDA:LiTf is comparable to the experimental value (-54.0°). However, in TMEDA:NaTf, the calculated N-C-C-N dihedral angle is only comparable to one of the dihedral angles in the crystal structure (-53.1, -60.3, 55.4, & 42.3°).

**Table 3.2: Experimental and calculated bond distances (Å)**  
**for TMEDA:LiTf and TMEDA:NaTf.**

	X = Li		X = Na		
	Calc.	Exp.	Calc.	Exp.	
X – N	2.098	2.066(5)	2.458	2.472(2)	2.5101(18)
	2.096	2.077(5)	2.436	2.489(3)	2.519(2)
				2.495(2)	2.521(2)
				2.502(2)	2.523(3)
X – O	1.990	1.805(6)	2.275	2.261(2)	2.283(2)
	1.967	1.836(6)	2.293	2.269(2)	2.2830(18)
		1.956(7)		2.270(2)	2.303(2)
		1.987(6)		2.2722(19)	2.3160(19)
					2.310(2)

In TMEDA:LiTf and TMEDA:NaTf, the cation is coordinated to two nitrogen atoms in the TMEDA and two oxygen atoms in the triflate ion. The calculated cation–N and cation–O bond distances are reported in **Table 3.2**. There are significant differences in the bond distances between TMEDA:LiTf and TMEDA:NaTf samples. The cation–O and cation–N bond distances are longer in TMEDA:NaTf than in TMEDA:LiTf. This is partly due to the sodium ions having a larger ionic radius compared to the lithium ions and to the sodium atom forming weaker bonds than the lithium atoms.

Selected calculated and experimental IR frequencies are described in **Table 3.3** (TMEDA & TMEDA:LiTf) and **Table 3.4** (TMEDA & TMEDA:NaTf). Some of the calculated vibrational frequencies and the nature of the modes change when one LiTf molecule is added to TMEDA. For instance, the calculated TMEDA band at 795 cm<sup>-1</sup> shifts to 805 cm<sup>-1</sup> upon the addition of one LiTf. Furthermore, the nature of the mode differs slightly when a LiTf is added such that the C–C stretching motion is not the dominant motion of the mode at 805 cm<sup>-1</sup>. In addition, the vibrational mode of the 1091 cm<sup>-1</sup> band in

**Table 3.3: Experimental and calculated IR frequencies ( $\text{cm}^{-1}$ ) of TMEDA and TMEDA:LiTf along with their corresponding mode descriptions.**

TMEDA				TMEDA:LiTf			
Mode Description	(xtx) Cal.	(x $\bar{g}$ x) Cal.	Exp.	20:1 Exp.	2:1 Crystal	2:1 Cal.	Mode Description
				763	763	757	$\nu_s(\text{CF}_3)$
				771	772	777	$\rho(\text{CH}_2)$
$\nu(\text{C-N})$ ; $\omega(\text{CH}_2)$ ; $\tau(\text{CH}_2)$ ; $\nu(\text{C-C})$		795	773	792	791	805	$\nu(\text{C-N})$ ; $\omega(\text{CH}_2)$ ; $\tau(\text{CH}_2)$
$\rho(\text{CH}_2)$		810	801	802			
$\nu(\text{C-N})$	844		830 835	830 835	830 835		
$\nu(\text{C-N})$	893		873	873			
$\rho(\text{CH}_2)$		952	938	938	938	954	$\nu(\text{C-C})$
				949	951	968	$\rho(\text{CH}_2)$
					1019	1001	$\omega(\text{CH}_3)$ ; $\rho(\text{CH}_2)$
xtx – $\omega(\text{CH}_3)$ x $\bar{g}$ x – $\omega(\text{CH}_3)$ ; $\nu(\text{C-N})$	1034	1025	1033	1033	1034	1018	$\omega(\text{CH}_3)$ ; $\rho(\text{CH}_2)$
					1038	1035	$\omega(\text{CH}_3)$ ; $\nu(\text{C-C})$
xtx – $\rho(\text{CH}_2)$ x $\bar{g}$ x – $\omega(\text{CH}_3)$ ; $\nu(\text{C-N})$	1056	1037	1043	1043	1043		
					1054	978	$\nu_s(\text{SO}_3)$
xtx – $\omega(\text{CH}_3)$ x $\bar{g}$ x – $\omega(\text{CH}_3)$ ; $\nu(\text{C-C})$	1091	1091	1097	1097	~1097	1038	$\omega(\text{CH}_3)$
xtx – $\omega(\text{CH}_3)$ x $\bar{g}$ x – $\omega(\text{CH}_3)$ ; $\nu(\text{C-C})$	1093	1096	~1099	1099	1099	1090	$\omega(\text{CH}_3)$

$\nu$  = stretch,  $\omega$  = wag,  $\rho$  = rock, and  $\tau$  = twist

TMEDA changes from a mixture of C–C stretching and  $\text{CH}_3$  wagging motions to a predominately  $\text{CH}_3$  wagging motion.

Quantum chemical computations are performed on one molecule in the gas phase, which is not the case in the experimental data. Therefore, the calculated vibrations do not reflect interactions with other molecules nor a constrained environment as such exists in crystalline domains, which could account for the major differences between experimental and calculated vibrational frequencies.

**Table 3.4: Experimental and calculated IR frequencies ( $\text{cm}^{-1}$ ) of TMEDA and**

**TMEDA:NaTf along with their corresponding mode descriptions.**

TMEDA				TMEDA:NaTf			
Mode Description	(xtx) Cal.	(x $\bar{g}$ x) Cal.	Exp.	20:1 Exp.	2:1 Crystal	2:1 Cal.	Mode Description
				760	760	753	$\delta_s(\text{CF}_3)$
				778	778	781	$\rho(\text{CH}_2)$
xtx $-\tau(\text{CH}_2)$ ; $\nu(\text{C-N})$ ; x $\bar{g}$ x $-\omega(\text{CH}_2)$ ; $\nu(\text{C-C})$		795	773	787	788	799	$\tau(\text{CH}_2)$
$\rho(\text{CH}_2)$		810	801	802			
$\nu(\text{C-N})$	844		830 835	830 835	830 835		
$\nu(\text{C-N})$	893		873	873			
$\rho(\text{CH}_2)$		952	938	938	940	949	$\nu(\text{C-C})$
				947	948	969	$\rho(\text{CH}_2)$ ; $\tau(\text{CH}_2)$
					1027	1033	$\rho(\text{CH}_2)$ ; $\omega(\text{CH}_3)$
xtx $-\omega(\text{CH}_3)$ x $\bar{g}$ x $-\omega(\text{CH}_3)$ ; $\nu(\text{C-N})$	1034	1025	1033	1033			
xtx $-\rho(\text{CH}_2)$ x $\bar{g}$ x $-\omega(\text{CH}_3)$ ; $\nu(\text{C-N})$	1056	1037	1043	1043	$\sim 1043$	1048	$\nu(\text{C-C})$
					1048	978	$\nu_s(\text{SO}_3)$
xtx $-\omega(\text{CH}_3)$ x $\bar{g}$ x $-\omega(\text{CH}_3)$ ; $\nu(\text{C-C})$	1091	1091	1097	1097	1099	1089	$\omega(\text{CH}_3)$
xtx $-\omega(\text{CH}_3)$ x $\bar{g}$ x $-\omega(\text{CH}_3)$ ; $\nu(\text{C-C})$	1096	1091	$\sim 1099$	$\sim 1100$	1101	1092	$\omega(\text{CH}_3)$

$\nu$  = stretch,  $\omega$  = wag,  $\rho$  = rock, and  $\tau$  = twist

In the conformation region ( $800\text{-}1000\text{ cm}^{-1}$ ), the vibrational frequencies between  $800$  and  $900\text{ cm}^{-1}$  are attributed to the TMEDA molecules with a trans N–C–C–N dihedral angle; all other frequencies are due to a gauche minus dihedral angle. However, the vibrational frequencies above  $1000\text{ cm}^{-1}$  are due to TMEDA molecules with a combination of both trans and gauche minus N–C–C–N dihedral angles. In TMEDA:LiTf and TMEDA:NaTf, the vibrational frequencies are due primarily to TMEDA molecules with a gauche minus N–C–C–N dihedral angle, based on the crystal structures of these systems.

When one molecule of NaTf is added to TMEDA, the changes in the vibrational frequencies and the nature of the modes are similar to those when LiTf is added. For

instance, the frequency of the band calculated at  $952\text{ cm}^{-1}$  shifts to  $949\text{ cm}^{-1}$  when NaTf is added. In addition, the nature of this mode changes from the mixed C–C stretching, and  $\text{CH}_2$  rocking motions to the predominant C–C stretching motion.

**3.2.4 Band Assignments.** Crystalline complexes have unambiguous local structures and distinct vibrations. These features can be utilized to understand the local environment of TMEDA:LiTf and TMEDA:NaTf in salt solutions. The vibrational analysis of TMEDA, TMEDA:LiTf, and TMEDA:NaTf will be focused on bands in the conformational and ionic association regions.

**Conformation Region.** In ethylene oxide-based systems, the frequencies and intensities of bands in the  $800\text{--}1000\text{ cm}^{-1}$  region are known to change when the backbone conformation changes (31). Similar changes in the backbone conformation occur in TMEDA systems. When LiTf is added to TMEDA, the broad distribution of TMEDA bands between  $765$  and  $800\text{ cm}^{-1}$  forms into two distinct bands at  $772$  and  $791\text{ cm}^{-1}$  (Figure 3.6a). The  $772\text{ cm}^{-1}$

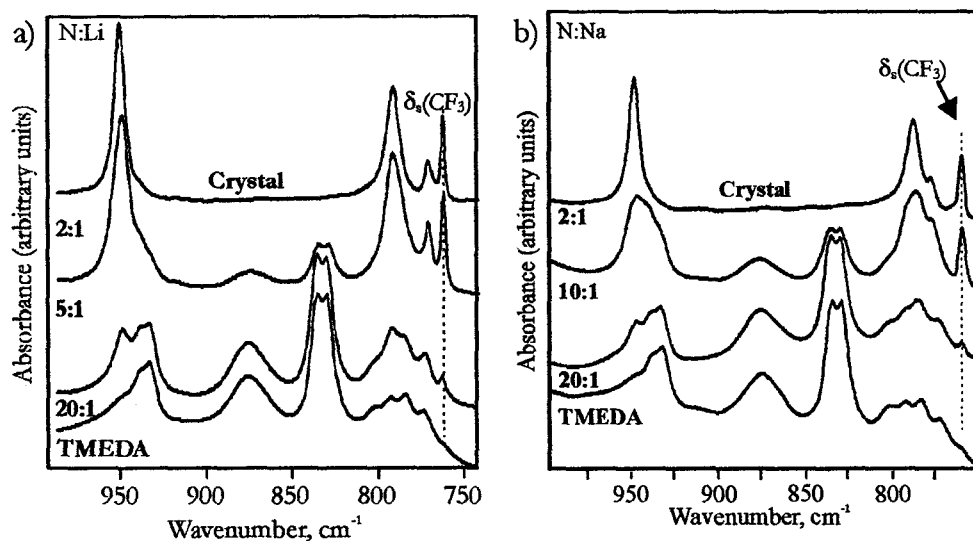


**Figure 3.6:** IR spectra of TMEDA with varying concentrations of **a) LiTf** and **b) NaTf** in the  $750$  to  $1000\text{ cm}^{-1}$  region.



band is attributed to the predominant CH<sub>2</sub> rocking motion, whereas the 791 cm<sup>-1</sup> band is assigned to mixed C–N stretching, CH<sub>2</sub> wagging, and CH<sub>2</sub> twisting motions. In the 800 to 900 cm<sup>-1</sup> region, the bands at 830, 835, and 876 cm<sup>-1</sup> are suppressed upon crystallization. These bands are due primarily to C–N stretching motion. In the 900 to 1000 cm<sup>-1</sup> region, the TMEDA band at 938 cm<sup>-1</sup> is attributed to a predominately CH<sub>2</sub> rocking motion. This band decreases in intensity as the ~949 cm<sup>-1</sup> band increases in intensity, reflecting changes in the conformation. The sharp band at 949 cm<sup>-1</sup> is predominantly CH<sub>2</sub> rocking motion. Similar changes mentioned above also occur in the Raman spectra.

In TMEDA:NaTf systems (**Figure 3.6b**), similar changes in vibrational frequencies and intensities occur upon crystallization. For instance, in the 765-800 cm<sup>-1</sup> region, two distinct bands at 778 and 788 cm<sup>-1</sup> emerge from the broad TMEDA bands, although these bands are as well separated as in the TMEDA:LiTf system. In TMEDA:NaTf, the 778 cm<sup>-1</sup> band is due to predominantly to CH<sub>2</sub> rocking motion, whereas the 788 cm<sup>-1</sup> band is assigned to predominantly CH<sub>2</sub> twisting motion. In the 800 to 900 cm<sup>-1</sup> region, there are no significant differences in the TMEDA bands when NaTf or LiTf is added. In the 900 to 1000 cm<sup>-1</sup> region, the major difference is that the new band at 940 cm<sup>-1</sup> does not shift to as high a frequency as in the TMEDA:LiTf spectra. In addition, the nature of the mode is attributed to the mixed CH<sub>2</sub> rocking and twisting motions, unlike in TMEDA:NaTf

*Ionic Association Region.* In crystalline TMEDA:LiTf and TMEDA:NaTf, the  $\delta(\text{CF}_3)$  bands occur at 763 and 760 cm<sup>-1</sup>, which are typically associated with an aggregate species. Because their local structures are known from the crystal structures, the aggregate species in crystalline TMEDA:LiTf and TMEDA:NaTf are attributed to an  $[\text{M}_2\text{Tf}]^+$  species ( $\text{M} = \text{Li}^+, \text{Na}^+$ ). In the TMEDA:LiTf and TMEDA:NaTf solutions, the  $[\text{M}_2\text{Tf}]^+$  species is present even at a 20:1 composition of salt. The  $\nu_s(\text{SO}_3)$  band in the infrared spectra appears at 1054

cm<sup>-1</sup> (TMEDA:LiTf crystal) and 1048 cm<sup>-1</sup> (TMEDA:NaTf crystal), which are also associated with an aggregate species.

### 3.3 PMDETA Complexed with LiTf and NaTf (*Paper III*)

PMDETA, CH<sub>3</sub>N(CH<sub>2</sub>CH<sub>2</sub>N(CH<sub>3</sub>)<sub>2</sub>)<sub>2</sub>, can be considered the smallest unit that is structurally similar to LPMEI. While studying PMDETA complexed with LiTf and NaTf as a possible model compound for LPMEI, crystalline compounds were discovered for PMDETA:LiTf and PMDETA:NaTf. PMDETA complexed with LiTf and NaTf is potentially an excellent model compound for LPMEI:LiTf and LPMEI:NaTf. Therefore attention was focused on this system.

**3.3.1 Crystal Structure.** Single crystals could not be isolated from crystalline PMDETA:LiTf, therefore its structure could not be determined using X-ray diffraction analysis. PMDETA:NaTf crystallizes in a triclinic unit cell with a P2<sub>1</sub>/c space group. The asymmetric unit of crystalline PMDETA:NaTf consist of one-half (PMDETA:NaTf)<sub>2</sub> molecules in which there is two different dimers that form. One of the dimers has center of symmetry [dimer (1)] whereas the other does not (**Figure 3.7**). In the unit cell, there are four dimer (1) structures and two dimer (2) structures. Both dimers have a five-coordinate sodium ion as illustrated in **Figure 3.7**. See Paper II for selected bond length and angles. The conformation of crystalline PMDETA is expressed as x<sub>1</sub>gx<sub>1</sub>-x<sub>2</sub> $\bar{g}$  x<sub>2</sub> (x<sub>1</sub> = t or g; x<sub>2</sub> = t or  $\bar{g}$ ) for both dimers. Dimer (1) has only one set of N-C-C-N dihedral angles (-62.3, 61.2°) because the atoms are related through the inversion center. However, in dimer (2), there are two sets of N-C-C-N dihedral angles (60.8 & -62.0 °; 61.4 & -58.9°), because the two TMEDA molecules are not related through the inversion center. There is no significant difference in the N-C-C-N dihedral angles between dimer (1) and dimer (2).

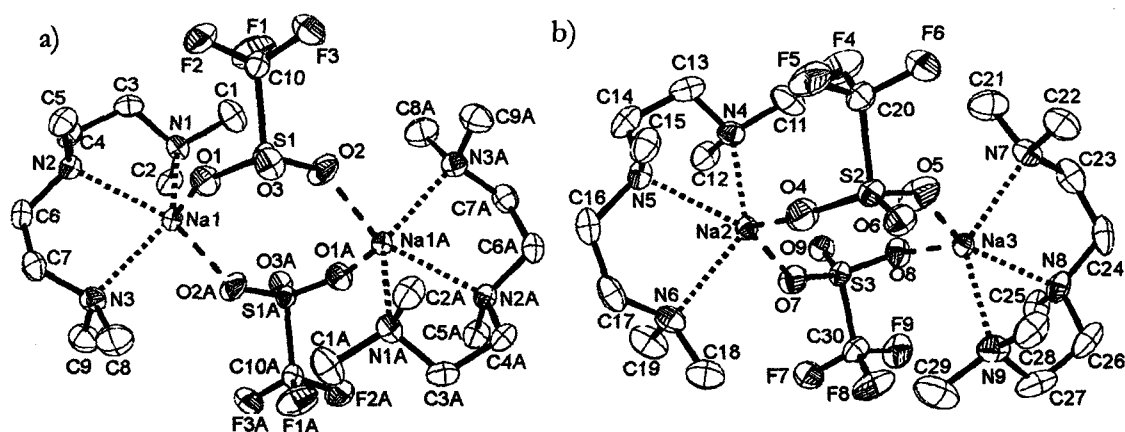


**Figure 3.7:** PMDETA:NaTf crystallizes into **a)** dimer (1) and **b)** dimer (2). The Na–O and Na–N bonds are represented as dots (\*\*\*) and dashes (---).

**3.3.2 Thermal Analysis.** PMDETA:NaTf melts at 237°C and recrystallizes at 238°C with no evidence of thermal hysteresis. There is another phase transition at 104°C that only occurs in the first heating cycle. During the second heating cycle, the 237°C peak becomes broader and smaller, indicating a decrease in the crystallinity of the sample.

**3.3.3 Quantum Chemical Computational Analysis.** Geometries were optimized for PMDETA with three different conformations;  $x_1gx_1-x_2\bar{g}x_2$  ( $g = 72.0^\circ$ ;  $\bar{g} = -48.2^\circ$ ),  $x_2\bar{g}x_2-x_1\bar{g}x_2$  ( $\bar{g} = -46.5$  &  $76.7^\circ$ ),  $x_2tx_1-x_2\bar{g}x_2$  ( $t = -175.8^\circ$ ;  $\bar{g} = -45.6^\circ$ ), and  $x_2tx_1-x_2tx_2$  ( $t = -173.6$  &  $-168.7^\circ$ ) where  $x_1$  is t or g, and  $x_2$  is t or  $\bar{g}$ . The PMDETA structure with a  $x_1gx_1-x_2\bar{g}x_2$  conformation has the lowest energy; PMDETA with a  $x_2tx_1-x_2tx_2$  conformation has the highest energy. For PMDETA:LiTf and PMDETA:NaTf, these geometries were optimized for PMDETA with a  $x_1gx_1-x_2\bar{g}x_2$  conformation based on the crystal structure of PMDETA:NaTf. The vibrational frequencies and modes were determined from the opti-

**Table 3.5: Calculated scaled IR frequencies ( $\text{cm}^{-1}$ ) of PMDETA and PMDETA:LiTf along with their corresponding mode descriptions.**

PMDETA					PMDETA LiTf	PMDETA NaTf	PMDETA LiTf & NaTf
Modes Description	t-t	t- $\bar{g}$	$\bar{g}-\bar{g}$	$\bar{g}-\bar{g}$	2:1	2:1	Mode Description
					757	758	$\delta(\text{CF}_3)$
					775		$\rho(\text{CH}_2)$ ; $\nu(\text{C-N})$
						775	$\rho(\text{CH}_2)$
$\bar{g}-\bar{g}$ : $\rho(\text{CH}_2)$ $\bar{g}-\bar{g}$ : $\rho(\text{CH}_2)$ ; $\nu(\text{C-N})$			788	784	785		$\rho(\text{CH}_2)$ ; $\nu(\text{C-N})$
$\bar{g}-\bar{g}$ : $\rho(\text{CH}_2)$ $\bar{g}-\bar{g}$ : $\rho(\text{CH}_2)$ ; $\nu(\text{C-N})$			797	799	797	786	LiTf: $\rho(\text{CH}_2)$ ; $\nu(\text{C-N})$ NaTf: $\rho(\text{CH}_2)$
t- $\bar{g}$ : $\rho(\text{CH}_2)$ ; $\nu(\text{C-N})$ $\bar{g}-\bar{g}$ : $\rho(\text{CH}_2)$		800	807				
$\rho(\text{CH}_2)$	816	806					
t-t $\nu(\text{C-N})$ t- $\bar{g}$ : $\rho(\text{CH}_2)$ ; $\nu(\text{C-N})$	850	822					
$\nu(\text{C-N})$	874						
$\nu(\text{C-N})$	908	879					
						914	$\nu(\text{C-C})$
					923		$\rho(\text{CH}_2)$ ; $\nu(\text{C-C})$
t- $\bar{g}$ ; $\bar{g}-\bar{g}$ : $\rho(\text{CH}_2)$ $\bar{g}-\bar{g}$ : $\rho(\text{CH}_2)$ ; $\nu(\text{C-N})$		955	960	973	954	953	$\rho(\text{CH}_2)$ ; $\nu(\text{C-N})$
t- $\bar{g}$ : $\nu(\text{C-N})$ $\bar{g}-\bar{g}$ : $\rho(\text{CH}_2)$		975	972		957		$\rho(\text{CH}_2)$ ; $\nu(\text{C-N})$
					999	993	$\rho(\text{CH}_2)$

mized geometries described above for PMDETA, PMDETA:LiTf, and PMDETA:NaTf.

Selected calculated vibrational frequencies of PMDETA, PMDETA:LiTf, and PMDETA:NaTf in the 760 to 1000  $\text{cm}^{-1}$  region are listed in Table 3.5. The vibrational frequencies calculated for PMDETA in the 800–910  $\text{cm}^{-1}$  region result from PMDETA with  $x_2\text{tx}_1-x_2\bar{g}x_2$  and  $x_2\text{tx}_1-x_2\text{tx}_2$  conformations. In the 910–1000  $\text{cm}^{-1}$  regions, the vibrational frequencies were determined from PMDETA with a  $x_1\bar{g}x_1-x_2\bar{g}x_2$ ,  $x_2\bar{g}x_2-x_1\bar{g}x_2$ , and  $x_2\text{tx}_1-x_2\bar{g}x_2$ . However, in the 760–800  $\text{cm}^{-1}$  region, the PMDETA bands are assigned based on

quantum chemical calculations of PMDETA with  $x_1gx_1-x_2\bar{g}x_2$  and  $x_2\bar{g}x_2-x_1\bar{g}x_2$  conformations. Because PMDETA ( $x_2tx_1-x_2\bar{g}x_2$ ) contains both a trans and gauche minus N–C–C–N dihedral angle, bands calculated for this system occur in both the 800–900  $\text{cm}^{-1}$  (trans) and 900–1000  $\text{cm}^{-1}$  (gauche & gauche minus) regions, which are specific to a particular conformation.

A majority of the PMDETA ( $x_1gx_1-x_2\bar{g}x_2$ ) bands in the 760–1000  $\text{cm}^{-1}$  region are due to predominantly  $\text{CH}_2$  rocking motion, whereas these bands in PMDETA with  $x_2tx_1-x_2\bar{g}x_2$  and  $x_2\bar{g}x_2-x_1\bar{g}x_2$  conformations are mostly attributed to mixed  $\text{CH}_2$  rocking and C–N stretching motions. In addition, the PMDETA bands that are associated with t-t N–C–C–N dihedral angles are due to a dominant C–N stretching motion.

When LiTf is added (Table 3.5), some of the calculated frequencies and the nature of the modes change. For instance, the calculated PMDETA ( $x_2\bar{g}x_2-x_1\bar{g}x_2$ ) band at 797  $\text{cm}^{-1}$  occurs at the same frequency in PMDETA:LiTf, but the nature of the mode changes from predominantly  $\text{CH}_2$  rocking motion to a mixture of  $\text{CH}_2$  rocking and C–N stretching motions. However, in PMDETA with a  $x_1gx_1-x_2\bar{g}x_2$  conformation, this band calculated at 799  $\text{cm}^{-1}$  shifts to 797  $\text{cm}^{-1}$  when LiTf is added, but the nature of the mode does not change. In some cases, both the frequencies and the nature of the modes change when LiTf is added. Some calculated bands in PMDETA are not assigned in PMDETA:LiTf or visa versa. For example, the  $\text{CH}_2$  rocking band at 807  $\text{cm}^{-1}$  in  $x_2\bar{g}x_2-x_1\bar{g}x_2$  PMDETA does not correlate to any of the calculated PMDETA:LiTf bands. Similar changes occur in the vibrational frequencies and the nature of the modes as when NaTf is added.

**3.3.4 Experimental Results.** Information about the local environment in PMDETA, PMDETA:LiTf, and PMDETA:NaTf solutions can be acquired by comparing these systems

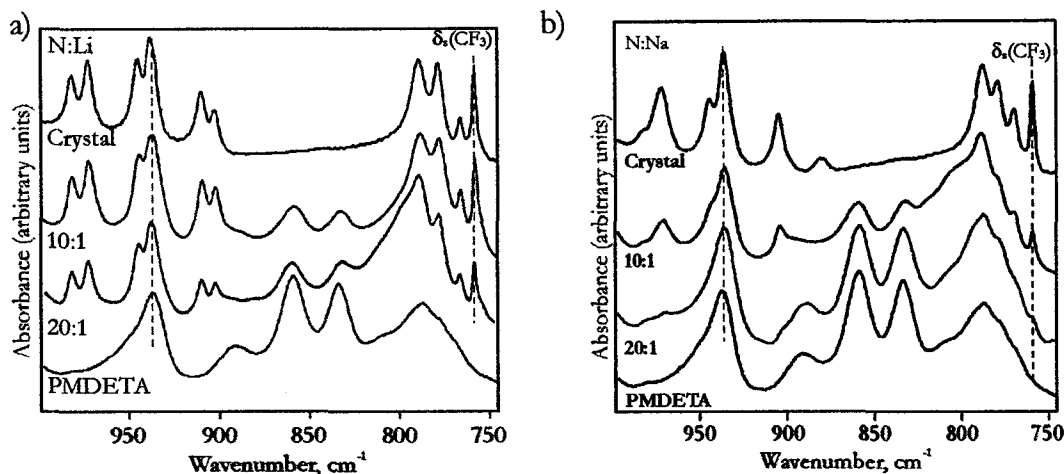


**Figure 3.8:** IR of PMDETA with varying concentrations of a) LiTf and b) NaTf in the 750 to 1000  $\text{cm}^{-1}$  region.

to crystalline PMDETA:LiTf and PMDETA:NaTf. This comparison is even more useful for the PMDETA:NaTf system in which its local structure of crystalline PMDETA:NaTf is unambiguous. Spectroscopic analysis will be confined to the 750 to 1000  $\text{cm}^{-1}$  regions, because it is the most sensitive to changes in the backbone due to host-cation and cation-anion interactions.

*Ionic Association Region.* In both PMDETA:LiTf and PMDETA:NaTf, the aggregate I species is dominant at all compositions of LiTf and NaTf based on the  $\delta(\text{CF}_3)$  bands (750 – 765  $\text{cm}^{-1}$ ). The aggregate I species in PMDETA:NaTf (759  $\text{cm}^{-1}$ ) vibrates as a  $[\text{Na}_2\text{Tf}]^+$  species based on its structural data from X-ray analysis. In PMDETA:LiTf, the aggregate I species (758  $\text{cm}^{-1}$ ) could not be determined because single crystals could not be isolated for X-ray analysis. However, based on similar vibrational frequencies of this band in PMDETA:LiTf and in PMDETA:NaTf, this aggregate I species in PMDETA:LiTf is assigned to an  $[\text{Li}_2\text{Tf}]^+$  species which is representative of a dimer structure.

In the PMDETA:NaTf system, there is only a small amount of contact ion pairs present at low NaTf compositions. The relative amount of these pairs decreases with increasing NaTf concentration and completely disappears upon crystallization. In the PMDETA:LiTf system at low LiTf compositions, there are relatively small amounts of “free” ions and aggregate II species and a moderate amount of contact ion pairs. At high LiTf compositions, the relative amount of “free” ions and aggregate II species is even smaller while the relative amount of  $[\text{Li}_2\text{Tf}]^+$  species increases. However, the relative amount of contact ion pairs does not change upon crystallization, within experimental error, but it still is the dominant species. These trends in the speciation of PMDETA:LiTf suggest that the relative amount of dimers increase with LiTf concentration. It is possible that the relative amount of dimers will increase as the relative amount of subunits decreases over time, which may result in single crystal formation.

*Conformation Region.* In the 760 –1000  $\text{cm}^{-1}$  region (**Figures 3.8a & b**), there are several major changes that occur when LiTf or NaTf is added to PMDETA, such as the narrowing of bandwidths, the formation of new bands, and decreasing band intensities. For example, in the 760 –800  $\text{cm}^{-1}$  region, the PMDETA bandwidths are broad, but these bands become more separated and have narrow bandwidths upon crystallization. In crystalline PMDETA:NaTf, these bands occur at 770, 779, and 789  $\text{cm}^{-1}$ . However, in crystalline PMDETA:LiTf, these bands occur at 766, 779, and 789  $\text{cm}^{-1}$ . These bands in PMDETA:LiTf and PMDETA:NaTf are also present in the corresponding solution spectra.

In the 800 to 900  $\text{cm}^{-1}$  region, the intensities of the PMDETA bands decreases upon crystallization, as illustrated in **Figures 3.8a and b**. This suggests conformational changes in PMDETA when LiTf or NaTf is added.

**Table 3.6: Experimental and calculated scaled IR frequencies ( $\text{cm}^{-1}$ ) of PMDETA and PMDETA:LiTf along with their corresponding mode descriptions.**

PMDETA						PMDETA:LiTf				
Mode Description	t - t Cal.	t - g Cal.	g - g Cal.	g - g Cal.	Exp.	20:1 Exp.	10:1 Exp.	crystal Exp.	2:1 Cal.	Mode Description
						758	758	758	757	$\delta(\text{CF}_3)$
						766	766	766	775	$\rho(\text{CH}_2)$ ; $\nu(\text{C-N})$
$\bar{g} - \bar{g}$ : $\rho(\text{CH}_2)$ $\bar{g} - \bar{g}$ : $\rho(\text{CH}_2)$ ; $\nu(\text{C-N})$			788	784	779	778	779	779	785	$\rho(\text{CH}_2)$ ; $\nu(\text{C-N})$
$\bar{g} - \bar{g}$ : $\rho(\text{CH}_2)$ $\bar{g} - \bar{g}$ : $\rho(\text{CH}_2)$ ; $\nu(\text{C-N})$			797	799	787	788	789	790	797	$\rho(\text{CH}_2)$ ; $\nu(\text{C-N})$
t - $\bar{g}$ : $\rho(\text{CH}_2)$ ; $\nu(\text{C-N})$ $\bar{g} - \bar{g}$ : $\rho(\text{CH}_2)$		800	807		791	791	~791			
$\rho(\text{CH}_2)$	816	806			~807	~807	~807			
t - t: $\nu(\text{C-N})$ t - $\bar{g}$ : $\rho(\text{CH}_2)$ ; $\nu(\text{C-N})$	850	822			834	833	833			
$\nu(\text{C-N})$	874				859	859	859			
$\nu(\text{C-N})$	908	879			~891	~891	~891			
						910	910	910	923	$\rho(\text{CH}_2)$ ; $\nu(\text{C-C})$
t - $\bar{g}$ ; $\bar{g} - \bar{g}$ : $\rho(\text{CH}_2)$ $\bar{g} - \bar{g}$ : $\rho(\text{CH}_2)$ ; $\nu(\text{C-N})$		955	960	973	937	937	937	938	954	$\rho(\text{CH}_2)$ ; $\nu(\text{C-N})$
t - $\bar{g}$ : $\nu(\text{C-N})$ $\bar{g} - \bar{g}$ : $\rho(\text{CH}_2)$		975	972		944	945	945	945	957	$\rho(\text{CH}_2)$ ; $\nu(\text{C-N})$
						972	972	973	999	$\rho(\text{CH}_2)$

$\nu$  = stretch,  $\omega$  = wag,  $\rho$  = rock, and  $\tau$  = twist

In the 900 to 1000  $\text{cm}^{-1}$  region (Figures 3.8a & b), a band at 945  $\text{cm}^{-1}$  (PMDETA:LiTf) and 943  $\text{cm}^{-1}$  (PMDETA:NaTf) arises upon crystallization from the broad PMDETA feature at ~944  $\text{cm}^{-1}$ . In the PMDETA:LiTf spectra, there are four new bands at 903, 910, 973, and 982  $\text{cm}^{-1}$ . In the PMDETA:NaTf, there are only two new distinct bands at 904 and 971  $\text{cm}^{-1}$  and a new shoulder at 982  $\text{cm}^{-1}$ .



**Table 3.7: Experimental and calculated IR frequencies ( $\text{cm}^{-1}$ ) of PMDETA and PMDETA:NaTf along with their corresponding mode descriptions.**

PMDETA						PMDETA:NaTf				
Mode Description	t-t Cal.	t-g Cal.	g-g Cal.	g-g Cal.	Exp.	20:1 Exp.	10:1 Exp.	2:1 Exp.	2:1 Cal.	Mode Description
							759	759	758	$\delta(\text{CF}_3)$
					770	770	770	770	775	$\rho(\text{CH}_2)$
$\bar{g}-\bar{g} : \rho(\text{CH}_2)$			788	784	779	779	779	779		$\rho(\text{CH}_2)$
$g-\bar{g} : \rho(\text{CH}_2); \nu(\text{C-N})$										
$\bar{g}-\bar{g} : \rho(\text{CH}_2)$			797	799	787	787	789	788	786	$\rho(\text{CH}_2)$
$g-\bar{g} : \rho(\text{CH}_2); \nu(\text{C-N})$										
$t-\bar{g} : \rho(\text{CH}_2); \nu(\text{C-N})$		800	807		791	791	~791		799	$\nu(\text{C-C}); \nu(\text{C-N}); \rho(\text{CH}_2); \tau(\text{CH}_2)$
$\bar{g}-\bar{g} : \rho(\text{CH}_2)$										
$\rho(\text{CH}_2)$	816	806			~807	~807	~807			
$t-t : \nu(\text{C-N})$	850	822			834	833	833			
$t-\bar{g} : \rho(\text{CH}_2); \nu(\text{C-N})$										
$\nu(\text{C-N})$	874				859	859	859			
$\nu(\text{C-N})$	908	879			~891	~891	~891			
					~903	903	904	904	914	$\nu(\text{C-C})$
$t-\bar{g}; \bar{g}-\bar{g} : \rho(\text{CH}_2)$		955	960	973	937	935	936	936	953	$\rho(\text{CH}_2); \nu(\text{C-N})$
$g-\bar{g} : \rho(\text{CH}_2); \nu(\text{C-N})$										
$t-\bar{g} : \nu(\text{C-N})$		975	972		944	943	943	944		$\rho(\text{CH}_2)$
$\bar{g}-\bar{g} : \rho(\text{CH}_2)$										
						970	971	972	993	$\rho(\text{CH}_2)$

$\nu = \text{stretch}$ ,  $\omega = \text{wag}$ ,  $\rho = \text{rock}$ , and  $\tau = \text{twist}$

**3.3.5 Band Assignments.** There are no significant differences between the calculated and experimental dihedral angles in PMDETA:NaTf. The experimental observed bands assigned to vibrational modes in PMDETA, PMDETA:LiTf, and PMDETA:NaTf are based on similarities in its IR intensities and frequencies with the computational results. These mode assignments were determined. The mode assignments of PMDETA, PMDETA:LiTf and PMDETA:NaTf are illustrated in Tables 3.6 and 3.7. The PMDETA bands in the 800 to 900  $\text{cm}^{-1}$  region are assigned by calculated vibrational frequencies from PMDETA with t-t

and t -  $\bar{g}$  N-C-C-N dihedral angles; the remaining bands are assigned from PMDETA with a g- $\bar{g}$ ,  $\bar{g}$ - $\bar{g}$ , and t -  $\bar{g}$  N-C-C-N dihedral angles.

In the 800-900  $\text{cm}^{-1}$  region, the spectral bands decrease in intensity upon crystallization, which is attributed to the PMDETA conformation changing from  $x_2tx_1 - x_2\bar{g}x_2$  and  $x_2tx_1-x_2tx_2$  to  $xgx-x\bar{g}x$ . based on quantum chemical calculations. In the 760-800 and 900-1000  $\text{cm}^{-1}$  regions, a clear spectral indication of conformational changes is evident in the narrowing bandwidths and formation of new bands in the PMDETA solutions when LiTf or NaTf is added. Based on computational analysis, the conformation changes from a mixture of  $x_1gx_1-x_2\bar{g}x_2$ ,  $x_2\bar{g}x_2-x_1\bar{g}x_2$ , and  $x_2tx_1-x_2\bar{g}x_2$  to mainly  $x_1gx_1-x_2\bar{g}x_2$  in the 900-1000  $\text{cm}^{-1}$  region upon addition of NaTf.

Utilizing quantum chemical calculations, vibrational modes assignments can be made for PMDETA, PMDETA:LiTf, and PMDETA:NaTf. In addition, the vibrational modes in the 800 to 1000  $\text{cm}^{-1}$  region are correlated to specific N-C-C-N dihedral angles of PMDETA.

*Studies of model compounds are contained in Papers IV and V.*

#### **4.1 LPMEI Complexed with LiTf and NaTf (Paper IV)**

There are limited research results reported for LPMEI systems, therefore a thorough investigation of LPMEI systems is necessary. LPMEI complexed with LiTf or NaTf has been investigated using infrared (IR) spectroscopy, differential scanning calorimetry (DSC), and complex impedance spectroscopy. While studying LPMEI:NaTf systems at moderate to high NaTf compositions (10:1 & 5:1), a crystalline compound was formed and characterized utilizing IR, DSC, and powder X-ray diffraction methods.

**4.1.1 Spectroscopic Analysis..** There are only a few reported spectra of LPMEI systems (115), but the spectra were never discussed in great detail. This section will focus on spectroscopic analysis of the conformation and ionic association regions because these regions are the most affected by cation-polymer and cation-anion interactions.

*Conformation Region.* In the 800 to 1000  $\text{cm}^{-1}$  region (**Figure 4.1**), there are several changes that occur when either LiTf or NaTf is added to LPMEI, such as decreasing band intensities and the formation of new bands. When LiTf is added to LPMEI, a band at  $\sim 799 \text{ cm}^{-1}$  in the 20:1 spectrum (data not shown) emerges from the broad distribution of bands between 760 to 830  $\text{cm}^{-1}$ . This band shifts to  $\sim 802 \text{ cm}^{-1}$  in the 10:1 spectra. At a 15:1 composition, the intensity of the  $\sim 785 \text{ cm}^{-1}$  band begins to increase in intensity; at high LiTf compositions (5:1), there are three bands at 772, 777, and 786  $\text{cm}^{-1}$ . Similar results are seen in LPMEI when NaTf is added, except the new bands in the 760 to 830  $\text{cm}^{-1}$  region are more distinct. These new bands occur at 771, 786, and 790  $\text{cm}^{-1}$  and are evident at all NaTf compositions. These distinct bands suggest that LPMEI:NaTf form a more locally

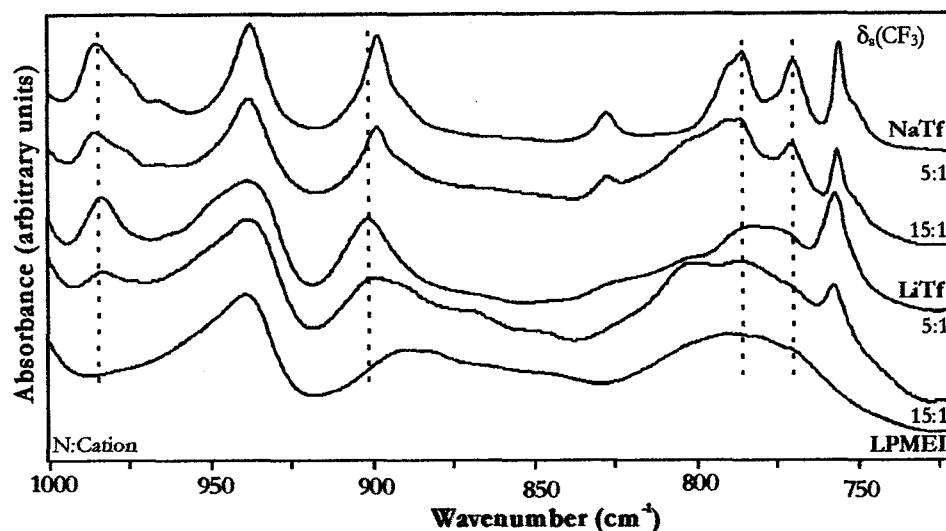


**Figure 4.1:** IR spectra of LPMEI with a 5:1 and 15:1 nitrogen:cation ratio of LiTf and NaTf in the 720–1000  $\text{cm}^{-1}$  region.

ordered system than LPMEI:LiTf.

In the 800 to 900  $\text{cm}^{-1}$  region (Figure 4.1), the LPMEI bands at  $\sim 850$  and  $\sim 869$   $\text{cm}^{-1}$  decrease in intensity as the LiTf composition increases. This phenomenon is more noticeable when NaTf is added to LPMEI where the band at 883  $\text{cm}^{-1}$  also decreases in intensity. A new LPMEI band forms at 828  $\text{cm}^{-1}$  upon addition of NaTf. This band occurs at all compositions of NaTf and is a result of a conformational change in the polymer backbone. The LPMEI band at  $\sim 889$   $\text{cm}^{-1}$  remains unchanged upon addition of LiTf or NaTf, even at high triflate compositions.

In the 900 to 1000  $\text{cm}^{-1}$  region (Figure 4.1), there are distinct bands forming at 899 and 983  $\text{cm}^{-1}$  in the 15:1 composition of LiTf. The 899  $\text{cm}^{-1}$  band shifts to 902  $\text{cm}^{-1}$  as the LiTf composition increases to 5:1. The 983  $\text{cm}^{-1}$  band is asymmetric, indicating the presence of an underlying band at  $\sim 980$   $\text{cm}^{-1}$ . At high LiTf compositions, there is evidence of bands forming at 949 and 962  $\text{cm}^{-1}$ . The addition of NaTf has similar effects on LPMEI as the

addition of LiTf, except there is no band at  $\sim 949\text{ cm}^{-1}$ . In addition, the bandwidth of the  $938\text{ cm}^{-1}$  band becomes smaller as the composition of NaTf increases, and new bands occur at 898, 966, 977, and  $986\text{ cm}^{-1}$ .

*Ionic Association Regions.* In LPMEI:LiTf systems, the contact ion pairs are the dominant species present, based on the  $\delta(\text{CF}_3)$  bands (**Table 4.1**). At low LiTf compositions, both contact ion pairs ( $757\text{-}758\text{ cm}^{-1}$ ) and “free” ions ( $752\text{ cm}^{-1}$ ) are present. However, at moderate LiTf compositions, an aggregate species ( $762\text{ cm}^{-1}$ ) forms. As the LiTf composition increases the relative amount of aggregate species increases, while the relative amount of “free” ions and contact ion pairs decreases. Similar trends occur in LPMEI:NaTf systems, except that the relative amount of “free” ions ( $751\text{-}752\text{ cm}^{-1}$ ) increases and contact ion pairs ( $756\text{ cm}^{-1}$ ) decreases to a greater extent. The frequency of the aggregate species ( $758\text{-}759\text{ cm}^{-1}$ ) is lower than in poly(ethylene oxide) systems, but it corresponds with the frequencies reported in LPEI:LiTf systems.

**Table 4.1: A comparison of the band center frequency in the  $\delta(\text{CF}_3)$  region for LPMEI:LiTf and LPMEI:NaTf at varying nitrogen:cation ratios.**

Composition (N:Cation)	Band center frequency (% relative intensity), $\text{cm}^{-1}$		
LiTf	Aggregate	Contact ion pairs	“Free”
20:1		757 (60)	752 (40)
15:1	762 (11)	757 (56)	753 (33)
10:1	762 (23)	757 (52)	752 (25)
5:1	762 (29)	758 (42)	752 (24)
NaTf			
20:1		756 (72)	751 (27)
15:1	758 (4)	756 (59)	751 (36)
10:1	759 (13)	756 (47)	751 (40)
5:1	758 (17)	756 (40)	752 (43)

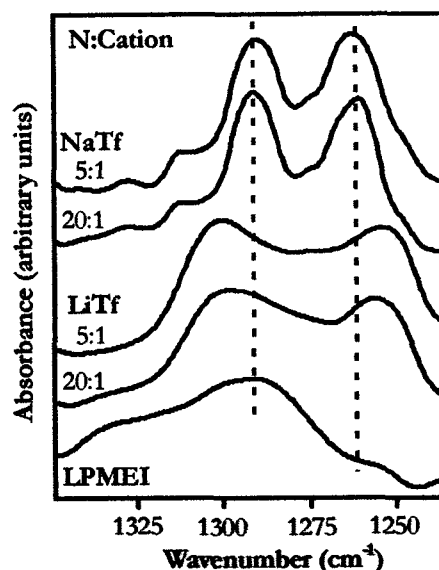


**Figure 4.2:** IR spectra of the  $\nu_{as}(\text{SO}_3)$  region of LPMEI with a 5:1 and 20:1 nitrogen:cation ratio of LiTf and NaTf.

The  $\nu_{as}(\text{SO}_3)$  region ( $\sim 1250\text{--}1320\text{ cm}^{-1}$ ) is also affected by cation-anion interactions. In **Figure 4.2**, the  $\nu_{as}(\text{SO}_3)$  bands occur at 1253,  $\sim 1272$ ,  $\sim 1276$ , and  $1300\text{ cm}^{-1}$  in LPMEI:LiTf and at 1261, 1273, and  $1291\text{ cm}^{-1}$  in LPMEI:NaTf. These bands in LPMEI:NaTf are more defined than those in LPMEI:LiTf. In addition, the  $\nu_{as}(\text{SO}_3)$  bands in LPMEI:LiTf are farther apart than those in LPMEI:NaTf. Furthermore, the separation of these bands becomes larger as the LiTf composition is increased. The differences in the  $\nu_{as}(\text{SO}_3)$  bands between LPMEI:LiTf and LPMEI:NaTf indicates that the coordination of the cation to the triflate anion is stronger in LPMEI:LiTf than in LPMEI:NaTf. Because the  $\nu_{as}(\text{SO}_3)$  mode has two-fold degeneracy, the splitting of the  $\nu_{as}(\text{SO}_3)$  band indicate that the degeneracy of this mode has been broken by the potential energy environment of the

system. A stronger perturbation of the vibrational potential energy environment will cause the component  $\nu_{as}(\text{SO}_3)$  bands to be further apart.

**4.1.2 Thermal Analysis.** The glass transition ( $T_g$ ) of LPMEI occurs at  $-91^\circ\text{C}$  (Table 4.2), which is similar to the results reported by Tanaka (95). As LiTf is added, the  $T_g$  increases to  $3^\circ\text{C}$  at a 5:1 LiTf composition. The coordination of the LiTf to LPMEI hinders the flexibility of the polymer, therefore increasing the  $T_g$  values. This trend in  $T_g$  does not occur in the LPMEI:NaTf systems.

When NaTf is added to LPMEI,  $T_g$  does not change within experimental error (Table 4.2). A  $T_g$  cannot be observed in the 5:1 LPMEI:NaTf sample because the crystalline domains are much larger than the amorphous domains. In all LPMEI:NaTf samples, melting temperatures are observed. However, in the 10:1 and 5:1 LPMEI:NaTf samples, the melting temperature is not sharply defined. In particular, there appear to be two superimposed thermal events in the 5:1 sample, with onsets at  $125$  and  $141^\circ\text{C}$ , respectively. However, these are only seen in freshly prepared samples and disappear upon cycling between  $50$  and  $150^\circ\text{C}$ , leaving a sharp melting transition with an onset at  $134^\circ\text{C}$  in the 5:1

**Table 4.2: Glass transition temperature ( $T_g$ ) and melting temperature ( $T_m$ ) of LPMEI, LPMEI:LiTf, and LPMEI:NaTf with varying nitrogen:cation molar ratios.**

Composition (N:Li)	$T_g$ ( $^\circ\text{C}$ )	Composition (N:Na)	$T_g$ ( $^\circ\text{C}$ )	$T_m$ ( $^\circ\text{C}$ )
LPMEI	-91			
20:1	-63	20:1	-90	119
15:1	-53	15:1	-89	119
10:1	-48	10:1	-88	128,133
5:1	3	5:1		125,141

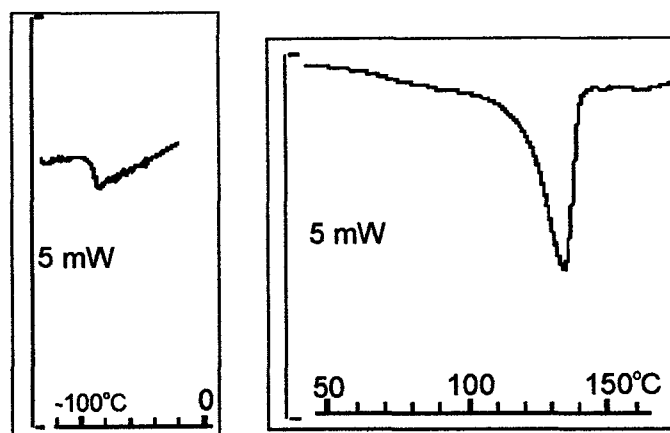


**Figure 4.3:** *T<sub>g</sub> and T<sub>m</sub> of 15:1 LPMEI:NaTf.*

LPMEI:NaTf sample. Based on the thermal analysis of LPMEI:NaTf, both amorphous and crystalline regions exist in the sample. **Figure 4.3** illustrates typical thermograms (*T<sub>g</sub>* & *T<sub>m</sub>*) recorded for LPMEI:NaTf systems.

**4.1.3 Powder X-ray Diffraction Analysis.** Diffraction patterns were acquired for LPMEI, LPMEI:NaTf of varying concentrations, and NaTf (**Figure 4.4**). Most of the peaks in the LPMEI:NaTf diffractograms do not correlate to the peaks in the NaTf diffractogram. The broad peak in LPMEI due to the amorphous domains is significantly decreased when NaTf is added, indicating an ordering of the system. The crystalline domains in LPMEI:NaTf are attributed to a complex involving both LPMEI and NaTf. In the diffractograms of LPMEI:NaTf, the crystalline growth can be observed in the sharper peaks (17-23°) and formation of new peaks (11-15°) as the NaTf composition increases.



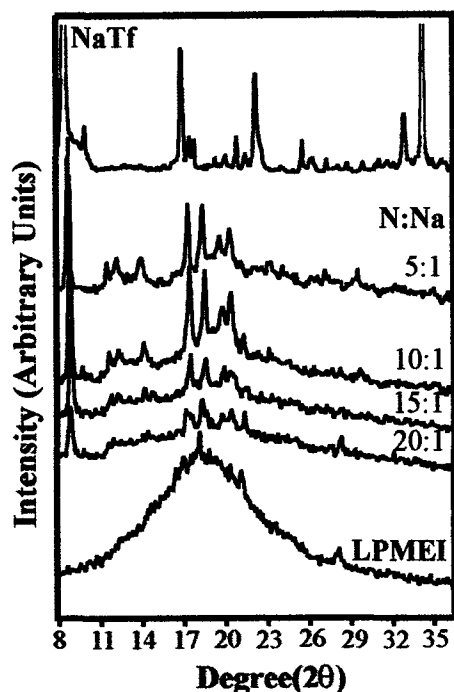


*Figure 4.4: XRD data of NaTf and LPMEI with varying concentrations of NaTf.*

**4.1.4 Ionic Conductivity Analysis.** The temperature dependent conductivity plots of LPMEI:LiTf are illustrated in **Figure 4.5a**. Note the lines tracing the conductivity curves are for a visual aid only. The 20:1 LPMEI:LiTf samples results in the highest conductivity values at all temperatures. At this composition, the dominant species present in the system are the contact ion pairs, based on curve-fitting analysis of the  $\delta(\text{CF}_3)$  region. This suggests that the ions quickly dissociate and reassociate to facilitate ion conduction (74). The conductivity decreases with increasing LiTf composition because the system becomes more locally ordered as described in section 4.1.1. As expected, the conductivity increases with temperature.

There are major differences between LPMEI:LiTf and LPEI:LiTf conductivity plots (**Figures 4.5a**); for example, the conductivity curves in LPEI:LiTf cross each other, unlike those in LPMEI:LiTf. A better comparison between LPMEI:LiTf and LPEI:LiTf is

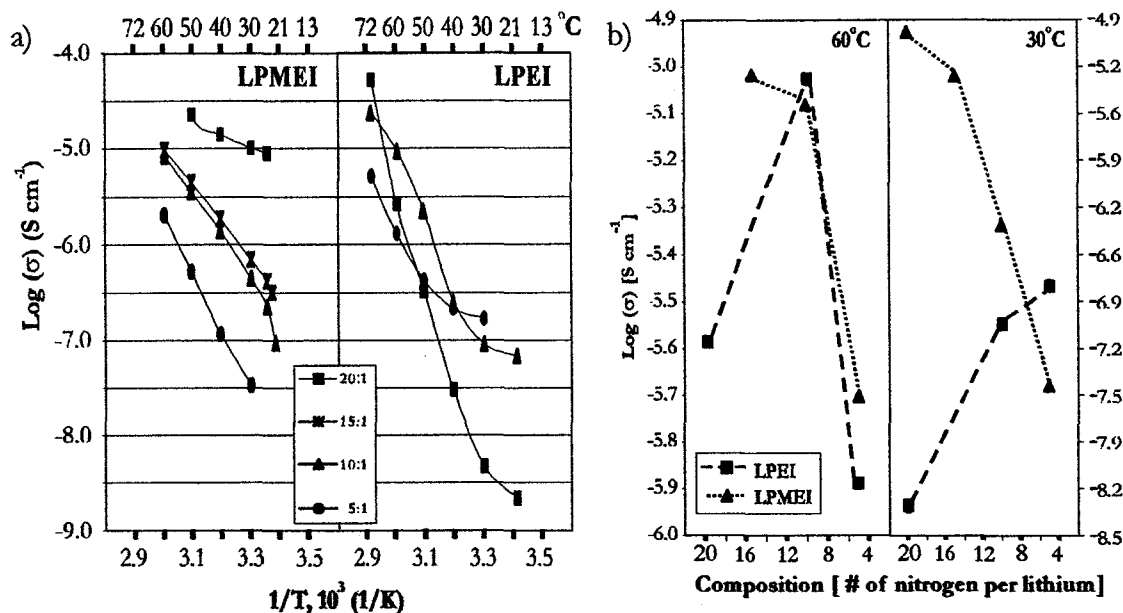


**Figure 4.5:** a) Temperature-dependent ionic conductivity data of LPMEI and LPEI with varying concentrations of LiTf. b) A comparison of ionic conductivity values at 30°C and 60°C of LPEI and LPMEI with LiTf at varying nitrogen:lithium molar ratios. (Note the lines tracing the conductivity curves are for a visual aid only.)

illustrated in **Figure 4.5b**. At 30°C (below the  $T_m$  of LPEI), LPMEI:LiTf has a higher conductivity than LPEI:LiTf at low LiTf compositions. As the LiTf composition increases, the conductivity of LPMEI:LiTf decreases and LPEI:LiTf increases. Eventually, the conductivity of LPEI:LiTf becomes greater than LPMEI:LiTf at ~12:1 ( $Li^+ : N$ , molar ratio). These trends in the conductivities are due to LPMEI becoming more locally ordered and LPEI becoming more locally disordered with increasing LiTf composition. At 60°C (above the  $T_m$  of LPEI), the conductivities of LPMEI:LiTf and LPEI:LiTf with a 10:1 and 5:1 compositions are similar within experimental error. At this temperature, LPEI has amorphous behavior similar to that of LPMEI at moderate to high LiTf compositions. However, at a 5:1 composition, LPMEI:LiTf has a higher conductivity value compared to

LPEI:LiTf, although at a 10:1 composition LPEI:LiTf has a slightly higher conductivity value.

## 4.2 LPMEI Characterized by Model Compounds (*Paper V*)

The vibrational mode assignments of the bands in LPMEI have not been reported. In order to be able to assign these modes to the bands in LPMEI, a model compound that mimics LPMEI vibrational signatures is helpful. The vibrational modes in model systems can be determined utilizing quantum chemical calculations. TMEDA and PMDETA systems have been investigated as possible model compounds for LPEI systems.

**4.2.1 LPMEI Modeled by TMEDA.** N,N,N',N'-tetramethylethylenediamine, TMEDA, (Figure 4.6a) is structurally similar to the LPMEI end groups (Figure 4.6b). However, TMEDA does not contain a nitrogen atom with only one methyl group attached. Spectroscopically, there are a few similarities in the spectral bands in TMEDA and LPMEI complexed with LiTf in the 760–1000 cm<sup>-1</sup> region (Figure 4.7). Both TMEDA and LPMEI have a number of bands with broad bandwidths in the 760–810 cm<sup>-1</sup> region. However, in this region there are small differences in the LPMEI:LiTf spectrum when LiTf is added, unlike the distinct band structures seen in the TMEDA:LiTf spectrum.

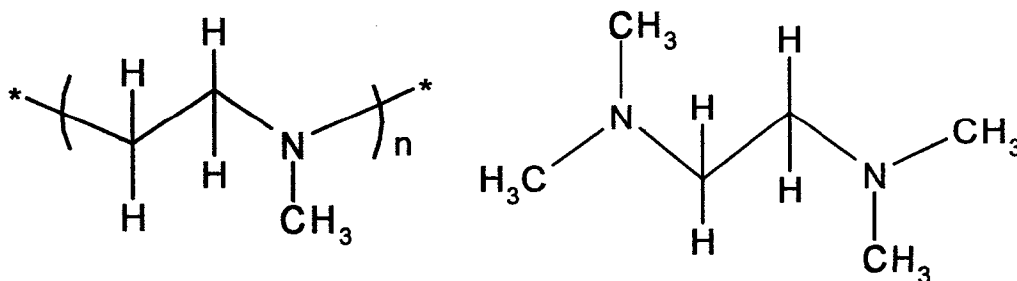


**Figure 4.6:** Structural Formula of **a)** LPMEI and **b)** TMEDA.

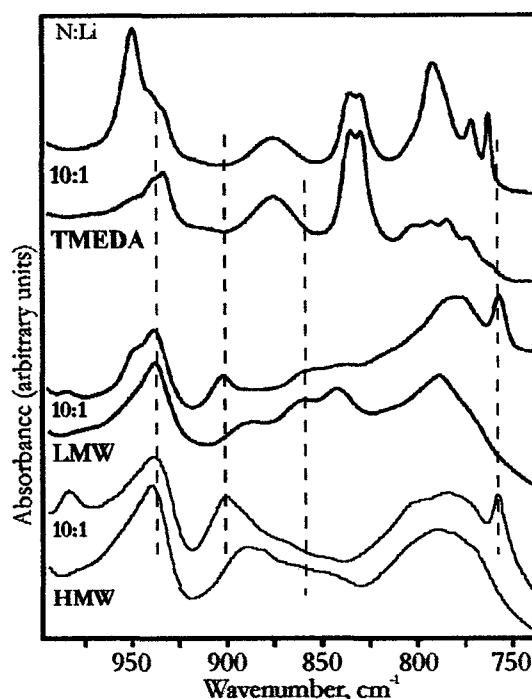


**Figure 4.7:** IR spectra of the of TMEDA, low molecular weight LPMEI (LMW), and high molecular weight LPMEI (HMW) with a 5:1 and 20:1 nitrogen:cation ratio of LiTf in the 750 to 1000  $\text{cm}^{-1}$  region.

In the 810–900  $\text{cm}^{-1}$  region, the TMEDA bands resembles those in LPMEI except that these TMEDA bands are much more intense relative to the 939  $\text{cm}^{-1}$  band. In the 900–1000  $\text{cm}^{-1}$  region, the LPMEI band at 939  $\text{cm}^{-1}$  has a similar band intensity and bandwidth as the TMEDA band in this region. However, when LiTf is added, there are a few changes in the LPMEI band, in which new bands are forming at 902, 949, and 984  $\text{cm}^{-1}$ , respectively, at high LiTf composition in both low and high molecular weight LPMEI. This band does not appear in the TMEDA:LiTf spectrum. Similar results are observed when comparing TMEDA:NaTf to LPMEI:NaTf.

In the  $\delta(\text{CF}_3)$  region of LPMEI:LiTf, the predominant species in all compositions is [LiTf] contact ion pairs (758  $\text{cm}^{-1}$ ). However, there are significant amounts of “free” ions and a few aggregate ions present at higher LiTf compositions. The cation-anion interactions

in LPMEI:LiTf are significantly different from those in TMEDA:LiTf, which consist of only the aggregate species  $[\text{Li}_2\text{Tf}]^+$ . These differences are attributed to the TMEDA forming a highly crystalline complex.

The spectroscopic differences between TMEDA and LPMEI are attributed to the structural differences between TMEDA and LPMEI. For example, all of the nitrogen atoms in TMEDA have two methyl groups attached, unlike LPMEI, which the majority of the nitrogen atoms have one methyl group attached. There are also spectroscopic differences in TMEDA and LPMEI when LiTf is added, which are due to the different coordinations of the lithium cation to the triflate anion. Because of the differences mentioned above, TMEDA systems are not the best model compound for LPMEI systems.

**4.2.2 LPMEI Modeled by PMDETA.** N,N,N',N',N''-pentamethylethylenediamine, PMDETA, is more structurally similar to LPMEI than TMEDA because PMDETA has a nitrogen atom that is attached by one methyl group (Figures 4.8a & b). In addition, PMDETA is more spectroscopically similar to high molecular weight LPMEI compared to TMEDA (Figures 4.9a & b). Low molecular weight LPMEI spectrum acts as an intermediate, because it exhibits spectral signatures of both PMDETA and high molecular weight LPMEI. The vibrational modes assignment of the LPMEI bands are listed in Table

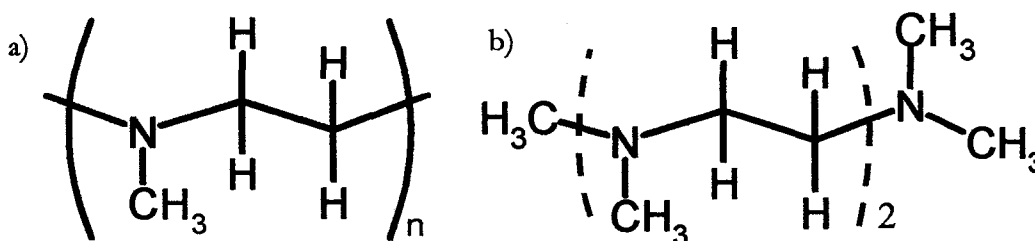


**Figure 4.8:** Structural Formula of **a)** LPMEI and **b)** PMDETA.

**Table 4.3. Vibrational modes and frequencies ( $\text{cm}^{-1}$ ) of PMDETA, high molecular weight (HMW), and low molecular weight (LMW) LPMEI.**

PMDETA	LMW LPMEI	HMW LPMEI	Mode Description
770-791	776-798	772-789	$\rho(\text{CH}_2)$ ; $\nu(\text{C-N})$
~807		~802	$\rho(\text{CH}_2)$
834	844	850	$\nu(\text{C-N})$ ; $\rho(\text{CH}_2)$
859	859	869	$\nu(\text{C-N})$
~891	~889	~889	$\nu(\text{C-N})$
937	938	939	$\rho(\text{CH}_2)$ ; $\nu(\text{C-N})$
~944	~947	~947	$\nu(\text{C-N})$ ; $\rho(\text{CH}_2)$

4.3. In PMDETA, there is a broad distribution of bands in the  $760$  to  $800\text{ cm}^{-1}$ , which are very similar to bands in this region in LPMEI, except the PMDETA bandwidths are not as large. These LPMEI bands are due predominantly to  $\text{CH}_2$  rocking motion. The vibrational mode assignment of the bands in the  $760$  to  $800\text{ cm}^{-1}$  region are based on quantum chemical calculations of PMDETA with  $g-\bar{g}$  and  $\bar{g}-\bar{g}$   $\text{N-C-C-N}$  dihedral angles..

In the  $800$  to  $900\text{ cm}^{-1}$  region, the PMDETA bands at  $\sim 807$ ,  $834$ ,  $859$ , and  $\sim 891\text{ cm}^{-1}$  correlate to the bands at  $844$ ,  $859$ , and  $\sim 889\text{ cm}^{-1}$  in low molecular weight LPMEI and at  $\sim 802$ ,  $850$ ,  $869$ ,  $882$ , and  $\sim 889\text{ cm}^{-1}$  in high molecular weight LPMEI. However, in high molecular weight LPMEI, bands at  $850$  and  $869\text{ cm}^{-1}$  are less intense relative to the  $882\text{ cm}^{-1}$  band as compared to PMDETA and low molecular weight LPMEI. The LPMEI band assignments in this region are determined from a quantum chemical calculation of a PMDETA molecule with a  $t-t$  and  $t-\bar{g}$   $\text{N-C-C-N}$  dihedral angles, because there were no bands in this region calculated from PMDETA with  $g-\bar{g}$  and  $\bar{g}-\bar{g}$   $\text{N-C-C-N}$  dihedral angles.

In the  $900$  to  $1000\text{ cm}^{-1}$  region, the PMDETA bands at  $937$  and  $\sim 944\text{ cm}^{-1}$  correlate to the LPMEI bands at  $938$  and  $\sim 947\text{ cm}^{-1}$  in the low molecular weight polymer and at  $939$

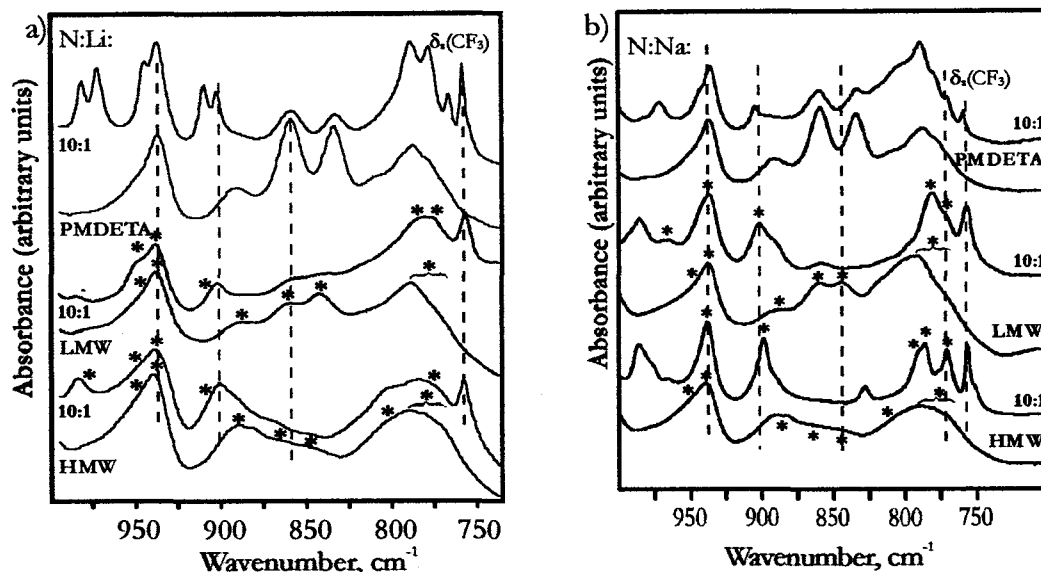


**Figure 4.9:** IR spectra of the of PMDETA low molecular weight LPMEI (LMW) and high molecular weight LPMEI (HMW) with a 5:1 and 20:1 nitrogen:cation molar ratio of a) LiTf and b) NaTf in the 750 to 1000  $\text{cm}^{-1}$  region. The asterisk (\*) indicates the bands that can be assigned to vibration modes. calculations of PMDETA with  $\bar{g}-\bar{g}$  and  $g-\bar{g}$  N-C-C-N dihedral angles.

and  $\sim 947 \text{ cm}^{-1}$  in the high molecular weight polymer. The  $938 \text{ cm}^{-1}$  band in LPMEI is attributed to a mixture of  $\text{CH}_2$  rocking and C-N stretching motions; the  $\sim 947 \text{ cm}^{-1}$  band is due to a predominately  $\text{CH}_2$  rocking motion. The vibrational mode assignment of the bands in this region are based on quantum chemical calculations of PMDETA with  $g-\bar{g}$ ,  $\bar{g}-\bar{g}$ , and  $t-\bar{g}$  N-C-C-N dihedral angles.

**PMDETA:LiTf.** There are also spectral similarities between the bands in PMDETA and LPMEI with LiTf added as summarized in Table 4.4. When LiTf is added to PMDETA, the bands in the 760 to  $800 \text{ cm}^{-1}$  region become more distinct (766, 779, 790, &  $\sim 797 \text{ cm}^{-1}$ ) as the bandwidths decrease. However, these bands in low (776, 792, &  $796 \text{ cm}^{-1}$ ) and high (772, 777, 786, &  $798 \text{ cm}^{-1}$ ) molecular weight LPMEI:LiTf are not as distinct as the

**Table 4.4. Vibrational modes and frequencies ( $\text{cm}^{-1}$ ) of PMDETA, high molecular weight (HMW), and low molecular weight (LMW) LPMEI complexed with LiTf or NaTf at a 10:1 molar ratio.**

PMDETA	LMW LPMEI	HMW LPMEI	Mode Description
<i>LiTf</i>			
779	776	777	$\rho(\text{CH}_2); \nu(\text{C-N})$
790	792		$\rho(\text{CH}_2); \nu(\text{C-N})$
903	902	902	
910	~910	~910	$\rho(\text{CH}_2); \nu(\text{C-C})$
938	938	939	$\rho(\text{CH}_2); \nu(\text{C-N})$
945	~948	~949	$\rho(\text{CH}_2); \nu(\text{C-N})$
973	973	974	$\rho(\text{CH}_2)$
982	984	984	
<i>NaTf</i>			
770	772	771	$\rho(\text{CH}_2); \nu(\text{C-N})$
788	781	786	$\rho(\text{CH}_2)$
~791		790	$\nu(\text{C-C}); \nu(\text{C-N}); \rho(\text{CH}_2); \tau(\text{CH}_2)$
904	901	898	$\nu(\text{C-C})$
936	938	939	$\rho(\text{CH}_2); \nu(\text{C-N})$
972	971		$\rho(\text{CH}_2)$
982	984	986	

PMDETA:LiTf bands in this region.

In the 800 to 900  $\text{cm}^{-1}$  region, the PMDETA bands decrease in intensity as the LiTf composition increases; a trend which is also evident in low and high molecular weight LPMEI but to a lesser extent. This phenomenon indicates a change in the N-C-C-N dihedral angles from t-t and t- $\bar{g}$  to g- $\bar{g}$  when significant amounts of LiTf is added. In addition, the frequencies of these bands increase with increasing chain length.

In the 900 to 1000  $\text{cm}^{-1}$  region, four new bands occur at 903, 910, 973, and 982  $\text{cm}^{-1}$  when LiTf is added to PMDETA. These bands occur at 902, ~910, 962, ~973, and 984  $\text{cm}^{-1}$  in low molecular weight and 902, ~910, 962, ~974, and 984  $\text{cm}^{-1}$  in high molecular weight LPMEI:LiTf. The PMDETA band at 938  $\text{cm}^{-1}$  is not affected by the addition of LiTf,



although, a band at  $\sim 944\text{ cm}^{-1}$  becomes more distinct. Similar results are seen in low and high molecular weight LPMEI:LiTf, except that the shoulder at  $\sim 949\text{ cm}^{-1}$  is not as prominent in the high molecular weight LPMEI:LiTf. This band in LPMEI:LiTf is assigned to the mixed  $\text{CH}_2$  rocking and C-N stretching motions.

*PMDETA:NaTf.* The vibrational mode assignments of PMDETA:LiTf bands are listed in **Table 4.4**. When NaTf is added to PMDETA and LPMEI systems, similar spectroscopic correlations can be made between the two systems. For instance, in the 760 to  $800\text{ cm}^{-1}$  region, there are three distinct PMDETA bands at 770, 779, 788, and  $\sim 791\text{ cm}^{-1}$  when NaTf is added. Similar results are seen in low (772, 781, &  $797\text{ cm}^{-1}$ ) and high (771, 786, &  $790\text{ cm}^{-1}$ ) molecular weight LPMEI:NaTf, except the bands in high molecular weight LPMEI are more prominent.

In the 800 to  $900\text{ cm}^{-1}$  region, the bands also decrease in intensity upon addition of NaTf in both PMDETA:NaTf and LPMEI:NaTf systems. In addition, the frequencies of these bands are also affected by the chain length to the same extent as PMDETA:LiTf and LPMEI:LiTf systems. There is a new band at  $828\text{ cm}^{-1}$  in high molecular weight LPMEI:NaTf, which does not occur in either PMDETA:NaTf or low molecular weight LPMEI.

In the 900 to  $1000\text{ cm}^{-1}$  region, the PMDETA:NaTf bands at 904, 936,  $\sim 944$ , 972, and  $982\text{ cm}^{-1}$  corresponds to the bands at 901, 938,  $\sim 942$ ,  $\sim 947$ , 971, and  $984\text{ cm}^{-1}$  in low molecular weight and  $\sim 898$ , 939,  $\sim 945$ , 977, and  $986\text{ cm}^{-1}$  in high molecular weight LPMEI:NaTf.

PMDETA systems are useful model compounds for assigning the vibrational modes in LPMEI systems, based on their spectroscopic similarities. Specifically, PMDETA systems model both the host-cation and cation-anion interactions in LPMEI systems.

## ***Chapter 5: CONCLUDING REMARKS***

---

There are several major points in this study:

1. Discovery of crystalline phases in DMEDA:NaTf, TMEDA:LiTf, TMEDA:NaTf, and PMDETA:NaTf; correlation of their vibrational modes to their local structures (ionically associated species and local backbone conformation) in the crystalline phase,
2. Demonstration that local structures observed in crystalline phases of DMEDA:NaTf, TMEDA:LiTf, TMEDA:NaTf, and PMDETA:NaTf are present in their solution phases,
3. Combined results of quantum chemical calculations, x-ray analysis, and spectroscopic measurements to understand relationship between the local structure and vibrational modes of TMEDA and PMDETA systems,
4. Demonstration of PMDETA:salt systems as useful models for understanding polymer-cation and cation-anion interactions in LPMEI:salt systems,
5. Discovery of a crystalline compound in the LPMEI:NaTf system,
6. Presentation of evidence that cation-anion interactions play a major role in the ionic conduction in LPMEI:LiTf systems, (less conductive at moderate to high LiTf compositions due to aggregate formation and local ordering of the system),
7. Proposal that 1) aggregate species in LPMEI:NaTf are due to a  $[\text{Na}_2\text{Tf}]^+$  species based on comparative spectroscopic studies of PMDETA:NaTf systems; 2) LPMEI:NaTf systems are more structurally ordered than LPMEI:LiTf systems, based on spectroscopic and thermal analysis.

Additional research would include:

- i. Crosslinking techniques to improve mechanical stability of the LPMEI-based electrolytes
- ii. Refining the crystalline phase in LPMEI:NaTf such that a crystal structure can be determined utilizing X-ray diffraction
- iii. Growth of single crystals of PMDETA:LiTf for X-ray analysis

LPMEI derivatives complexed with salts can be a useful resource in finding polymer electrolytes that exhibits great mechanical properties and has conductivity values acceptable for lithium battery applications.

## REFERENCES

- (1) Meyer, W. H. *Adv. Mater.* **1998**, *10*, 439-448.
- (2) Tarascon, J.-M.; Armand, M. *Nature* **2001**, *414*, 359-367.
- (3) Armand, M. B.; Chabagno, J. M.; Duclot, M. J. *Sec. Int. Conf. on Solid Elect.* **1978**, *St. Andrews, Scotland*.
- (4) Armand, M. B.; Chabagno, J. M.; Duclot, M. J. Polyethers as Solid Electrolytes. In *Fast Ion Transport in Solids*; Vashista, P., Mundy, J. M., Shenoy, G. K., Eds.; Elsevier: Amsterdam, 1979; pp 131-136.
- (5) Murphy, D. W.; Salvo, F. J. D.; J. N. Carides, J. N.; Waszczak, J. V. *Mat. Res. Bull.* **1978**, *13*, 1395-1402.
- (6) Armand, M.; Gauthier, M. Polymeric Solid Ion Conductors: The Immobile Solvent Concept. In *In High Conductivity Solid Ionic Conductors: recent trends and applications*; Takahashi, T., Ed.; World Scientific: New Jersey, 1989; pp 114 - 145.
- (7) Fenton, D. E.; Parker, J. M.; Wright, P. V. *Polymer* **1973**, *14*, 589.
- (8) *Handbook of Batteries*, 3rd ed.; McGraw-Hill: New York, 2002.
- (9) Vincent, C. A. *Prog. Solid St. Chem.* **1987**, *17*, 145-261.
- (10) Allcock, H. R.; O'Connor, S. J. M.; Olmeijer, D. L.; Napierala, M. E.; Cameron, C. G. *Macromolecules* **1996**, *29*, 7544-7552.
- (11) Nishimoto, A.; Watanabe, M.; Ikeda, Y.; Kohjiya, S. *Electrochim. Acta* **1998**, *43* (10-11), 1177-1184.
- (12) Pearson, R. G. *J. Chem. Ed.* **1968**, *45*, 581-587.
- (13) Pearson, R. G. *J. Am. Chem. Soc.* **1963**, *85*, 3533-3539.
- (14) Gray, F. M. *Solid Polymer Electrolytes: Fundamentals and Technological Applications*; VCH Publishers, Inc.: New York, 1991.
- (15) Pearson, R. G. *J. Chem. Ed.* **1968**, *45*, 643 - 648.
- (16) Bruce, P. G.; Gray, F. M. Polymer Electrolytes II: Physical Principles. In *Solid State Electrochemistry*; Bruce, P. G., Ed.; Cambridge University Press: Cambridge, 1995; pp 119-162.
- (17) Bruce, P. G.; Vincent, C. A. *Solid State Ionics* **1990**, *40-41*, 607-611.
- (18) Lourenco, M. A.-V. *Compt. Rend.:hebdomadaires des seances de l'Academie des sciences* **1859**, *49*, 619-620.
- (19) Wurtz, A. *Compt. Rend.: hebdomadaires des seances de l'Acad. des sciences* **1859**, *49*, 813-817.
- (20) Berthier, C.; Gorecki, W.; Minier, M.; Armand, M. B.; Chabagno, P. R. *Solid State Ionics* **1983**, *11*, 91-95.
- (21) *Polymer Handbook*; Interscience Publishers: New York, 1966.
- (22) Dong, H.; Hyun, J.-K.; Rhodes, C. P.; Frech, R.; Wheeler, R. A. *J. Phys. Chem. B* **2002**, *106*, 4878-4885.
- (23) Rhodes, C. Crystalline and Amorphous Phases in Polymer Electrolytes and Model Systems. Dissertation, University of Oklahoma, 2001.
- (24) Rhodes, C. P.; Frech, R. *Macromolecules* **2001**, *34*, 2660-2666.
- (25) Frech, R.; Huang, W. *Macromolecules* **1995**, *28*, 1246-1251.
- (26) Yoshida, H.; Matsuura, H. *J. Phys. Chem. A* **1998**, *102*, 2691-2699.
- (27) Petrowsky, M.; Rhodes, C. P.; Frech, R. *J. Soln. Chem.* **2001**, *30*, 171-181.
- (28) Rhodes, C. P.; Khan, M.; Frech, R. *J. Phys. Chem. B* **2002**, *106*, 10330-10337.
- (29) Bruce, P. G. *Faraday Discuss. Chem. Soc.* **1989**, *88*, 43-54.
- (30) Papke, B. L.; Ratner, M. A.; Shriver, D. F. *J. Electrochem. Soc.* **1982**, *129*, 1434-1438.
- (31) Matsuura, H.; Fukuhara, K. *J. Poly. Sci. B* **1986**, *24*, 1383-1400.

- (32) Wright, P. V. Structure, Morphology and Thermal Properties of Crystalline Complexes of Poly(ethylene oxide) and Alkali Salts. In *Polymer Electrolyte Reviews - 2*; MacCallum, J. R., Vincent, C. A., Eds.; Elsevier Applied Science: New York, 1989; pp 61-119.
- (33) Painter, P. C.; Coleman, M. M. *Fundamentals of Polymer Science: an introductory text*, 2nd ed.; Technomic Publishing Co. Inc.: Lancaster, 1997.
- (34) Shriver, D. F.; Bruce, P. G. Polymer Electrolytes I: General Principles. In *Solid State Electrochemistry*; Bruce, P. G., Ed.; Cambridge University Press: New York, 1995; pp 95-162.
- (35) Chintapalli, S.; Frech, R. *Electrochim. Acta* **1998**, *43*, 1395-1400.
- (36) Vallée, A.; Besner, S.; Prud'homme, J. *Electrochim. Acta* **1992**, *37*, 1579-1583.
- (37) Besner, S.; Vallée, A.; Bouchard, G.; Prud'homme, J. *Macromolecules* **1992**, *25*, 6480-6488.
- (38) Fauteux, D. Phase Equilibria. In *Polymer Electrolyte Reviews - 2*; MacCallum, J. R., Vincent, C. A., Eds.; Elsevier Applied Science: New York, 1989; pp 121-155.
- (39) Stainer, M.; Hardy, L. C.; Whitmore, D. H.; Shriver, D. F. *J. Electrochem. Soc.* **1984**, *131*, 784-790.
- (40) Robitaille, C. D.; Fauteux, D. *J. Electrochem. Soc.* **1986**, *133*, 315-325.
- (41) Siddiqui, J. A.; Wright, P. V. *Faraday Discuss. Chem. Soc.* **1989**, *88*, 113-22.
- (42) Angell, C. A. *Solid State Ionics* **1986**, *18-19*, 72-88.
- (43) Ratner, M. A.; Johansson, P.; Shriver, D. F. *MRS Bulletin* **2000**, *25*, 31-37.
- (44) Ratner, M. A.; Nitzan, A. *Faraday Discuss. Chem. Soc.* **1989**, *88*, 19-42.
- (45) Bruce, P. G. Electrical Measurements on Polymer Electrolytes. In *Polymer Electrolyte Reviews - I*; MacCallum, J. R., Vincent, C. A., Eds.; Elsevier Applied Science: New York, 1987; pp 237-274.
- (46) Ansari, S. M.; Brodwin, M. *Solid State Ionics* **1985**, *17*, 101-106.
- (47) Shriver, D. F.; Dupon, R.; Stainer, M. *J. Power Sources* **1983**, *9*, 383-388.
- (48) Wright, P. V. *Br. Polym. J.* **1975**, *7*, 319-327.
- (49) Bruce, P. G.; Vincent, C. A. *J. Chem. Soc. Faraday Trans.* **1993**, *89*, 3187-3203.
- (50) Sorensen, P. R.; Jacobsen, T. *Electrochim. Acta* **1982**, *27*, 1671-1675.
- (51) Gadjourova, Z.; Andreev, Y. G.; Tunstall, D. P.; Bruce, P. G. *Nature* **2001**, *412*, 520-523.
- (52) Ratner, M. A. Aspects of the Theoretical Treatment of Polymer Solid Electrolytes: Transport Theory and Models. In *Polymer Electrolyte Reviews -1*; MacCallum, J. R., Vincent, C. A., Eds.; Elsevier Applied Science: New York, 1987; pp 173-236.
- (53) Ratner, M. A.; Shriver, D. F. *Chem. Rev.* **1988**, *88* (1), 109-113.
- (54) Druger, S. D.; Nitzan, N.; Ratner, M. A. *J. Chem. Phys.* **1983**, *79*, 3133-3142.
- (55) Nitzan, A.; Ratner, M. A. *J. Phys. Chem.* **1994**, *98*, 1765-1775.
- (56) Bouridah, A.; Dalard, F.; Deroo, D.; Armand, M. B. *J. Appl. Electrochem.* **1987**, *17*, 625-634.
- (57) Cameron, G. G.; Ingram, M. D.; Harvie, J. L. *Faraday Discuss. Chem. Soc.* **1989**, *88*, 55-63.
- (58) Fritz, H. P.; Kuhn, A. *J. Power Sources* **1993**, *41*, 253-261.
- (59) Cameron, G. G.; Harvie, J. L.; Ingram, M. D. *Solid State Ionics* **1989**, *34*, 65-68.
- (60) Ferry, A.; Doeff, M. M.; DeJonghe, L. C. *Electrochim. Acta* **1998**, *43*, 1387-1393.
- (61) Arumugam, S.; Shi, J.; Tunstall, D. P.; Vincent, C. A. *J. Phys.: Condens. Matter* **1993**, *5*, 153-160.
- (62) Ferry, A.; Orädd, G.; Jacobson, P. *J. Chem. Phys.* **1998**, *108*, 7426-7433.

- (63) Lindsey, S. E.; Whitmore, D. H.; Halperin, W. P. *Polym. Prepr. (Am. Chem. Soc., Div. Polym. Chem.)* **1989**, *30*, 442-443.
- (64) Walls, H. J.; Zawodzinski, T. A. J. *Electrochem. Solid-State Lett.* **2000**, *3*, 321-324.
- (65) Doyle, M.; Newman, J. J. *Electrochem. Soc.* **1995**, *142*, 3465-3468.
- (66) Bruce, P. G.; Hardgrave, M. T.; Vincent, C. A. *Electrochim. Acta* **1992**, *37*, 1517-1520.
- (67) Doeff, M. M.; Edman, L.; Sloop, S. E.; Kerr, J.; De Jonghe, L. C. J. *Power Sources* **2000**, *89*, 227-231.
- (68) Munshi, M. Z. A.; Owens, B. B. *Polymer J.* **1988**, *20*, 577-586.
- (69) Ma, Y.; Doyle, M.; Fuller, T. F.; Doeff, M. M.; Jonghe, L. C. D.; Newman, J. J. *Electrochem. Soc.* **1995**, *142*, 1859-1868.
- (70) McLin, M. G.; Angell, C. A. J. *Phys. Chem. B* **1996**, *100*, 1181-1188.
- (71) Huang, W.; Frech, R.; Johansson, P.; Lindgren, J. *Electrochim. Acta* **1995**, *40*, 2147-2151.
- (72) Frech, R.; Manning, J. P. *Electrochim. Acta* **1992**, *37*, 1499-1503.
- (73) Frech, R.; Huang, W. *Solid State Ionics* **1993**, *66*, 183-188.
- (74) York, S. R. S. Local Structures and Conductivity in Polyethylenimine and Polyphosphazene Polymer Electrolytes. Dissertation, University of Oklahoma, 2002.
- (75) Schantz, S.; Sandahl, J.; Borjesson, L.; Torell, L. M.; Stevens, J. R. *Solid State Ionics* **1988**, *28-30*, 1047-1053.
- (76) Frech, R.; Huang, W. *Solid State Ionics* **1994**, *72*, 103-107.
- (77) Frech, R.; Huang, W.; Dissanayake, M. A. K. L. *Mat. Res. Soc. Symp. Proc.* **1995**, *369*, 523-534.
- (78) Huang, W.; Frech, R.; Wheeler, R. A. J. *Phys. Chem.* **1994**, *98*, 100-110.
- (79) Rhodes, C. P.; Frech, R. *Solid State Ionics* **1999**, *121*, 91-99.
- (80) Saegusa, T. Y.; Akira; Taoda, Hiroshi; Kobayashi, Shiro. *Macromolecules* **1978**, *11*, pp. 435-6.
- (81) Takahashi, T.; Davis, G. T.; Chiang, C. K.; Harding, C. A. *Solid State Ionics* **1986**, *18-19*, 321-325.
- (82) Johnson, T. W. K.; Irving M. *Macromolecules* **1974**, *7*, pp. 149-53.
- (83) Harris, C. S.; Ratner, M. A.; Shriver, D. F. *Macromolecules* **1987**, *20*, 1778-1781.
- (84) Park, I. H.; Choi, E.-J. *Polymer* **1996**, *37*, 313-319.
- (85) Paul, J.-L.; Jegat, C.; Lassegues, J.-C. *Electrochim. Acta* **1992**, *37*, 1623-1625.
- (86) Chiang, C. K.; Davis, G. T.; Harding, C. A.; Takashi, T. *Solid State Ionics* **1986**, *18&19*, 300-305.
- (87) Chiang, C. K.; Davis, G. T.; Harding, C. A.; Takashi, T. *Macromolecules* **1985**, *18*, 825-827.
- (88) Hirata, M.; Yamada, K.; Kokufuta, E. *Polym. Prepr.* **1993**, *34*, 978-979.
- (89) Hirata, M. Y.; Kazunori; Matsuda, Kiyomi; Kokufuta, Etsuo. *ACS Symp. Ser.*, *548 (Macro-ion Characterization)* **1994**, pp. 493-8.
- (90) Jin, J. H.; Hong, S. U.; Won, J.; Kang, Y. S. *Macromolecules* **2000**, *33*, 4932-4935.
- (91) Johansson, P. *Polymer* **2001**, *42*, 4367-4373.
- (92) Kokufuta, E.; Suzuki, H.; Yoshida, R.; Yamada, K.; Hirata, M.; Kaneko, F. *Langmuir* **1998**, *14*, 788-795.
- (93) Tanaka, R.; Fujita, T.; Nishibayashi, H.; Saito, S. *Solid State Ionics* **1993**, *60*, 119-123.
- (94) Tanaka, R.; Yamamoto, H.; Iwase, T. *Electrochim. Acta* **1995**, *40*, 2421.
- (95) Tanaka, R.; Sakurai, M.; Sekiguchi, H.; Mori, H.; Murayama, T.; Ooyama, T. *Electrochim. Acta* **2001**, *46*, 1709-1715.
- (96) York, S.; Frech, R.; Snow, A.; Glatzhofer, D. *Electrochim. Acta* **2001**, *46*, 1533-1537.
- (97) Saegusa, T.; Ikeda, H.; Fujii, H. *Macromolecules* **1972**, *5*, 108.

- (98) Chatani, Y.; Irie, T. *Polymer* **1988**, *29*, 2126-2129.
- (99) Tanaka, R.; Ueoka, I.; Takaki, Y.; Kataoka, K.; Saito, S. *Macromolecules* **1983**, *16*, 849-853.
- (100) Chatani, Y.; Kobatake, T.; Tadokoro, H.; Tanaka, Y. *Macromolecules* **1982**, *15*, 170-176.
- (101) Watanabe, M.; Ikezawa, R.; Sanui, K.; Ogata, N. *Macromolecules* **1987**, *20*, 968-973.
- (102) Chatani, Y.; Tadokoro, H.; Saugus, T.; Ikede, H. *Macromolecules* **1981**, *14*, 315-321.
- (103) Chatani, Y.; Kobatake, T.; Tadokoro, H. *Macromolecules* **1983**, *16*, 199-204.
- (104) Buckner, M.; York, S. S.; Frech, R.; Glatzhofer, D. T. *Polym. Prepr.* **2003**, *44*, 1085-1086.
- (105) York, S. S.; Buckner, M.; Frech, R.; Glatzhofer, D. T. **manuscript in progress.**
- (106) Harris, C. S.; Shriver, D. F.; Ratner, M. A. *Macromolecules* **1986**, *19*, 987-989.
- (107) Chatani, Y.; Yakura, Y.; Ishioka, T. *Polymer* **1990**, *31*, 208-211.
- (108) Begun, G. M.; Rutenberg, A. C. *Inorg. Chem.* **1967**, *6*, 2212-2216.
- (109) Gadajourova, Z.; Marero, D. M.; Andersen, K. H.; Andreev, Y. G.; Bruce, P. G. *Chem. Mater.* **2001**, *13*, 1282-1285.
- (110) Seneviratne, V.; Frech, R.; Furneaux, J.; Kahn, M. **manuscript in progress.**
- (111) Sanders, R. A. *The  $\text{LiSbF}_6$  band in 10:1 (N:Li molar ratio) LPMEI:LiSbF<sub>6</sub> occurs at 623, 643, and 658  $\text{cm}^{-1}$  in the IR and Raman spectra. unreported results.*
- (112) Chedulaeva, I. A.; Trokhova, S. S.; Ignatenko, A. V.; Ponomarenko, V. A. *Vysok. Soed. Ser. B, Krat. Soob.* **1984**, *26*, 231-234.
- (113) Chedulaeva, I. A.; Ignatenko, A. V.; Ponomarenko, V. A. *Vysok. Soed. Ser. B* **1985**, *27*, 601-604.
- (114) Sanders, R. A.; Boesch, S. A.; Snow, A. G.; Hu, L.; Frech, R.; Wheeler, R. A.; Glatzhofer, D. T. **manuscript in progress.**
- (115) Tanaka, R.; Koike, M.; Tsutsui, T.; Tanaka, T. *J. Poly. Sci. : Poly. Letters ed* **1978**, *16*, 13-19.
- (116) Sanders, R. A.; Snow, A. G.; Frech, R.; Glatzhofer, D. T. *Electrochim. Acta* **2003**, *48* (14-16), 2247-2253.
- (117) Sanders, R. A.; Boesch, S. E.; Snow, A. G.; Hu, L. R.; Frech, R.; Wheeler, R. A.; Glatzhofer, D. T. *Polym. Prepr.* **2003**, *44*, 996-997.
- (118) Ponomarenko, V. A.; Chedulaeva, I. A.; Bogacheva, N. B.; Ignatenko, A. V. *Vysok. Soed. Ser. B, Krat. Soob.* **1981**, *23*, 1981.
- (119) Ponomarenko, V. A.; Chedulaeva, I. A.; Gorodetskaya, E. Y.; Ignatenko, A. V.; Kechina, A. G. *Vysok. Soed. Ser. B, Krat. Soob.* **1974**, *16*, 815-817.
- (120) Nedel'ko, V. V.; Korsunskii, B. L.; Dubovitskii, F. I.; Anan'ina, O. V. *Vysokom. Sodin. Ser. A* **1977**, *19*, 1599-1604.
- (121) Erickson, M.; Glatzhofer, D. T.; Frech, R. *Electrochim. Acta* **2003**, *48* (14-16), 2059-2063.
- (122) Snow, A. G.; Sanders, R. A.; Frech, R.; Glatzhofer, D. T. *Electrochim. Acta* **2003**, *48* (14-16), 2065-2069.
- (123) York, S. S.; Boesch, S. E.; Wheeler, R. A.; Frech, R. *Phys. Chem. Comm.* **2002**, 99-111.
- (124) Boesch, S. E.; York, S. S.; Frech, R.; Wheeler, R. A. *Phys. Chem. Comm.* **2001**, 1.
- (125) York, S. S.; Boesch, S. E.; Wheeler, R. A.; Frech, R. *Macromolecules in press* **2003**.
- (126) Daniel, M. F.; Desbat, B.; Cruege, F.; Trinquet, O.; Lassegues, J. C. *Solid State Ionics* **1988**, *28-30*, 637-641.
- (127) Sanders, R. A.; Frech, R.; Kahn, M. J. *Phys. Chem. B* **2003**, *107* (33), **in press.**
- (128) Sanders, R. A.; Frech, R.; Kahn, M. J. *Phys. Chem. B* **manuscript in progress.**
- (129) Scott, A. P.; Random, L. J. *Phys. Chem.* **1996**, 16502-16513.
- (130) Tadokoro, H. *Structure of Crystalline Polymers*. John Wiley & Sons, New York, 1979.

## **I. DMEDA complexed with LiTf and NaTf**



**Characterization of the Crystalline and Solution Phases in N,N'-Dimethylethylenediamine (DMEDA) with Sodium Triflate (NaCF<sub>3</sub>SO<sub>3</sub>).**

**Rebecca A. Sanders, Roger Frech\*, and Masood A. Khan.**

*Department of Chemistry and Biochemistry, University of Oklahoma, 620 Parrington Oval,  
Norman, OK 73019*

Linear poly(ethylenimine), [LPEI], is a synthetically versatile polymer host compared to poly(ethylene oxide), in that various groups can be attached to the backbone nitrogen atoms. The interactions of LPEI with sodium cations are modeled by solutions of N,N'-dimethylethylenediamine, DMEDA, containing dissolved sodium triflate [NaTf]. During these studies, a crystalline compound was discovered and characterized by X-ray diffraction, differential scanning calorimetry, Fourier transform infrared spectroscopy, and Raman spectroscopy. The DMEDA:NaTf crystallizes into polymeric-like chains in a triclinic unit cell of the  $P\bar{1}$  space group. In the crystal, the sodium ions are both five- and six-coordinate. A spectroscopic comparison of DMEDA, DMEDA:NaTf crystal, and DMEDA:NaTf salt solutions over a composition range of 15:1 to 3:1 [N:Na<sup>+</sup>, molar ratio] was conducted using infrared and Raman spectroscopy. In the DMEDA:NaTf crystal, the triflate ions vibrate as either [Na<sub>2</sub>Tf]<sup>+</sup> or [Na<sub>3</sub>Tf]<sup>2+</sup> species due to the coordination of the triflate ion by sodium ions. However, in solution, only the [Na<sub>2</sub>Tf]<sup>+</sup> species is present at high NaTf compositions. At a 15:1 DMEDA:NaTf composition, contact ion pairs [NaTf] are the dominant species.

## 1. Introduction

The most widely studied polymer electrolyte is poly(ethylene oxide), PEO, complexed with various salts to form ionically-conducting polymers<sup>1</sup>. Polymer-based electrolytes with lithium salts have attracted worldwide attention because of their applications in lithium rechargeable batteries<sup>2</sup>. The mechanism of ionic transport in these systems is not well understood, especially at the molecular level. Cation-anion interactions<sup>3</sup> and cation-polymer interactions<sup>4</sup> are believed to play a major role in the mechanism. The cation-polymer interactions<sup>4</sup> result in changes in the polymer backbone conformation<sup>5</sup>, whereas the cation-anion interactions<sup>3</sup> are associated with the formation of associated ionic species<sup>6</sup>. These, local structures (ionically associated species and local backbone conformation) may be used to study the nature of those important interactions and provide essential insight needed to understand the mechanism of ionic transport.

Linear poly(ethylenimine), LPEI, is a highly crystalline polymer host that also has been studied as a polymer electrolyte since the mid 1980s<sup>7-11</sup>. However, LPEI-based polymer electrolytes exhibit

poor conductivity due to the high crystallinity of LPEI. On the other hand, LPEI is a synthetically versatile polymer host compared to PEO, in that various groups can be attached to the backbone nitrogen atom. By adding various side chains (e.g., -CH<sub>3</sub>, -CH<sub>2</sub>CH<sub>3</sub>, -CH<sub>2</sub>CH<sub>2</sub>CN) to LPEI, the crystallinity of the polymer host decreases, opening many possibilities for the preparation of new polymer electrolytes. However, a basic knowledge of LPEI is needed to better understand the behavior of the LPEI derivatives, therefore model compounds can be useful. Model compounds with vibrational modes similar to the analogous high molecular weight polymer have proved helpful in making vibrational assignments in the latter system, in part because the low molecular weight models are amenable to computational studies<sup>12,13</sup>. Further, studies of ion-polymer coordinations in model compounds complexed with salts provide useful information about ion-polymer coordinations in the corresponding polymer-salt complex. This is especially true when a solved crystal structure of the model compound-salt complex is available. York *et al.* have previously reported work on N,N'-dimethylethylenediamine [(CH<sub>3</sub>NHCH<sub>2</sub>)<sub>2</sub>], DMEDA, with dissolved

$\text{LiCF}_3\text{SO}_3$  (LiTf) as a model compound for LPEI complexed with  $\text{LiTf}^{2,14,15}$ . However, the DMEDA:NaTf system has not been examined as a model for LPEI:NaTf systems. While studying solutions of DMEDA with NaTf, the formation of a crystalline compound was discovered. This paper describes the characterization of the crystalline and amorphous phases in DMEDA:NaTf systems using X-ray diffraction, Fourier transform infrared spectroscopy, Raman spectroscopy, and differential scanning calorimetry (DSC). Structural information obtained from the DMEDA:NaTf crystal provides a better understanding of the local environment of DMEDA and the triflate anion in DMEDA:NaTf solutions.

## 2. Experimental

**2.1 Sample Preparation.** DMEDA and NaTf were obtained from Aldrich. DMEDA was used as received. NaTf was heated under vacuum at  $120^\circ\text{C}$  for 48 hours. The chemicals were stored and used in a dry nitrogen glovebox ( $\text{VAC}, \leq 1\text{ ppm H}_2\text{O}$ ) at room temperature. To prepare the solutions, NaTf was dissolved into DMEDA at various concentrations and stirred for at least 4 hours. The compositions of the solutions are reported as a nitrogen to sodium ion molar ratio ( $\text{N}:\text{Na}^+$ ). At a 3:1 composition, the DMEDA:NaTf solution contained both a viscous liquid and a gel-like phase. After about 6 months, a thin plate of crystals had formed at the liquid-air interface, with a viscous liquid still present underneath the crystals. The crystals were isolated and allowed to dry in a nitrogen atmosphere.

**2.2 X-ray.** A single crystal suitable for X-ray diffraction measurements was isolated from a 3:1 composition of DMEDA:NaTf. X-ray data were collected at 173 (2) K on a Bruker P4 diffractometer using  $\text{MoK}\alpha$  radiation ( $\lambda = 0.71073 \text{ \AA}$ ). The data were corrected for Lorentz and polarization effects; an absorption correction was not applied as it was judged to be insignificant. The structure was solved by the direct method using the SHELXTL system and refined by full-matrix least squares on  $F^2$  using all reflections. All nonhydrogen atoms were refined anisotropically, and all hydrogen atoms were included with idealized parameters. The final  $R_1 = 0.053$  is based on 5863 "observed reflections" [ $I > 2\sigma(I)$ ], and  $wR^2 = 0.156$  is based on all reflections (6999 unique data).

**2.3 Differential Scanning Calorimetry.** A single crystal weighing approximately 2 mg was sealed in a 40  $\mu\text{L}$  aluminum pan. The DSC data were collected using a Mettler DSC 820 calorimeter with Star<sup>c</sup> software (v.6.10) under dry

nitrogen purge. Data were collected during two heating and cooling cycles between  $0^\circ\text{C}$  and  $280^\circ\text{C}$  at a heating and cooling rate of  $5^\circ\text{C}/\text{min}$ .

**2.4 IR & Raman Spectroscopy.** For IR measurements, the DMEDA and DMEDA:NaTf solutions were placed between zinc selenide windows in a sealed sample holder. Finely ground DMEDA:NaTf crystals were prepared as a KBr pellet and a Nujol mull. IR data were recorded on a Bruker IFS66V with a KBr beam splitter over a range of  $500\text{--}4000 \text{ cm}^{-1}$  ( $1 \text{ cm}^{-1}$  resolution; 64 scans). The spectra of the solutions were measured under a dry air purge; the crystal data were collected under vacuum (8 mbar). For the Raman measurements, the DMEDA and DMEDA:NaTf solutions were placed in a solution well and covered with a glass cover plate; the single crystal was sealed into a quartz cuvette in the glovebox. Raman data were recorded with a Jobin-Yvon T64000 system in the triple subtractive mode with a CCD detector using the 532 nm line of a diode-pumped Nd:YVO<sub>4</sub> laser for excitation. All Raman data were collected in a  $180^\circ$  scattering geometry at a laser power of 200 mW measured at the laser head.

## 3. Results and Discussion

### 3.1 Crystal structure. The DMEDA:NaTf

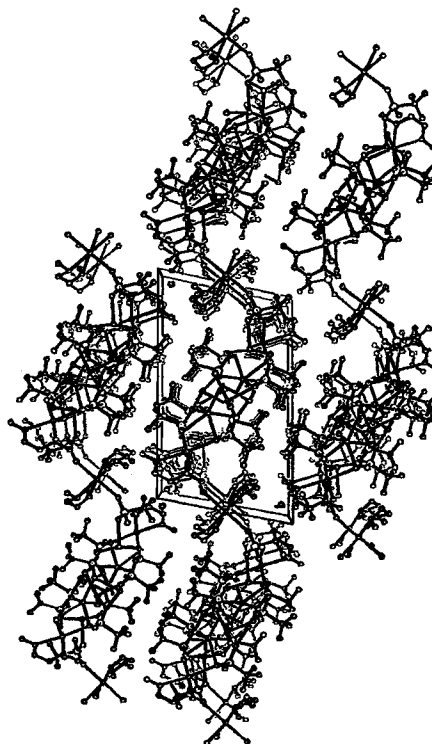


**Figure 1:** Packing diagram of the DMEDA:NaTf crystal. The crystals form a polymeric chain-like structures that are stacked on top of each other.

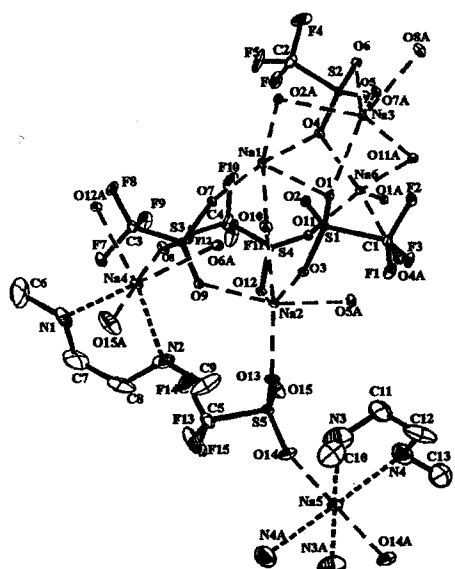


**Figure 2:** A complex structure of the DMEDA:NaTf crystal. The structure does not include the hydrogen atoms. The Na–O bonds are represented as long dashes (---) and the Na–N bonds are represented as short dashes (\*\*\*).

**Table 1:** Structural data of the DMEDA:NaTf crystal obtained from x-ray diffraction study.

Parameters	
Crystal system	Triclinic
Space group	$P\bar{1}$
Temperature	173 (2) K
a (Å)	9.762 (2)
b (Å)	11.4111 (15)
c (Å)	18.989 (2)
$\alpha$	99.664 (9)°
$\beta$	97.195 (12)°
$\gamma$	103.435 (13)°
Volume (Å <sup>3</sup> )	1998.2 (5)
Z	2
Density (Mg/m <sup>3</sup> )	1.723
R1	0.0530
Crystal size (mm <sup>3</sup> )	0.48 x 0.46 x 0.32

crystals form a triclinic unit cell in the  $P\bar{1}$  space group, with a  $[(\text{DMEDA})_2:(\text{NaTf})_5]$  asymmetric units in the cell as illustrated in **Figure 1**. However, there are six Na cation positions because the Na(5) and Na(6) atoms are situated at the inversion center and each component has a fifty percent occupancy. The packing forms a polymeric chain-like network in the  $a$  direction. In this network, two of the Na ions coordinate to the DMEDA molecules; while the remaining NaTf

**Table 2:** Selected bond lengths (Å) and angles (°) for DMEDA:NaTf crystal.

Bond		
Na(4)–N	2.424 (3)	2.436 (4)
Na(5)–N	2.480 (4)	2.490 (4)*
	2.480 (5)*	2.490 (4)
Bond sequence		
N1–Na(4)–N2	74.63 (10)	
N3–Na(5)–N4	73.02 (12)	
Dihedral angle		
C–N1–C–C	-171.7 (6)	t
N1–C–C–N2	-34.5 (8)	$\bar{g}$
C–C–N2–C	172.1 (6)	t
C–N3–C–C	105.8 (6)	s
N3–C–C–N4	56.9 (7)	g
C–C–N4–C	175.8 (6)	t

\*Symmetry transformation ( $-x-2, -y+1, -z$ ) used to generate equivalent atoms.

units form a cluster that does not coordinate with the DMEDA molecules (**Figure 2**). In the DMEDA:NaTf crystal, the sodium ions occupy either five- or six-coordinate sites. Here, coordination is defined as a sodium-oxygen (Na–O) or a sodium-nitrogen (Na–N) bond length of 2.80 Å or less which is based on typical bond lengths of crystal structures of dimethyl ethers of ethylene oxides or glymes, i.e.  $\text{CH}_3(\text{OCH}_2\text{CH}_2)_n\text{OCH}_3$  with  $n = 1-4$ , complexed with NaTf<sup>16</sup>.

All sodium atoms coordinated to DMEDA molecules are six-coordinate. However, one of the these sodium atoms is coordinated to two nitrogen atoms and four triflate oxygen atoms; the other sodium atom is attached to four nitrogen atoms and only two triflate oxygen atoms. The remaining sodium atoms are coordinated only to the triflate oxygen atoms. Structural data of the DMEDA:NaTf crystal are summarized in **Table 1**; selected bond lengths and angles for the DMEDA:NaTf crystal are listed in **Tables 2 and 3**.

The conformation of the DMEDA oligomers can be characterized in terms of the C–N–C–C and N–C–C–N dihedral angles (gauche, g,  $60^\circ \pm 30^\circ$ ; gauche minus,  $\bar{g}$ ,  $-60^\circ \pm 30^\circ$ ; s,  $120^\circ \pm 30^\circ$  trans, t,  $\pm 180^\circ \pm 30^\circ$ ). The N–C–C–N dihedral angle is of particular interest because it is most directly affected by the coordination of the cation to the nitrogen atoms. In the DMEDA:NaTf crystal (**Table 2**), the N–C–C–N dihedral angle of the DMEDA molecules is gauche (56.9°) and gauche minus ( $-34.5^\circ$ ), which results in  $t\bar{g}t$  and  $sgt$  conformations.

**Table 3: The five symmetrically inequivalent triflate anions (Tf) in the asymmetric unit exhibit different degrees of coordination with the sodium anions based on their bond lengths (Å).**

	Bond	Bond length
Tf(1)	O(13)-Na(2)	2.329 (3)
	O(14)-Na(5)	2.427 (3)
Tf(2)	O(3)-Na(2)	2.3297 (18)
	O(1)-Na(3)	2.4050 (18)
	O(1)-Na(1)	2.7499 (19)
Tf(3)	O(7)-Na(1)	2.2587 (19)
	O(9)-Na(2)	2.379 (2)
	O(8)-Na(4)	2.394 (2)
Tf(4)	O(4)-Na(6)	2.316 (3)
	O(4)-Na(1)	2.344 (18)
	O(6)-Na(3)	2.445 (2)
Tf(5)	O(10)-Na(1)	2.307 (2)
	O(11)-Na(6)	2.350 (3)
	O(10)-Na(1)	2.682 (3)
	O(12)-Na(2)	2.785 (2)

**3.2 Thermal Analysis.** Differential scanning calorimetry (DSC) was used to characterize melting and recrystallization processes in the DMEDA:NaTf crystal. In the DSC thermogram of the DMEDA:NaTf crystal (figure not shown), there are several small broad endothermic peaks before 200°C and one sharp endothermic peak at 250°C. The small broad peaks may be due to the loss of residual solvent and unresolved phase transitions. The sharp peak at 250°C represents the melting of the crystalline compound. In the cooling cycle, the onset of recrystallization occurs at 249°C. In a second thermal analysis cycle, the melting and recrystallization temperatures are consistent at 249 and 250°C, respectively, indicating no thermal hysteresis.

### 3.3 Vibrational Spectroscopy.

**3.3.1 Ionic Association in the Crystalline Phase.** The  $\delta(\text{CF}_3)$  region contains distinct bands due to different ionically-associated species. In poly(ethylene oxide):NaTf systems, the ionically associated species and their Raman-active bands are "free" ions at 753  $\text{cm}^{-1}$ , contact ion pairs [MTf] ( $M = \text{cation}$ ) at 756  $\text{cm}^{-1}$ , the aggregate (I) species at 761  $\text{cm}^{-1}$ , and the aggregate (II) species at 769  $\text{cm}^{-1}$ <sup>17</sup>. In poly(ethylenimine):NaTf systems, the "free" ions, contact ion pairs, and the aggregate species occur at 754, 756–757, and 762  $\text{cm}^{-1}$ , respectively<sup>18</sup>. For DMEDA:LiTf solutions, York *et al.* have reported Raman frequencies of the ionic species occurring at 755  $\text{cm}^{-1}$  ("free" ions), 758–760  $\text{cm}^{-1}$  (contact ion pairs), and 763  $\text{cm}^{-1}$

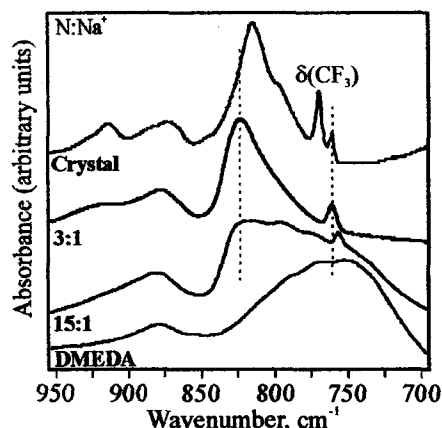


**Figure 3a:** IR spectra of DMEDA with varying concentrations of NaTf in the  $\delta(\text{CF}_3)$  and conformation regions.

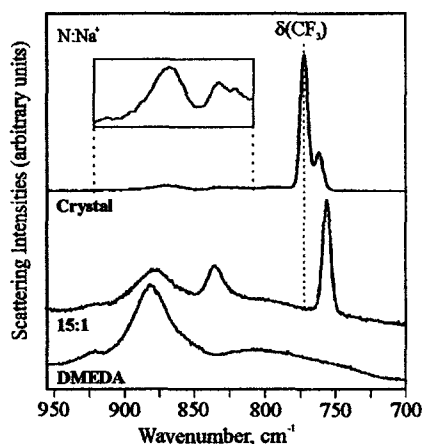


**Figure 3b:** Raman spectra of DMEDA with varying concentrations of NaTf in the  $\delta(\text{CF}_3)$  and conformation regions.

(aggregate species at)<sup>19</sup>. Therefore, a spectral study of this region can provide information about the coordination of the triflate ion by the sodium ion(s). In the DMEDA:NaTf crystal, the  $\delta(\text{CF}_3)$  bands occur at 761, 770, and 772  $\text{cm}^{-1}$  in the IR spectra (Figure 3a) and at 762 and 772  $\text{cm}^{-1}$  in the Raman spectra (Figure 3b). These bands will be discussed in detail later in this section.

The crystal structure reveals a complicated pattern for the coordination of the triflate oxygen atoms by the sodium ions, which is summarized in Table 3. Triflate ion number one, Tf(1), is coordinated by two sodium ions and vibrates as an  $[\text{Na}_2\text{Tf}]^+$  species. Tf(2), Tf(3), and Tf(4) each appear to be coordinated by three sodium ions, although, the relatively long O(1)-Na(1) bond distance (2.7499 Å) in Tf(2) might indicate that this triflate ion essentially vibrates as an  $[\text{Na}_2\text{Tf}]^+$  species. However, Tf(3) and Tf(4) clearly vibrate

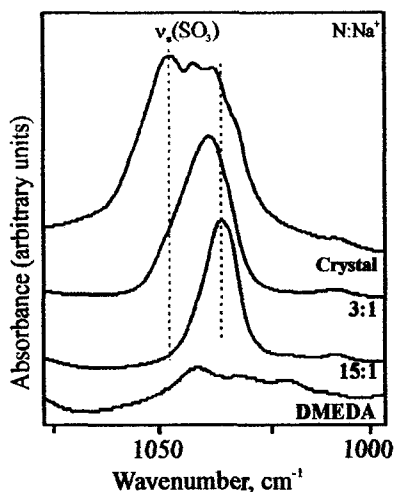


**Figure 4a:** IR spectra of DMEDA with varying concentrations of NaTf in the 1000–1075  $\text{cm}^{-1}$  region. This region includes the  $\nu_s(\text{SO}_3)$  mode.

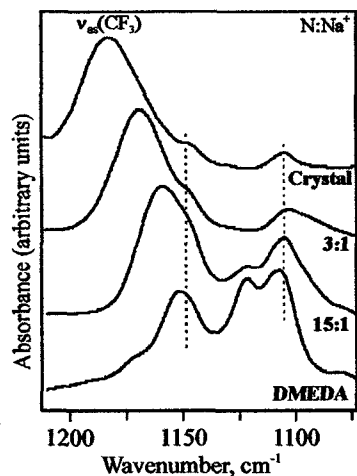


**Figure 4b:** IR spectra of DMEDA with varying concentrations of NaTf in the 1075–1200  $\text{cm}^{-1}$  region. This region includes the  $\nu_{as}(\text{CF}_3)$  mode.

as an  $[\text{Na}_3\text{Tf}]^{2+}$  species. Tf(5) is coordinated by two sodium ions with a relatively short Na-O distance and two sodium ions with a relatively long Na-O bond distance; it essentially vibrates as an  $[\text{Na}_2\text{Tf}]^+$  species. The bands at 770  $\text{cm}^{-1}$  (IR) and 772  $\text{cm}^{-1}$  (Raman) are assigned to the  $[\text{Na}_3\text{Tf}]^{2+}$  species, while the bands at 761 (IR) and 762 (Raman)  $\text{cm}^{-1}$  are attributed to the  $[\text{Na}_2\text{Tf}]^+$  species. These ionic species along with these correlated frequencies will be discussed later using factor group analysis.

The frequency of the  $\text{SO}_3$  symmetric stretch,  $\nu_s(\text{SO}_3)$ , is also affected by the coordination of the triflate ion with the cation. The Raman-active bands at 1032, 1037, and 1050–1058  $\text{cm}^{-1}$

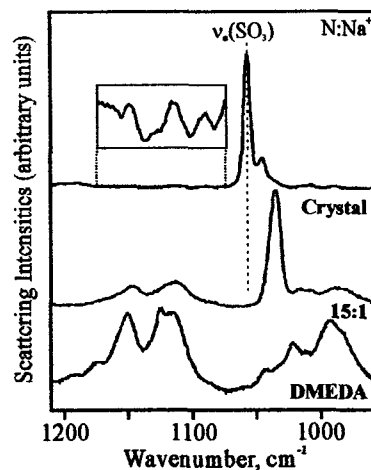


**Figure 4c:** Raman spectra of DMEDA with varying concentrations of NaTf in the 1000–1200  $\text{cm}^{-1}$  region. This region includes only the  $\nu_s(\text{SO}_3)$  mode.

correspond to “free” ions, contact ion pairs, and aggregate species in poly(ethylene oxide):NaTf systems<sup>17,20</sup>. Similar assignments are made for the IR-active bands. For the DMEDA:LiTf solutions, York *et al.* have reported the triflate species to be composed of “free” ions at 1032–1036  $\text{cm}^{-1}$ , contact ion pairs at 1038–1044  $\text{cm}^{-1}$ , and aggregate species at 1050–1054  $\text{cm}^{-1}$  based on Raman measurements<sup>19</sup>. In the DMEDA:NaTf crystal, the  $\nu_s(\text{SO}_3)$  region in IR contains bands at 1047, 1042, 1037, and  $\sim 1033$   $\text{cm}^{-1}$  as illustrated in **Figure 4a**. In the Raman spectrum of the  $\nu_s(\text{SO}_3)$  region (**Figure 4c**), there is a strong band at 1057  $\text{cm}^{-1}$  and a weak band at 1045  $\text{cm}^{-1}$  associated with the  $\nu_s(\text{SO}_3)$  mode.

The intramolecular vibrations of the triflate ion in a unit cell are correlated through intermolecular forces, yielding a vibrational multiplet structure that can be described by a symmetry-based analysis<sup>21</sup>. The resulting normal modes belong to the various irreducible representations of the unit cell group (factor group). For modes originating in the  $A_1$  vibration of an isolated triflate ion, a factor group analysis predicts five Raman active  $A_g$  modes and five IR active  $A_u$  modes for both the symmetric  $\text{SO}_3$  stretching modes and the symmetric  $\text{CF}_3$  deformation modes, i.e.

$$\Gamma(\nu_s(\text{SO}_3)) = \Gamma(\delta_s(\text{CF}_3)) = 5A_g + 5A_u$$

The observation of four IR active modes (1033, 1037, 1042, & 1047  $\text{cm}^{-1}$ ) and two Raman active modes (1045 & 1057  $\text{cm}^{-1}$ ) in the  $\nu_s(\text{SO}_3)$  region, none of which are coincident in frequency,

indicates that the vibrations of the triflate ions in the unit cell are indeed correlated through the center of inversion.

The case of the  $\delta_s(\text{CF}_3)$  modes presents a very different situation. Here there are three IR-active modes (761, 770, & 772  $\text{cm}^{-1}$ ), two of which are coincident with the two Raman-active modes (762 & 772  $\text{cm}^{-1}$ ). This lack of coincidence argues that the modes are not correlated through the inversion. The IR data show that the intensities of the  $\delta_s(\text{CF}_3)$  modes are very weak compare with the strong, sharp  $\nu_s(\text{SO}_3)$  absorptions.

Vibrationally induced dipoles are the major contribution to the intermolecular forces that couple the vibrations of the triflate ions in the unit cell. Therefore, it is not surprising that the vibrations of modes originating in  $\nu_s(\text{SO}_3)$  are highly correlated, whereas the modes originating in  $\delta_s(\text{CF}_3)$  show little or no correlation. The existence of three  $\delta_s(\text{CF}_3)$  bands in the IR is due to the different potential energy environments of the triflate ions in an asymmetric unit (see Table 3). In other words, the vibrations of the two asymmetric units are the same, since the vibrations of the triflate ions in one unit are more or less independent of the vibrations of its symmetrically equivalent partner in the cell. An asymmetric unit has trivial  $C_1$  symmetry, therefore the symmetry species of the triflate ion vibrations may be written

$$\Gamma(\nu_s(\text{SO}_3)) = \Gamma(\delta_s(\text{CF}_3)) = 5A$$

The combined infrared and Raman data show three distinct bands, two of which occur in a frequency range usually attributed to a  $[\text{Na}_3\text{Tf}]^{2+}$  species and the other band to a  $[\text{Na}_2\text{Tf}]^+$  species. An examination of Table 3 shows that the triflate ion Tf(1), Tf(2), and Tf(5) each have two Na–O distances in the range 2.30–2.43 Å, with the remaining Na–O distances greater than 2.74 Å. (Tf(5) is the exception to this generalization, with an additional Na–O distance = 2.682 Å). To a first approximation, if the perturbation of the triflate ion by sodium ion at a Na–O distance greater than 2.43 Å is negligible, those three triflate ions each vibrate independently as  $[\text{Na}_2\text{Tf}]^+$  species with essentially the same frequency.

Tf(3) and Tf(4) each have three Na–O distances less than 2.45 Å. These two ions vibrate as  $[\text{Na}_3\text{Tf}]^{2+}$  species, although the perturbation of the two triflate ions differs sufficiently so that two  $[\text{Na}_3\text{Tf}]^{2+}$  bands can be distinguished with a separation of 2  $\text{cm}^{-1}$ .

**3.3.2 Ionic Association in the Solution Phase.** In the spectra of the 15:1 DMEDA:NaTf solution

(Figures 3a & b), the  $\delta(\text{CF}_3)$  band occurs at 757 (IR) and 756  $\text{cm}^{-1}$  (Raman), a frequency range that is assigned to contact ion pairs. In the 3:1 DMEDA:NaTf solution, there are contact ion pairs ( $\sim 757 \text{ cm}^{-1}$ ) and the  $[\text{Na}_2\text{Tf}]^+$  aggregate species (761  $\text{cm}^{-1}$ ) present.

In the DMEDA:NaTf solutions, the  $\nu_s(\text{SO}_3)$  band (IR) is centered at 1035  $\text{cm}^{-1}$  in the 15:1 solution and 1038  $\text{cm}^{-1}$  in the 3:1 solution (Figure 4a), which correspond to contact ion pairs. However, this band in the 3:1 DMEDA:NaTf solution appears to have two weak shoulders at  $\sim 1035$  and  $\sim 1042 \text{ cm}^{-1}$ . This latter band probably corresponds to the  $[\text{Na}_2\text{Tf}]^+$  species. Therefore, there are ionically-associated species present in the solutions that appear to be similar to certain associated species found in the crystal.

**3.3.3 Comparison of the Cation-DMEDA Interactions in Crystalline and Solution Phases.** The frequencies and intensities of bands from 800 to 1000  $\text{cm}^{-1}$  are sensitive to conformational changes that result from the coordination of the cation by the nitrogen atom in DMEDA<sup>19</sup>. Similar conformational studies have been reported in salt complexes of ethylene oxide-based systems<sup>5,17,22–26</sup>.

Because the bands in this spectral region of the crystal are relatively weak, they are shown in the inset of Figure 3b. Particularly noteworthy is the new band that appears at 831  $\text{cm}^{-1}$  in the crystal, and the shift in the broad DMEDA band at 881  $\text{cm}^{-1}$  to 868  $\text{cm}^{-1}$ . In the 15:1 solution spectrum, the new band is at 836  $\text{cm}^{-1}$ , and the broad band is centered at  $\sim 878 \text{ cm}^{-1}$ , which is intermediate between its values in pure DMEDA and in the crystal. This vibrational pattern is the spectroscopic signature of the t $\bar{g}$ t–sgt conformational sequence seen in the crystal and probably reflects the  $\bar{g} \ g$  sequence of the two N–C–C–N dihedral angles. The fact that this vibrational pattern appears in the 15:1 solution argues that the sodium ions interact with the DMEDA molecules to produce a conformation that bears a significant resemblance to the conformation found in the crystal.

In the 1000–1200  $\text{cm}^{-1}$  region, there are several spectral differences in the crystal and solution DMEDA:NaTf data (Figure 4a, b, and c). Modes in this region consist of a mixture of C–C and C–N stretching,  $\text{CH}_2$  rocking and twisting,  $\text{CH}_3$  asymmetric deformation, and N–H parallel bending motions with a significant amount of C–N stretching<sup>14</sup>. The IR band at 1107  $\text{cm}^{-1}$  in DMEDA (Figure 4b) decreases in intensity and shifts to a slightly lower frequency upon crystallization. In

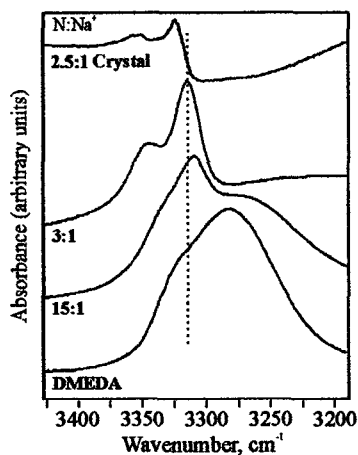


**Figure 5:** IR spectra of DMEDA with varying concentrations of NaTf in the NH stretching region.

addition, the intensity of the DMEDA band at  $1122\text{ cm}^{-1}$  diminishes with increasing NaTf composition. In the Raman spectra (Figure 4c), the bands at  $1125$  and  $1150\text{ cm}^{-1}$  in DMEDA shift to  $1114$  and  $1140\text{ cm}^{-1}$  when NaTf is added. This is due to the sodium atoms coordinating the nitrogen atoms, which delocalizes the electron densities in the C-N bonds thus lowering these band frequencies. We note in passing that the band associated with the  $\text{CF}_3$  asymmetric stretching motion in the 15:1 sample ( $1160\text{ cm}^{-1}$ ) shifts to higher frequencies ( $1182\text{ cm}^{-1}$ ) upon crystallization.

The IR spectra of the NH stretching region shown in Figure 5 are especially interesting. There is a large broad feature in DMEDA centered at  $3282\text{ cm}^{-1}$  with a shoulder at  $3330\text{ cm}^{-1}$ . Upon addition of NaTf to bring the solution to a 15:1 composition, the shoulder shifts to  $\sim 3335\text{ cm}^{-1}$  and a new band at  $3310\text{ cm}^{-1}$  rises out of a very broad feature. In the 3:1 solution, this new band is more intense and shifts to  $3315\text{ cm}^{-1}$ , while the shoulder shifts to  $3344\text{ cm}^{-1}$  and becomes more prominent. Upon crystallization, these two bands shift to  $3324$  and  $3352\text{ cm}^{-1}$ , respectively. These shifts in band frequencies in the NH region are due to the formation of intermolecular hydrogen bonding in the crystal and the loss of intramolecular hydrogen bonding networks based on computational analysis<sup>19</sup>.

#### 4. Conclusions

Single crystals of DMEDA:NaTf have been isolated and characterized using X-ray diffraction, DSC, IR, and Raman techniques. The complex structure of the DMEDA:NaTf crystal, in particular the formation of polymeric-like chains, reflects the

hydrogen bonding interactions of the DMEDA NH group  $[(\text{CH}_3\text{NHCH}_2)_2]$ . By contrast, these interactions are nonexistent in the crystal structure of the related N,N,N',N'-tetramethylethylenediamine: NaTf or  $((\text{CH}_3)_2\text{NCH}_2)_2\text{:NaTf}$  compound, whose unit cells contain discrete tetrameric units.

The coordination of the triflate ion by sodium ion consists primarily of contact ion pairs in the 15:1 composition. In the 3:1 solution, spectra of the triflate ion in the  $\nu_s(\text{SO}_3)$  region suggest the presence of more highly coordinated  $[\text{Na}_2\text{Tf}]^+$  species such as are found in the crystal. However, there is no evidence for the presence of an  $[\text{Na}_3\text{Tf}]^{2+}$  species in solution.

The similarity of the vibrational mode frequencies and intensities in the spectral region sensitive to the conformation of the DMEDA molecule argues that the conformation of DMEDA in the more concentrated salt solutions is similar to that in the crystal. This conclusion is supported by the comparison of modes in the  $1100\text{--}1200\text{ cm}^{-1}$  range.

#### 5. Acknowledgements

Thanks to Shawna York for the spectroscopic IR and Raman data of DMEDA. This work was partially supported by funds from the National Science Foundation, Contract No. DMR-0072544.

#### 6. References

- (1) Fenton, D. E.; Parker, J. M.; Wright, P. V. Complexes of alkali metal ions with poly(ethylene oxide). *Polymer* **1973**, *14*, 589.
- (2) Armand, M. B.; Chabagno, J. M.; Duclot, M. *J. Sec. Int. Conf. on Solid Elect.* **1978**, *St. Andrews, Scotland*.
- (3) Papke, B. L.; Ratner, M. A.; Shriver, D. F. Vibrational Spectroscopic Determination of Structure and Ion Pairing in Complexes of Poly(ethylene oxide) with Lithium Salts. *J. Electrochem. Soc.* **1982**, *129*, 1434.
- (4) Armand, M. B.; Chabagno, J. M.; Duclot, M. J. Polyethers as solid electrolytes. In *Fast Ion Transport in Solids*; Vashista, P., Mundy, J. M., Shenoy, G. K., Eds.; Elsevier: Amsterdam, 1979; pp 131.
- (5) Huang, W.; Frech, R.; Johansson, P.; Lindgren, J. Cation-Polymer Interaction and Ionic Association in Diglyme- $\text{LiCF}_3\text{SO}_3$  and Diglyme-Propylene carbonate- $\text{LiCF}_3\text{SO}_3$  Complexes. *Electrochim. Acta* **1995**, *40*, 2147.
- (6) Bruce, P. G. Effect of Ion Association on Transport in Polymer Electrolytes. *Faraday Discuss. Chem. Soc.* **1989**, *88*, 43.

- (7) Takahashi, T.; Davis, G. T.; Chiang, C. K.; Harding, C. A. Chemical Modification of Poly(ethylene imine) for Polymeric Electrolyte. *Solid State Ionics* **1986**, *18* -19, 321.
- (8) Harris, C. S.; Shriver, D. F.; Ratner, M. A. Complex Formation of Poly(ethylenimine) with Sodium Triflate and Conductivity Behavior of the Complexes. *Macromolecules* **1986**, *19*, 987.
- (9) Harris, C. S.; Ratner, M. A.; Shriver, D. F. Ionic Conductivity in Branched Polyethylenimine-Sodium Trifluoromethanesulfonate Complexes. Comparisons to Analogous Complexes Made with Linear Polyethyleneimine. *Macromolecules* **1987**, *20*, 1778.
- (10) Chiang, C. K.; Davis, G. T.; Harding, C. A.; Takashi, T. Polyethyleneimine-sodium iodide complexes. *Macromolecules* **1985**, *18*, 825.
- (11) Chiang, C. K.; Davis, G. T.; Harding, C. A.; Takashi, T. Polymeric electrolyte based on Poly(ethylene imine) and Lithium salts. *Solid State Ionics* **1986**, *18&19*, 300.
- (12) York, S. S.; Boesch, S. E.; Wheeler, R. A.; Frech, R. Vibrational Assignments for High Molecular Weight Linear Polyethylenimine (LPEI) based on Monomeric and Tetrameric Model Compounds. *Macromolecules* **submitted 2003**.
- (13) Sanders, R. A.; Boesch, S. A.; Snow, A. G.; Hu, L.; Frech, R.; Wheeler, R. A.; Glatzhofer, D. T. Spectroscopic Investigation of Linear Poly(N-methylethylenimine), LPMEI, using a model Compound: N,N,N',N',N"-Pentamethyldiethylenetriamine (PMDETA) with LiCF<sub>3</sub>SO<sub>3</sub> and NaCF<sub>3</sub>SO<sub>3</sub>. **manuscript in progress**.
- (14) Boesch, S. E.; York, S. S.; Frech, R.; Wheeler, R. A. An Experimental and Computational Investigation of the Structure and Vibrations of Dimethylethylenediamine, a model for poly(ethylenimine). *Phys. Chem. Comm.* **2001**, *1*.
- (15) York, S. R. S. Local Structures and Conductivity in Polyethylenimine and Polyphosphazene Polymer Electrolytes. Dissertation, University of Oklahoma, 2002.
- (16) Rhodes, C. P.; Khan, M.; Frech, R. Crystalline Phases of Poly(Ethylene Oxide) Oligomers and Sodium Triflate: Changes in Coordination and Conformation with Chain Length. *J. Phys. Chem. B* **2002**, *106*, 10330.
- (17) Rhodes, C. P.; Frech, R. Cation-anion and cation-polymer interactions in (PEO)<sub>n</sub>NaCF<sub>3</sub>SO<sub>3</sub> (n=1-80). *Solid State Ionics* **1999**, *121*, 91.
- (18) York, S.; Frech, R.; Snow, A.; Glatzhofer, D. A Comparative Vibrational Spectroscopic Study of Lithium Triflate and Sodium Triflate in Linear Poly(ethylenimine). *Electrochimica Acta* **2001**, *46*, 1533.
- (19) York, S. S.; Boesch, S. E.; Wheeler, R. A.; Frech, R. The Effects of Lithium Triflate and Lithium Bromide on the Vibrational Frequencies of DMEDA. *Phys. Chem. Comm.* **2002**, 99.
- (20) Kakihana, M.; Schantz, S.; Torell, L. M. Dissociated Ions and Ion-Ion Interactions in Poly(ethylene oxide) Based NaCF<sub>3</sub>SO<sub>3</sub> Complexes. *Solid State Ionics* **1990**, *40/41*, 641.
- (21) Fately, W. G.; Dollish, F. R.; McDevitt, N. T.; Bentley, F. F. *Infrared and Raman Selection rules for molecular and lattice vibrations: The Correlation Method*; Wiley-Interscience: New York, 1972.
- (22) Matsuura, H.; Fukuhara, K. Vibrational Spectroscopic Studies of Conformation of Poly(oxyethylene). II. Conformation-Spectrum Correlations. *J. Poly. Sci. B* **1986**, *24*, 1383.
- (23) Frech, R.; Huang, W. Polymer Conformation and Ionic Association in Complexes of Lithium, Sodium and Potassium Triflate with Poly(ethylene oxide) Oligomers. *Solid State Ionics* **1994**, *72*, 103.
- (24) Frech, R.; Huang, W. Conformational Changes in Diethylene Glycol Dimethyl Ether and Poly(ethylene oxide) Induced by Lithium Ion Complexation. *Macromolecules* **1995**, *28*, 1246.
- (25) Goutev, N.; Ohno, K.; Matsuura, H. Raman Spectroscopic Study on the Conformation of 1,2-Dimethoxyethane in the Liquid Phase and in Aqueous Solution. *J. Phys. Chem. A* **2000**, *104*, 9226.
- (26) Murcko, M. A.; DiPaola, R. A. Ab Initio Molecular Orbital Conformational Analysis of Prototypical Organic Systems. 1. Ethylene Glycol and 1,2-Dimethoxyethane. *J. Am. Chem. Soc.* **1992**, *114*, 10010.



## **II. TMEDA complexed with LiTf and NaTf**

**Structural Investigation of Crystalline and Solution Phases in N,N,N',N'-Tetramethylethylenediamine (TMEDA) with Lithium Triflate (LiCF<sub>3</sub>SO<sub>3</sub>) and Sodium Triflate (NaCF<sub>3</sub>SO<sub>3</sub>).**

**Rebecca A. Sanders, Roger Frech\*, and Masood A. Khan.**

*Department of Chemistry and Biochemistry, University of Oklahoma, 620 Parrington Oval,  
Norman, OK 73019*

Linear poly(N-methylethylenimine) [LPMEI], a methylated derivative of linear poly(ethylenimine) [LPEI], shows potential as a polymer electrolyte host. The interactions of LPMEI with lithium and sodium cations are modeled by solutions of N, N, N', N'-tetramethylethylenediamine, TMEDA, containing either dissolved lithium triflate [LiTf] or sodium triflate [NaTf]. During these studies, crystalline compounds were discovered and characterized by x-ray diffraction, differential scanning calorimetry, and Fourier transform infrared spectroscopy (FT-IR). The TMEDA:LiTf crystallizes as dimers in an orthorhombic unit cell in the Pccn space group; however the TMEDA:NaTf crystallizes as tetramers in a triclinic unit cell in the P $\bar{1}$  space group. A spectroscopic comparison of TMEDA, TMEDA:LiTf crystal, TMEDA:NaTf crystal, and their corresponding salt solutions over a composition range of 5:1 to 20:1[nitrogen:cation, molar ratio] is carried out using FT-IR and Raman spectroscopy. The triple cation species [Li<sub>2</sub>Tf]<sup>+</sup> is the dominant species in the TMEDA:LiTf solution and exclusively present in the crystal. However, the dominant species in the TMEDA:NaTf samples is the aggregate [Na<sub>3</sub>Tf]<sup>2+</sup>. The N-C-C-N dihedral angle, which appears to be a mixture of gauche minus and trans in both LiTf and NaTf solutions, changes to gauche minus upon crystallization. Finally, the vibrations of individual TMEDA molecules appear to be completely decoupled in the TMEDA:LiTf crystal, in spite of the fact that each dimeric unit contains two TMEDA molecules.

## 1. Introduction

Polymer electrolytes offer a number of advantages for lithium rechargeable battery technology including high energy density, processibility, low environmental impact, and enhanced consumer safety<sup>1</sup>. The most widely studied polymer electrolyte is poly(ethylene oxide), PEO, complexed with various salts such as LiCF<sub>3</sub>SO<sub>3</sub>, LiN(CF<sub>3</sub>SO<sub>2</sub>)<sub>2</sub>, LiSbF<sub>6</sub>, LiBF<sub>4</sub>, and LiClO<sub>4</sub>. The mechanism of ionic transport in these systems is not well understood, especially at the molecular level. However, it is known that cation-anion interactions<sup>2</sup> and cation-polymer interactions<sup>3</sup> play critical roles in ion transport. Both cation-anion and cation-polymer interactions presumably affect the ionic mobilities; in addition, the former are expected to significantly affect the number of effective charge carriers. Cation-anion interactions lead to the formation of associated ionic species, while cation-polymer interactions are

manifested in changes of the polymer backbone conformation. Thus local structures (ionically associated species and local backbone conformation) may be used to directly study the nature of those important interactions and provide essential insight needed to understand the mechanism of ionic transport<sup>4</sup>. Since polymer electrolytes are very complex structures, model compounds can provide crucial information about local structures in polymer electrolytes. Some of the compounds studied as models for PEO-based electrolytes include the dimethyl ethers of ethylene oxides or glymes, i.e. CH<sub>3</sub>(OCH<sub>2</sub>CH<sub>2</sub>)<sub>n</sub>OCH<sub>3</sub> with n = 1–4, complexed with various salts.

Glymes with dissolved salts are useful models of structure and dynamics in high molecular weight PEO-salt systems. In several cases, studies have shown that the conformational changes in the glyme-salt systems are strikingly similar to conformational changes in PEO

complexed with the corresponding salt<sup>5,6</sup>. Further, polymers have been developed with ethylene oxide side chains as polymer electrolyte hosts; most notable among these is the family of polyphosphazenes with oligoethyleneoxy side groups<sup>7</sup>. Finally, computational studies have been performed on glyme-salt systems to gain insight into the nature of the ion transport mechanism is high molecular weight PEO-salt complexes<sup>8,9</sup>.

Linear poly(ethylenimine) or LPEI is a synthetically versatile polymer host compared to PEO, in that various groups can be attached to the backbone nitrogen atom. Pure LPEI has highly crystalline domains, therefore it exhibits poor conductivity. By adding various side chains (e.g.,  $-\text{CH}_3$ ) to LPEI, the crystallinity is decreased. Linear poly(*N*-methylethylenimine), LPMEI, is a methyl-substituted derivative of LPEI. LPMEI is completely amorphous at room temperature unlike LPEI, which melts at 58°C<sup>10-12</sup>. To achieve a better understanding of LPMEI, *N,N,N',N'*-tetramethylethylenediamine (TMEDA) is used as a model compound for LPMEI. While studying solutions of TMEDA with  $\text{LiCF}_3\text{SO}_3$  (LiTf) and  $\text{NaCF}_3\text{SO}_3$  (NaTf) in TMEDA, crystalline compounds were discovered. This paper describes the characterization of the crystalline and amorphous phases in TMEDA:LiTf and TMEDA:NaTf systems using x-ray diffraction, Fourier transform infrared spectroscopy (FT-IR), Raman spectroscopy, and differential scanning calorimetry (DSC). Structural information obtained from the TMEDA:LiTf and TMEDA:NaTf crystals provides a better understanding of the local environment of TMEDA and the triflate anion in TMEDA:LiTf and TMEDA:NaTf solutions.

## 2. Experimental

**2.1 Sample Preparation.** *N,N,N',N'*-tetramethylethylenediamine (TMEDA), LiTf, and NaTf were obtained from Aldrich. TMEDA was distilled over sodium metal. LiTf and NaTf were heated under vacuum at 120°C for 48 hours. The chemicals were stored and used in a dry nitrogen glovebox ( $\text{VAC}_2 \leq 1 \text{ ppm H}_2\text{O}$ ) at room temperature. To prepare the solutions, LiTf was dissolved into TMEDA at various concentrations and stirred for at least 48 hours. Similar sample preparation was used for the NaTf samples except the samples were stirred only for 4 hours. The compositions of the solutions are reported as a nitrogen to cation molar ratio (*N:M*, *M* = Li, Na). At higher triflate compositions, the solutions contained both a liquid and a gel-like phase that formed within 24 hours of preparing the sample. Eventually, all the samples become phase-

separated. Several months later, a fine-grained, gritty textured material had formed at the gel-liquid interface and on the glass surface just above the sample. After about 6 months, the entire sample was composed of crystals with only a small amount of residual solvent in the vial. The crystals were allowed to completely dry in a nitrogen atmosphere. The formation of crystals was evident in all of the TMEDA:LiTf and TMEDA:NaTf samples prepared.

**2.2 X-ray.** Single crystals for x-ray analysis were grown and isolated from a 38:1 TMEDA:LiTf solution and a 20:1 TMEDA:NaTf solution. X-ray data were collected at 173 (2) K on a Bruker P4 diffractometer using  $\text{MoK}\alpha$  radiation ( $\lambda = 0.71073 \text{ \AA}$ ). The data were corrected for Lorentz and polarization effects; an absorption correction was not applied since it was judged to be insignificant. The structure was solved by the direct method using the SHELXTL system and refined by full-matrix least squares on  $F^2$  using all reflections. All nonhydrogen atoms were refined anisotropically, and all hydrogen atoms were included with idealized parameters.

For the TMEDA:LiTf crystal, the final  $R_1 = 0.068$  is based on 1541 "observed reflections" [ $I > 2\sigma(I)$ ], and  $wR^2 = 0.201$  is based on all reflections (2406 unique data). For the TMEDA:NaTf crystal, the final  $R_1 = 0.056$  is based on 6277 "observed reflections" [ $I > 2\sigma(I)$ ], and  $wR^2 = 0.153$  is based on all reflections (9715 unique data). In the TMEDA:NaTf crystal, some parts of the TMEDA are disordered as evident by the large thermal parameters of these atoms. In addition, the positions of the C17 and C18 atoms are not well defined; therefore, these atoms were resolved in two components with a fifty percent occupancy for each component.

**2.3 Differential Scanning Calorimetry.** A single crystal weighing approximately 3.5 mg was sealed in a 40  $\mu\text{L}$  aluminum pan. For both crystals, DSC data were collected using a Mettler DSC 820 calorimeter with Star<sup>c</sup> software (v.6.10) under dry nitrogen purge. The TMEDA:LiTf crystal data were collected during two heating and cooling cycles between 0°C and 250°C at a heating and cooling rate of 5°C/min. However, the TMEDA:NaTf crystals were cycled between 0°C and 300°C at rate of 5°C/min.

**2.4 FT-IR & Raman Spectroscopy.** For FT-IR measurements, the TMEDA, TMEDA:LiTf solutions, and TMEDA:NaTf solutions were placed between zinc selenide windows in a sealed sample holder. Finely ground crystals were prepared as KBr pellets. FT-IR data were recorded on a Bruker IFS66V with a KBr beam splitter over a

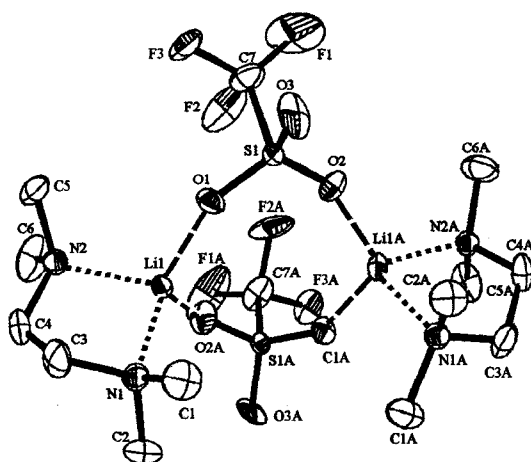


**Figure 1:** Dimer of the TMEDA:LiTf crystal showing the four-fold coordination of the lithium atom.

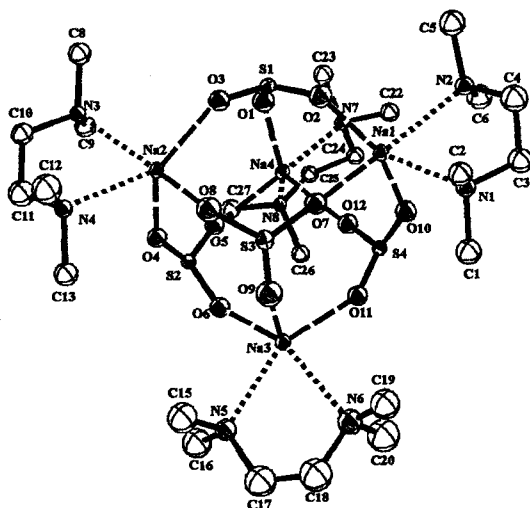


**Figure 2:** Tetramer of the TMEDA:NaTf crystal. The CF<sub>3</sub> groups of the triflate ions are not shown for clarity of the figure.

range of 500–4000 cm<sup>-1</sup> (1 cm<sup>-1</sup> resolution). The spectra of the solutions were measured under a dry air purge; the crystal data were collected under vacuum (8 mbar). For the Raman measurements, the TMEDA and TMEDA:LiTf solutions were placed in a solution well and covered with a glass cover plate; the single crystal was sealed into a quartz cuvette in the glovebox. Raman data were recorded with a Jobin-Yvon T64000 system in the triple subtractive mode with a CCD detector using the 514.5 nm line of an argon laser for excitation. All Raman data were collected in a 180° scattering geometry at a laser power of 300 mW measured at the laser head.

### 3. Results and Discussion

#### 3.1 Crystal structure. The TMEDA:LiTf crystal

**Table 1:** Structural data of the TMEDA:LiTf and TMEDA:NaTf crystals.

Parameters	TMEDA LiTf	TMEDA NaTf
Crystal system	Orthorhombic	Triclinic
Space group	Pccn	$P\bar{1}$
Temperature	173 (2) K	173 (2) K
a (Å)	12.272 (3)	10.6695 (14)
b (Å)	13.544 (3)	12.5383 (16)
c (Å)	16.425 (4)	22.392 (3)
$\alpha$	90°	92.054 (9)°
$\beta$	90°	100.104 (9)°
$\gamma$	90°	107.611 (9)°
Volume (Å <sup>3</sup> )	2730.1 (12)	2798.3 (7)
Z	8	2
Density (Mg/m <sup>3</sup> )	1.325	1.369
R1	0.068	0.056
Crystal size (mm <sup>3</sup> )	0.54 x 0.52 x 0.24	0.38 x 0.36 x 0.32

forms an orthorhombic unit cell in the Pccn space group with Z = 8; the structure consists of independent (TMEDA:LiTf)<sub>2</sub> dimers (**Figure 1**). Each lithium ion is coordinated by two nitrogen atoms and two triflate oxygen atoms, one from each of the two triflate ions in the dimer. The TMEDA:NaTf crystal forms a triclinic unit cell in the  $P\bar{1}$  space group, which contains two tetramers (TMEDA:NaTf)<sub>4</sub> as illustrated in **Figure 2**. The sodium ion is coordinated to three triflate oxygen atoms and two nitrogen atoms. Structural data are summarized in **Table 1**; selected bond lengths and angles for the TMEDA:LiTf and TMEDA:NaTf crystals are listed in **Tables 2 and 3**.

The dimeric TMEDA:LiTf crystal structure is similar to the dimeric crystal structure of diglyme [CH<sub>3</sub>(OCH<sub>2</sub>CH<sub>2</sub>)<sub>2</sub>OCH<sub>3</sub>]:LiTf or G2:LiTf, although in the G2:LiTf crystal the lithium atom is coordinated to three oxygen atoms of G2 and two triflate oxygen atoms<sup>5</sup>. An additional structural comparison can also be made with monoglyme [CH<sub>3</sub>(OCH<sub>2</sub>CH<sub>2</sub>)OCH<sub>3</sub>]:LiTf, G1:LiTf, where the lithium ion is four-coordinate in the crystalline compound<sup>13</sup>. Both TMEDA and G1 have two heteroatoms that provide coordinating sites for the lithium ion. However, TMEDA has two methyl groups attached to the nitrogen atom, whereas G1 has only one methyl group coordinated to the ether oxygen. Therefore, the greater steric hindrance in TMEDA plays a role in its coordination chemistry. For example, in the G1:LiTf crystal each G1

**Table 2:** Selected bond lengths (Å) and angles (°) for the TMEDA:LiTf and TMEDA:NaTf crystals.

bond	$X = Li$	$X = Na$
X-N	2.077 (5)	2.502 (2)
	2.066 (5)	2.521 (2)
		2.472 (2)
		2.519 (2)
		2.489 (3)
		2.523 (3)
		2.495 (2)
		2.5101 (18)
X-O	1.805 (6)	2.269 (2)
	1.836 (6)*	2.283 (2)
	1.956 (7)*	2.2830 (18)
	1.987 (6)	2.276 (2)
		2.2779 (19)
		2.2864 (19)
		2.261 (2)
		2.303 (2)
		2.3160 (19)
		2.270 (2)
<i>bond sequence</i>		2.2722 (19)
		2.310 (2)
<hr/>		
<i>bond sequence</i>		
N-X-N	89.18 (18)	73.19 (7)
		72.67 (7)
		71.29 (9)
		72.22 (7)

molecule is coordinated to two different lithium atoms<sup>13</sup>. Further, the lithium ion in the G1:LiTf crystal is also coordinated to three different triflate oxygen atoms, unlike the lithium ion-triflate ion coordination in the TMEDA:LiTf crystal<sup>13</sup>.

The conformational structures of the TMEDA oligomers can be characterized in terms of the C-N-C-C and N-C-C-N dihedral angles (gauche, g,  $60^\circ \pm 30^\circ$ ; gauche minus,  $\bar{g}$ ,  $-60^\circ \pm 30^\circ$ ; s,  $120^\circ \pm 30^\circ$ ; s minus,  $\bar{s}$ ,  $-120^\circ \pm 30^\circ$  trans, t,  $\pm 180^\circ \pm 30^\circ$ ). An individual TMEDA molecule can occur in four different conformations because of the two methyl groups attached to each nitrogen atom. However, the N-C-C-N dihedral angle is of most interest because it is directly affected by the coordination of the cation to the nitrogen atoms. In the TMEDA:LiTf crystal (Table 3), the N-C-C-N dihedral angle ( $-54.0^\circ$ ) leads to conformations  $x\bar{g}x'$  where  $x, x' = t$  or  $\bar{g}$ . However, the TMEDA:NaTf crystal has four different N-C-C-N dihedral angles ( $-53.1^\circ$ ,  $-60.3^\circ$ ,  $55.4^\circ$ ,  $42.3^\circ$ ) which leads to two TMEDA molecules with  $x\bar{g}x'$  ( $x, x' = t$  or  $\bar{g}$ ), one with  $x_1gx_1'$  ( $x_1, x_1' = t$  or  $g$ ), and one

**Table 3:** Dihedral angles of TMEDA:LiTf and TMEDA:NaTf crystals with the corresponding conformations.

TMEDA:NaTf		
<i>bond sequence</i>	<i>dihedral angle. (°)</i>	<i>conformation</i>
C-N1-C-C	154.6 (3)	t
C-N1-C-C	-84.1 (3)	$\bar{g}$
N1-C-C-N2	-53.1 (4)	$\bar{g}$
C-C-N2-C	-85.8 (4)	$\bar{g}$
C-C-N2-C	156.0 (3)	t
C-N3-C-C	-154.0 (2)	t
C-N3-C-C	85.7 (3)	g
N3-C-C-N4	55.4 (3)	g
C-C-N4-C	74.4 (3)	g
C-C-N4-C	-164.9 (2)	t
C-N5-C-C	-145.0(6), 158.2(4)	$\bar{s}, t$
C-N5-C-C	95.9(7), -83.1(5)	s, $\bar{g}$
N5-C-C-N6	42.3(8), -65.4(6)	g, $\bar{g}$
C-C-N6-C	105.2(5), -69.9(7)	s, $\bar{g}$
C-C-N6-C	-138.1(5), 166.8(5)	$\bar{s}, t$
C-N7-C-C	167.2 (2)	t
C-N7-C-C	-72.3 (3)	$\bar{g}$
N7-C-C-N8	-60.3 (3)	$\bar{g}$
C-C-N8-C	-77.0 (3)	$\bar{g}$
C-C-N8-C	162.3 (2)	t
<hr/>		
TMEDA:LiTf		
C1-N-C3-C4	158.0 (3)	t
C2-N-C3-C4	-80.6 (4)	$\bar{g}$
N-C3-C4-N	-54.0 (5)	$\bar{g}$
C3-C4-N-C5	-81.2 (4)	$\bar{g}$
C3-C4-N-C6	158.3 (4)	t

\*The symmetry transformation ( $-x + 1/2, -y + 1/2, z$ ) used to generate equivalent atoms.

with either  $x_2gx_2'$  ( $x_2, x_2' = \bar{s}$  or s) or  $x_3\bar{g}x_3'$  ( $x_3, x_3' = \bar{g}$  or t) conformations. There are two possible conformations about the C17 and C18 bond because these atoms are disordered.

The TMEDA conformations in the TMEDA:LiTf crystal ( $x\bar{g}x'$ ) differ from those in the crystals of G1:LiTf (ttt) and G2:LiTf (tgt - t $\bar{g}$ t). The major difference is in the x-C-C-x dihedral angles ( $x = N, O$ ), which are gauche minus in TMEDA:LiTf, trans in G1:LiTf, and gauche/gauche minus in G2:LiTf<sup>5,13</sup>. These differences are mainly due to packing requirements originating in the different molecular structures of the organic constituents.

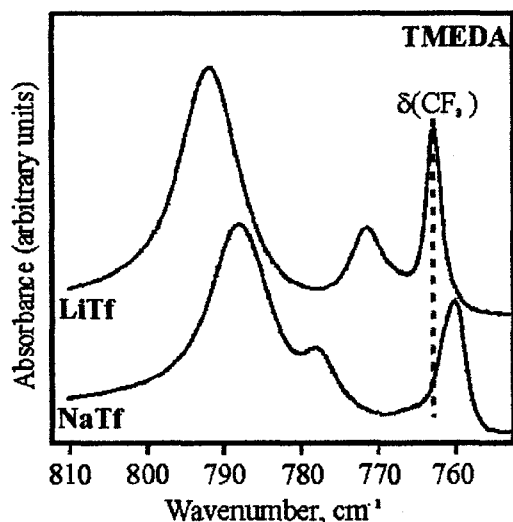


**Figure 3:** FT-IR spectra of crystalline TMEDA:LiTf and TMEDA:NaTf in the 750 – 810  $\text{cm}^{-1}$  region.

The Li–N bond length ( $\sim 2.08$  Å) in the TMEDA:LiTf crystal is 0.42 Å shorter than the Na–N bond length ( $\sim 2.50$  Å) in the TMEDA:NaTf crystal (Table 2). In addition, the Li–O bond length ( $\sim 1.90$  Å) is 0.38 Å shorter than the Na–O bond length ( $\sim 2.28$  Å). These differences are greater than the differences in their ionic radii; therefore, suggesting the lithium ion is more strongly coordinated to both the nitrogen and oxygen atom compared to the sodium ion. There is also a  $17^\circ$  difference between the N–Li–N ( $\sim 89^\circ$ ) and N–Na–N ( $\sim 72^\circ$ ) bond angles, which correlates with the differences in the cation–nitrogen bond lengths. However, changing the cation does not significantly affect the F–C–F bond angles, or the C–C and C–N bond distances (data not shown).

The Li–N bond length ( $\sim 2.08$  Å) in the TMEDA:LiTf crystal is slightly longer than the Li–O (ether oxygen) bond length in G1:LiTf (1.93 Å) and similar to that in the G2:LiTf crystals (2.10 Å)<sup>5</sup>. In addition, the Li–O (triflate oxygen) bond distances in the TMEDA:LiTf crystal (1.81 – 1.99 Å) have a greater spread of values compared to G1:LiTf (1.93 – 1.94 Å) and G2:LiTf (1.94 – 1.97 Å)<sup>5,13</sup>. The Li–O–S angles in the TMEDA:LiTf crystal ( $136.9 - 68.0^\circ$ ) are very similar to the Li–O–S (triflate oxygen) bond angles in the G2:LiTf crystal ( $144 - 161^\circ$ )<sup>14</sup>.

**3.2 Thermal Analysis.** Differential scanning calorimetry (DSC) was used to characterize melting and recrystallization processes in the TMEDA:LiTf and TMEDA:NaTf crystals. In the DSC thermogram of the TMEDA:LiTf crystal (figure not shown), there is an endothermic sharp

peak at  $154^\circ\text{C}$  due to the melting of the crystalline compound. The onset of recrystallization occurs at  $110^\circ\text{C}$ . In a second thermal analysis cycle, the melting and recrystallization temperatures decrease to  $128$  and  $107^\circ\text{C}$ , respectively, indicating some degree of thermal hysteresis. However, the data may also be interpreted as incongruent melting/recrystallization. In addition, the melting peak becomes smaller and broader, indicating a loss of crystallinity of the sample. The TMEDA:LiTf crystal is more thermally stable compared to the G1:LiTf or the G2:LiTf crystals, which melt at  $-3$  and  $27^\circ\text{C}$ , respectively<sup>5,13</sup>.

The thermogram of the TMEDA:NaTf crystal (figure not shown) is different than the thermogram of the TMEDA:LiTf crystal. For instance, TMEDA:NaTf has four endothermic phase transitions occurring at  $128$ ,  $193$ ,  $199$ , and  $237^\circ\text{C}$  in the first heating cycle. Only the two transitions at  $128$  and  $237^\circ\text{C}$  appear in the cooling cycles and are observed at  $110$  and  $238^\circ\text{C}$ . During the second heating cycle these transitions occur at  $118$  and  $238^\circ\text{C}$ . In addition, the peak at  $\sim 110^\circ\text{C}$  becomes broader and smaller, indicating a decrease in the crystallinity of the sample. However, the phase transition at  $237^\circ\text{C}$  is completely reversible, with no hysteresis within experimental error. The melting temperature of the TMEDA:NaTf crystal is higher than the TMEDA:LiTf crystal, partly because the crystal consists of a much larger network structure.

**3.3 Vibrational Spectroscopy.** Knowledge of the TMEDA:LiTf and TMEDA:NaTf crystal structures provides unambiguous information about the local structures in the crystals. In turn, this knowledge can result in critical insight into local structures in TMEDA:LiTf and TMEDA:NaTf solutions through comparative spectroscopic studies of both crystalline and solution phases. This is accomplished by identifying the spectral signatures of local structures in the TMEDA:LiTf and TMEDA:NaTf crystals, with particular attention to the bands from  $770$  to  $1000$   $\text{cm}^{-1}$ . The frequencies and intensities of bands in this region are sensitive to conformational changes in the TMEDA backbone. Bands in this region have also been shown to provide information about backbone conformation in ethylene oxide-based systems<sup>15</sup>. Figure 3 shows that there are some differences between the crystalline TMEDA:LiTf and TMEDA:NaTf spectra in this conformation-sensitive region. The bands at  $772$  (TMEDA:LiTf) and  $778$   $\text{cm}^{-1}$  (TMEDA:NaTf) are predominately due to  $\text{CH}_2$  rocking motion<sup>15</sup>. In addition, the TMEDA band at  $792$   $\text{cm}^{-1}$  in the TMEDA:LiTf crystal spectrum is  $4$   $\text{cm}^{-1}$  higher than in the

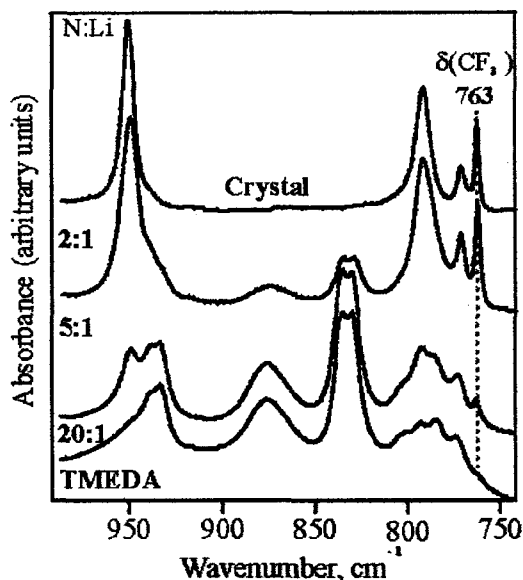


**Figure 4a:** FT-IR spectra of TMEDA with varying concentrations of LiTf in the  $\delta(\text{CF}_3)$  and conformation regions.

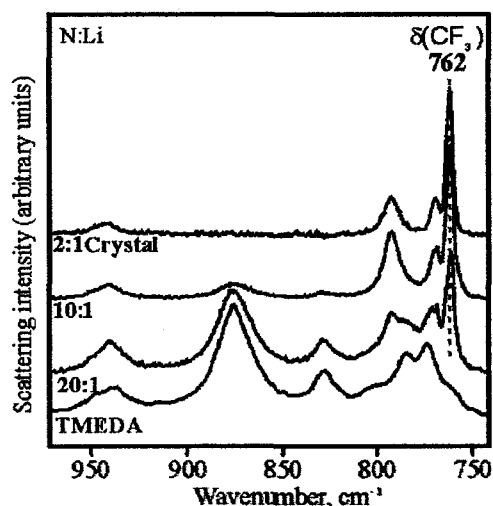


**Figure 4b:** Raman spectra of TMEDA with varying concentrations of LiTf in the  $\delta(\text{CF}_3)$  and conformation regions.

TMEDA:NaTf crystal spectrum. It is important to note that in the TMEDA:NaTf crystal, the  $788\text{ cm}^{-1}$  band is attributed primarily to a predominant  $\text{CH}_2$  twisting motion<sup>16</sup>. However, the  $792\text{ cm}^{-1}$  band in the TMEDA:LiTf crystal is due to a mixed mode of C-N stretching,  $\text{CH}_2$  twisting and  $\text{CH}_2$  wagging motions<sup>15</sup>.

From parallel studies of crystalline TMEDA:LiTf, TMEDA, and solutions of LiTf in TMEDA, information about the conformational

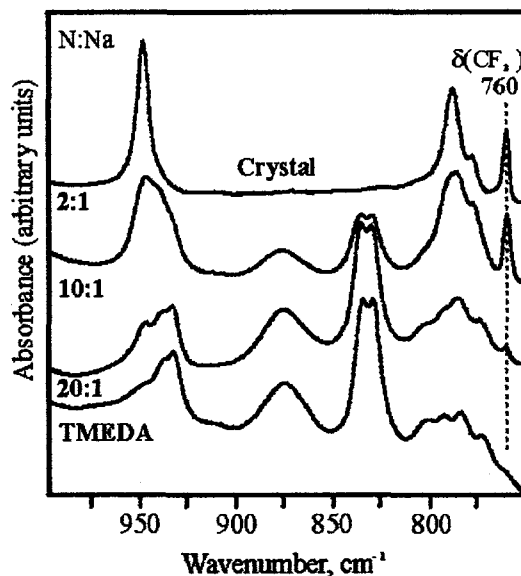


**Figure 5:** FT-IR spectra of TMEDA with varying concentrations of NaTf in the  $\delta(\text{CF}_3)$  and conformation regions.

bands in the predominantly  $\nu(\text{C-N})$  region at  $830$ ,  $835$ , and  $876\text{ cm}^{-1}$  diminish in intensity with increasing LiTf concentration and completely disappear in the spectrum of the TMEDA:LiTf crystal<sup>16</sup>. Computational studies of TMEDA in the gas phase attribute these bands to TMEDA a trans N-C-C-N dihedral angle<sup>16</sup>. However, the bands in the  $700$  to  $800\text{ cm}^{-1}$  and  $900$  to  $1000\text{ cm}^{-1}$  regions are due to a TMEDA molecule with a gauche minus N-C-C-N dihedral angle<sup>16</sup>. Therefore, the N-C-C-N dihedral angle, which is a mixture of gauche and trans in the TMEDA:LiTf solutions, appears to change to gauche minus upon crystallization. This interesting phenomenon is also observed in the Raman spectra (Figure 4b) and TMEDA:NaTf spectra (Figure 5). Striking differences between solution spectra and crystalline spectra reflecting dramatic conformational changes upon crystallization were also observed in the G1:LiTf system<sup>13</sup>. However, in that system the O-C-C-O dihedral angle of G1 changes from gauche in solution to trans upon crystallization<sup>13</sup>.

Bands between  $770$ – $810\text{ cm}^{-1}$  and  $930$ – $940\text{ cm}^{-1}$  are also affected by the conformational changes during crystallization of the TMEDA:LiTf and TMEDA:NaTf compounds. In TMEDA (Figure 4a), there are at least four bands in the  $770$ – $810\text{ cm}^{-1}$  region. A computational analysis established that the TMEDA bands in this region are a complex mixture of C-C and C-N stretching,  $\text{CH}_2$  wagging,  $\text{CH}_2$  twisting, and  $\text{CH}_2$  rocking motions<sup>17</sup>. The bands at  $772$  and  $792\text{ cm}^{-1}$  become

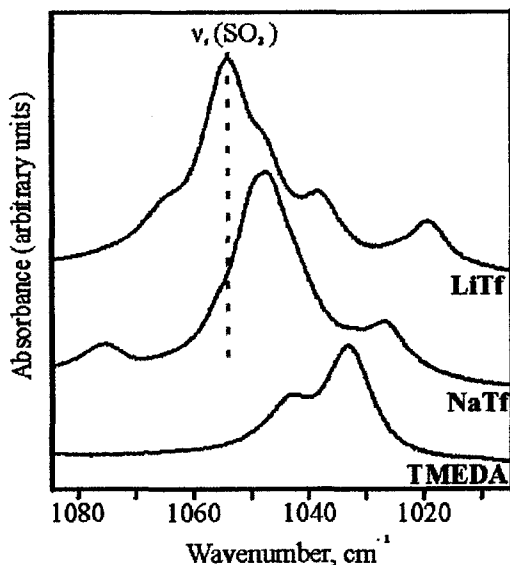


**Figure 6:** FT-IR spectra of TMEDA with varying LiTf and NaTf concentrations in the  $\nu_s(\text{SO}_3)$  region.

more prominent with increasing LiTf concentrations until, in the crystal, they are the dominant TMEDA bands in this region. Similar results are seen in the TMEDA:NaTf samples (Figure 5) where the two prominent bands in the crystal are at 778 and 788  $\text{cm}^{-1}$ .

The nature of the vibrational modes of the TMEDA bands in this region ( $\sim 780 \text{ cm}^{-1}$ ) changes upon addition of salt. When NaTf is added to TMEDA, the TMEDA modes change from C-C and C-N stretching,  $\text{CH}_2$  wagging, and  $\text{CH}_2$  twisting motions to a predominately  $\text{CH}_2$  twisting motion<sup>17</sup>. However when LiTf is added, the TMEDA modes in this region involve primarily C-N stretching,  $\text{CH}_2$  wagging and  $\text{CH}_2$  twisting motions<sup>17</sup>.

The change in TMEDA conformation has a more dramatic effect on the 930–940  $\text{cm}^{-1}$  region, which is comprised mostly of  $\text{CH}_2$  rocking, C-C stretching, and  $\text{CH}_3$  wagging motions<sup>17</sup>. Even in a 20:1 solution composition of TMEDA:LiTf or TMEDA:NaTf, a few bands suggest the early formation of local structures similar to those in the crystal. In Figure 4a, the band at 949  $\text{cm}^{-1}$  increases in intensity and shifts to a higher frequency (951  $\text{cm}^{-1}$ ) with increasing LiTf concentration. Similar behavior is seen in the Raman data shown in Figure 4b. However, when NaTf is added to TMEDA, the 949  $\text{cm}^{-1}$  band does not shift upon crystallization within experimental error (1  $\text{cm}^{-1}$ ). In TMEDA:LiTf, this band (949  $\text{cm}^{-1}$ ) consist primarily of  $\text{CH}_2$  rocking motion,

however in TMEDA:NaTf, this band (948  $\text{cm}^{-1}$ ) is due to both  $\text{CH}_2$  rocking and  $\text{CH}_2$  twisting motions<sup>17</sup>.

The  $\text{CF}_3$  symmetric deformation,  $\delta(\text{CF}_3)$ , region contains distinct bands due to different ionically associated species: "free" ions at 752–753  $\text{cm}^{-1}$ , contact ion pairs  $[\text{MTf}]$  ( $\text{M} = \text{cation}$ ) at 756–758  $\text{cm}^{-1}$ , and the aggregate species  $[\text{M}_2\text{Tf}]^+$  or  $[\text{M}_3\text{Tf}]^{2+}$  at 761–763  $\text{cm}^{-1}$ <sup>18–21</sup>. Therefore, a spectral study of this region can provide additional local structural information about the coordination of the triflate ion by the lithium and sodium ion(s). The spectra-structure correlations of the triflate ion species quoted above have been determined in ethylene oxide-based systems. Therefore, it is necessary to either develop a similar set of correlations in TMEDA or confirm that the ethylene oxide-based correlations may be used in TMEDA systems. In the TMEDA:LiTf crystal, the  $\delta(\text{CF}_3)$  band is measured at 763  $\text{cm}^{-1}$  (IR) and 762  $\text{cm}^{-1}$  (Raman), Figures 4a and 4b. Based on the crystal structure, this frequency is associated with an aggregate species where one triflate ion is coordinated to two lithium ions,  $[\text{Li}_2\text{Tf}]^+$ . The  $[\text{Li}_2\text{Tf}]^+$  aggregate is the dominant species in all TMEDA:LiTf solutions. The frequency of  $[\text{Li}_2\text{Tf}]^+$  in the TMEDA:LiTf crystal agrees well with its frequency in the G2:LiTf crystal, where it is observed at 763  $\text{cm}^{-1}$  (Raman)<sup>5</sup>.

In the TMEDA:NaTf crystal, the  $\delta(\text{CF}_3)$  band is at 760  $\text{cm}^{-1}$ , which can be unambiguously associated with the aggregate species  $[\text{Na}_3\text{Tf}]^{2+}$ . This species dominates even in the solution phase. As illustrated in Figure 3, there is a 3  $\text{cm}^{-1}$  difference in the  $\delta(\text{CF}_3)$  band maximum between TMEDA:LiTf and TMEDA:NaTf crystal spectra. Even though the TMEDA:NaTf forms a higher order aggregate species than TMEDA:LiTf, this species has a slightly lower frequency because the sodium atom is not as strongly coordinated to the triflate ion. In addition, the  $\delta(\text{CF}_3)$  band in the TMEDA:NaTf spectra has a larger bandwidth than in the TMEDA:LiTf spectra.

The frequency of the  $\text{SO}_3$  symmetric stretch,  $\nu_s(\text{SO}_3)$ , is also affected by the coordination of the triflate ion with the cation. Raman-active bands at 1032–1033  $\text{cm}^{-1}$ , 1037–1042  $\text{cm}^{-1}$ , and 1044–1056  $\text{cm}^{-1}$  correspond to "free" ions, contact ion pairs, and aggregate species, respectively, in ethylene oxide-based systems<sup>18–21</sup>. In Figure 6, the  $\nu_s(\text{SO}_3)$  band in the infrared spectra appears at 1054  $\text{cm}^{-1}$  (TMEDA:LiTf crystal) and 1048  $\text{cm}^{-1}$  (TMEDA:NaTf crystal). This frequency difference in the  $\nu_s(\text{SO}_3)$  band is again due to the relatively weaker coordination of the sodium atom with the



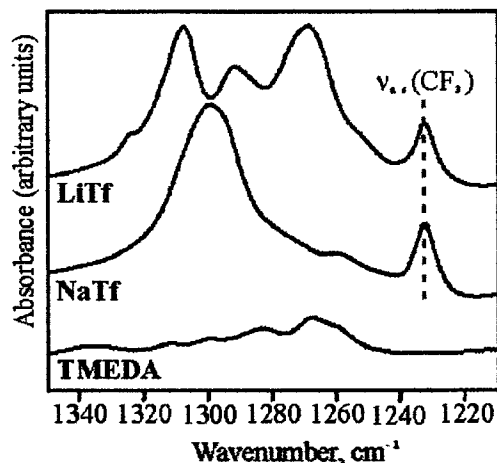


**Figure 7:** FT-IR spectra of the TMEDA and TMEDA crystals with NaTf and LiTf the  $\nu_{as}(\text{SO}_3)$  and  $\nu_{as}(\text{CF}_3)$  regions.

triflate ion oxygen atoms. The latter frequency is the same, within experimental error, as in the ethylene oxide systems. The Raman frequency of the  $\nu_s(\text{SO}_3)$  mode in the TMEDA:LiTf crystal ( $1051 \text{ cm}^{-1}$ ) is comparable to that in the G2:LiTf crystal ( $1053 \text{ cm}^{-1}$ ) because the triflate ion vibrates as a  $[\text{Li}_2\text{Tf}]^+$  species in both crystals<sup>5</sup>. The  $\nu_s(\text{SO}_3)$  frequency (Raman) is higher in the G1:LiTf crystal ( $1056 \text{ cm}^{-1}$ ) because there the triflate ion is coordinated to three lithium ions<sup>5,13</sup>.

The  $\text{SO}_3$  asymmetric stretch,  $\nu_{as}(\text{SO}_3)$ , of the triflate ion is also affected by coordination to the cations, as illustrated in Figure 7. The apparent simplicity of the TMEDA:NaTf crystal spectrum in this region is deceptive. The two-fold degeneracy of the  $\nu_{as}(\text{SO}_3)$  mode in an isolated triflate ion is broken by the potential energy environment in the crystal. Formally, each of the four triflate ions in the asymmetric unit yields two components resulting from the broken degeneracy, for a total of eight vibrational degrees of freedom. However, there are two tetrameric units in the unit cell, i.e.  $Z=2$ . Therefore, there are a total of sixteen vibrational degrees of freedom originating in the  $\nu_{as}(\text{SO}_3)$  mode. These vibrational components are then correlated through intermolecular interactions, resulting in a vibrational multiplet structure that can be analyzed by standard group theoretical methods<sup>22</sup>. The irreducible representations of these modes under the  $P\bar{1}$  unit cell group are given by

$$\Gamma(\nu_{as}(\text{SO}_3)) = 8A_g + 8A_u \quad (1)$$

This analysis predicts eight infrared-active  $\nu_{as}(\text{SO}_3)$  vibrational modes. The data in Figure 7 show that

the splitting in this mode induced by the interaction with the sodium ion and the subsequent coupling interaction of the eight triflate ions in the unit cell are not sufficient to resolve the individual modes predicted by Eq. 1. However the breadth of the feature in Figure 7 probably originates in the overlap of these components.

There are also sixteen degrees of vibrational freedom arising from  $\nu_{as}(\text{SO}_3)$  in the TMEDA:LiTf crystal. A correlation field analysis shows that the  $\nu_{as}(\text{SO}_3)$  modes can be classified according to the irreducible representations of the Pccn unit cell group as

$$\Gamma(\nu_{as}(\text{SO}_3)) = 2A_g + 2B_{1g} + 2B_{2g} + 2B_{3g} + 2A_u + 2B_{1u} + 2B_{2u} + 2B_{3u} \quad (2)$$

Because the sample was in the form of a microcrystalline powder, in principle all six infrared-active components ( $2B_{1u} + 2B_{2u} + 2B_{3u}$ ) are observed in a transmission experiment. In the spectrum, prominent bands are observed at  $1307$  and  $1268 \text{ cm}^{-1}$ , with a smaller, asymmetric band at  $1292 \text{ cm}^{-1}$ . In addition, a very weak band occurs at  $1324 \text{ cm}^{-1}$ . Without an oriented single crystal and a complete set of polarized infrared reflection spectra, a detailed assignment of these four bands in terms of their symmetry species is not possible. In this region, the  $\text{CF}_3$  asymmetric stretching mode occurs at  $1230 \text{ cm}^{-1}$  in both the TMEDA:LiTf and TMEDA:NaTf crystal spectra.

#### 4. Conclusions

Single crystals of TMEDA:LiTf and TMEDA:NaTf have been isolated and characterized using x-ray diffraction, DSC, FT-IR, and Raman techniques. The TMEDA:LiTf crystal (dimer) is structurally different than the TMEDA:NaTf crystal (tetramer), where the lithium ion is four-coordinate and the sodium ion is five-coordinate.

Since the TMEDA:LiTf crystal structure is described by the Pccn ( $D_{2h}^{10}$ ) space group, it has a center of symmetry. Therefore, modes should be either Raman active or infrared active, but none should be simultaneously Raman and infrared active except by coincidence. However, in the TMEDA:LiTf crystal, the majority of the vibrational bands are both IR and Raman active. This suggests that the two TMEDA molecules are vibrationally decoupled, i.e. the vibrations of each TMEDA molecule are sufficiently independent such that the role of the inversion center in coupling vibrations is negligible.

This work demonstrates that spectroscopic studies of the TMEDA:LiTf and TMEDA:NaTf crystals can provide insight into the local structures present in solutions of TMEDA:LiTf and TMEDA:NaTf. Specifically, local structures similar to those in the crystal are present in the TMEDA:LiTf and TMEDA:NaTf solutions, even at a 20:1 composition. In addition, there is evidence of conformational changes occurring in the solutions upon crystallization. A comparison of computational studies in the gas phase, x-ray analyses of the crystal structures, and vibrational measurements of crystalline and solution phases leads to the conclusion that conformation of TMEDA in the TMEDA:LiTf and TMEDA:NaTf solutions changes from a mixture of  $x\bar{g}x$  and  $xtx$  to  $x\bar{g}x$  upon crystallization of the TMEDA:LiTf and TMEDA:NaTf compounds. In addition, the ionic association in TMEDA:LiTf and TMEDA:NaTf solutions is similar to that in the TMEDA:LiTf and TMEDA:NaTf crystals, where the  $[Li_2Tf]^+$  and  $[Na_2Tf]^{2+}$  aggregate species are the primary ionic species present, even in a 20:1 composition.

The lithium ion is more strongly coordinated to both the nitrogen and oxygen atoms than is the sodium ion. Therefore, small frequency shifts in similar bands and changes in the vibrational modes are observed when comparing TMEDA:LiTf to TMEDA:NaTf. Similar results are seen in the poly(ethylene oxide) systems where the lithium ion is more strongly coordinated to the ether oxygen atoms than is the sodium ion.

Finally there are some striking similarities between the TMEDA:LiTf crystal and several glyme:LiTf crystals. Both TMEDA:LiTf and G2:LiTf crystallize as discrete dimers comprised of two cations, two anions, and two solvent molecules. However, the lithium ion is four-fold coordinated in the TMEDA:LiTf crystal and five-fold coordinated in the G2:LiTf crystal. Upon crystallization, the solvent molecules in both TMEDA:LiTf and G1:LiTf undergo dramatic changes in conformation as shown by the values of the N-C-C-N and O-C-C-O dihedral angles, respectively.

## 5. Acknowledgements

This work was partially supported by funds from the National Science Foundation, Contract No. DMR-0072544. We appreciate the assistance of Scott Boesch in the ab initio calculations.

## 6. References

- 1) Gauthier, M.; Bélanger, A.; Kapfer, B.; Vassort, G.; Armand, M. *Polymer Electrolyte Reviews Volume 2*; Elsevier: London, 1989.
- 2) Papke, B. L.; Ratner, M. A.; Shriver, D. F. *J. Electrochem. Soc.* **1982**, *129*, 1434-1438.
- 3) Armand, M. B.; Chabagno, J. M.; Duclot, M. *J. Sec. Int. Conf. on Solid Elect.* **1978**, *St. Andrews, Scotland*.
- 4) Bruce, P. G. *Faraday Discuss. Chem. Soc.* **1989**, *88*, 43-54.
- 5) Rhodes, C. P.; Frech, R. *Macromolecules* **2001**, *34*, 2660-2666.
- 6) Rhodes, C. P.; Khan, M.; Frech, R. *J. Phys. Chem. B* **2002**, *106*, 10330-10337.
- 7) Allcock, H. R.; O'Connor, S. J. M.; Olmeijer, D. L.; Napierala, M. E.; Cameron, C. G. *Macromolecules* **1996**, *29*, 7544-7552.
- 8) Borodin, O.; Smith, G. D. *Macromolecules* **1998**, *31*, 8396-8406.
- 9) Sutjianto, A.; Curtiss, L. A. *J. Phys. Chem. A* **1998**, *102*, 968-974.
- 10) Saegusa, T.; Ikeda, H.; Fujii, H. *Macromolecules* **1972**, *5*, 108.
- 11) Chatani, Y.; Irie, T. *Polymer* **1988**, *29*, 2126-2129.
- 12) Tanaka, R.; Ueoka, I.; Takaki, Y.; Kataoka, K.; Saito, S. *Macromolecules* **1983**, *16*, 849-853.
- 13) Rhodes, C. P.; Khan, M.; Frech, R.; Ruf, M. *J. Phys. Chem.*, **submitted**.
- 14) Rhodes, C. *X-ray data of the diglyme: LiTf crystal, unreported results*.
- 15) Matsuura, H.; Fukuhara, K. *J. Poly. Sci. B* **1986**, *24*, 1383-1400.
- 16) Boesch, S.; Wheeler, R. *Calculation of TMEDA:LiTf in the ttt conformation were preformed using B3LYP, a hybrid Hartree-Fock density functional method, with a basis set of 6-31G(d), unreported results*.
- 17) Boesch, S.; Wheeler, R. *Calculations (for vibrational mode assignments) of TMEDA, TMEDA:LiTf and TMEDA:NaTf were preformed using B3LYP, a hybrid Hartree-Fock/density functional method, with a 6-31G(d) basis set, unreported results*.
- 18) Schantz, S.; Sandahl, J.; Borjesson, L.; Torell, L. M.; Stevens, J. R. *Solid State Ionics* **1988**, *28-30*, 1047-1053.
- 19) Frech, R.; Huang, W. *Solid State Ionics* **1994**, *72*, 103-107.
- 20) Huang, W.; Frech, R.; Wheeler, R. A. *J. Phys. Chem.* **1994**, *98*, 100-110.
- 21) Frech, R.; Huang, W.; Dissanayake, M. A. K. *L. Mat. Res. Soc. Symp. Proc.* **1995**, *369*, 523-534.

- 22) Fately, W. G., Dollish, F. R., McDevitt, N. T., and Bentley, F. F. *Infrared and Raman Selection rules for molecular and lattice vibrations: The Correlation Method*; Wiley-Interscience: New York, 1972.

### **III. PMDETA complexed with LiTf and NaTf**

**Characterization of the Crystalline and Solution Phases in N,N,N',N',N'' – Pentamethyldiethylenetriamine (PMDETA) with Lithium Triflate (LiCF<sub>3</sub>SO<sub>3</sub>) and Sodium Triflate (NaCF<sub>3</sub>SO<sub>3</sub>).**

**Rebecca A. Sanders, Roger Frech\*, and Masood A. Khan.**

*Department of Chemistry and Biochemistry, University of Oklahoma, 620 Parrington Oval, Norman, OK 73019*

Linear poly(N-methylethylenimine) [LPMEI], a methylated derivative of linear poly(ethylenimine) [LPEI], shows potential as a polymer electrolyte host. The interactions of LPMEI with lithium and sodium cations are modeled by solutions of N,N,N',N',N''-pentamethyldiethylenetriamine, PMDETA, containing either dissolved lithium triflate [LiTf] or sodium triflate [NaTf]. During these studies, crystalline compounds were discovered and characterized by differential scanning calorimetry, Fourier transform infrared spectroscopy (IR), and Raman spectroscopy. The crystals of the PMDETA:NaTf complex were of sufficient size to allow a structure determination by X-ray diffraction. The PMDETA:NaTf crystallizes as two dimers with different symmetries in a monoclinic unit cell in the P2<sub>1</sub>/c space group. A spectroscopic comparison of PMDETA, crystalline PMDETA:LiTf, crystalline PMDETA:NaTf, and their corresponding salt solutions over a composition range of 5:1 to 20:1[nitrogen:cation, molar ratio] is carried out using IR and Raman spectroscopy. The dominant species in the PMDETA:NaTf solutions are the triple cation [Na<sub>2</sub>Tf]<sup>+</sup>, even at a 20:1 NaTf composition.

## 1. Introduction

The most widely studied polymer electrolyte is poly(ethylene oxide), PEO, complexed with various salts, such as LiCF<sub>3</sub>SO<sub>3</sub>, LiN(CF<sub>3</sub>SO<sub>2</sub>)<sub>2</sub>, LiSbF<sub>6</sub>, LiBF<sub>4</sub>, and LiClO<sub>4</sub>. The mechanism of ionic transport in these systems is not well understood especially at the molecular level, although cation-anion interactions<sup>1</sup> and cation-polymer interactions<sup>2</sup> play a major role. Cation-polymer interactions lead to changes of the polymer backbone conformation<sup>3</sup>, while cation-anion interactions<sup>1</sup> result in the formation of associated ionic species<sup>4</sup>. Thus, local structures (ionically associated species and local backbone conformation) may be used to study those important interactions and provide essential insight needed to understand the mechanism of ionic transport. Model compounds have proven useful in fundamental studies of local structures in polymer electrolytes. Model compounds for PEO-based electrolytes include the dimethyl ethers of ethylene oxides (CH<sub>3</sub>(OCH<sub>2</sub>CH<sub>2</sub>)<sub>n</sub>-OCH<sub>3</sub>, n = 1–4), otherwise known as glymes, i.e., monoglyme, diglyme, triglyme, and tetraglyme<sup>3,5–11</sup>.

Linear poly(ethylenimine), LPEI, is a highly crystalline polymer that is analogous to PEO. LPEI-based electrolytes exhibit poor conductivity because of the crystallinity of the host matrix. In spite of this

drawback, there have been attempts to understand ionic association and ion-polymer interactions in LPEI complexed with lithium and sodium salts. These attempts have been aided by the use of salt complexes of N,N'-dimethylethylenediamine<sup>12–15</sup>.

The addition of side chains (e.g., –CH<sub>3</sub>, –CH<sub>2</sub>CH<sub>3</sub>) to LPEI decreases the crystallinity. Linear poly(N-methylethylenimine), LPMEI, is a methyl-substituted derivative of LPEI. LPMEI is completely amorphous at room temperature, unlike LPEI, which melts at 58°C<sup>16–18</sup>. The LPMEI-based electrolytes have been explored by Tanaka *et al.* and Sanders *et al.*<sup>18–21</sup> There is very limited knowledge about the local structures in LPMEI; therefore, model compounds that mimic vibrational modes of LPMEI and LPMEI-based polymer electrolytes can be useful. N,N,N',N'-tetramethylethylenediamine (TMEDA), monomeric LPMEI, has been investigated by Sanders *et al.* as a possible model compound for LPMEI<sup>22</sup>. However, the short chain length of TMEDA limits its usefulness. Therefore, N,N,N',N',N''-pentamethyldiethylenetriamine (PMDETA), which is essentially LPMEI with two repeat units, is being investigated<sup>23,24</sup>. While studying solutions of PMDETA with LiCF<sub>3</sub>SO<sub>3</sub> (LiTf) and NaCF<sub>3</sub>SO<sub>3</sub> (NaTf) in PMDETA,

crystalline compounds were discovered. This paper characterizes the crystalline and amorphous phases in PMDETA:LiTf and PMDETA:NaTf systems using X-ray diffraction, Fourier transform infrared spectroscopy (IR), Raman spectroscopy, and differential scanning calorimetry (DSC). Structural information obtained from the PMDETA:NaTf crystal provides a better understanding of the local environment of PMDETA and the triflate anion in the PMDETA:NaTf solutions.

## 2. Experimental

**2.1 Sample Preparation.** N,N,N',N',N''-pentamethyldiethylenetriamine (PMDETA), LiTf, and NaTf were obtained from Aldrich. PMDETA was distilled over sodium metal. LiTf and NaTf were heated under vacuum at 120°C for 48 hours. The chemicals were stored and used in a dry nitrogen glovebox (VAC,  $\leq 1$  ppm H<sub>2</sub>O) at room temperature. To prepare the solutions, LiTf was dissolved into PMDETA at various concentrations and stirred for at least 4 hours. A similar sample preparation was used for the PMDETA:NaTf samples except the samples were heated to completely dissolve the salt and stirred for 24 hours. The compositions of the solutions are reported as a nitrogen to cation molar ratio (N:M, M = Li, Na). At higher salt compositions, the solutions contained both a liquid and a gel-like phase that formed within 24 hours. Eventually, all the samples became phase-separated. Approximately three months later, a fine-grained, gritty textured material had formed at the gel-liquid interface and on the glass surface just above the sample. After about 6 months, the gel-liquid interface and on the glass surface just above the sample was composed of crystals. However, the solutions were still in a gel-like phase. The crystals were allowed to completely dry in a nitrogen atmosphere. The formation of crystals was evident in most of the PMDETA:LiTf and all of the PMDETA:NaTf samples prepared. However, single crystals suitable for X-ray diffraction measurements could be isolated only from the PMDETA:NaTf samples.

**2.2 X-ray Diffraction.** Single crystals for X-ray analysis were grown and isolated from the 10:1 PMDETA:NaTf solution. X-ray data were collected at 110 (2) K on a Bruker Apex diffractometer using MoK $\alpha$  radiation ( $\lambda = 0.71073$  Å). The data were corrected for Lorentzian and polarization effects; an absorption correction was not applied since it was judged to be insignificant. The structure was solved by the direct method using the SHELXTL system and refined by full-matrix least squares on F<sup>2</sup> using all reflections. All nonhydrogen atoms were refined anisotropically, and all hydrogen atoms were included with idealized parameters. The final R1 = 0.042 is based on 7629 “observed reflections” [ $I > 2\sigma(I)$ ], and

$wR^2 = 0.107$  is based on all reflections (10798 unique reflections).

**2.3 Differential Scanning Calorimetry.** Single crystals of PMDETA:NaTf weighing in total approximately 1.0 mg were sealed in a 40  $\mu$ L aluminum pan. DSC data were collected using a Mettler DSC 820 calorimeter with Star<sup>c</sup> software (v.6.10) under dry nitrogen purge. Data were collected during two heating and cooling cycles between 25°C and 300°C at a heating and cooling rate of 5°C/min.

**2.4 IR & Raman Spectroscopy.** For IR measurements, the PMDETA, PMDETA:LiTf solutions, and PMDETA:NaTf solutions were placed between zinc selenide windows in a sealed sample holder. Finely ground crystals of PMDETA:LiTf and PMDETA:NaTf samples were prepared as KBr pellets. IR data were recorded on a Bruker IFS66V with a KBr beam splitter over a range of 500–4000 cm<sup>-1</sup> (1 cm<sup>-1</sup> resolution). The spectra of the solutions were measured under a dry air purge; the crystal data were collected under vacuum (8 mbar). For the Raman measurements, the PMDETA, PMDETA:LiTf, and PMDETA:NaTf solutions were placed in a round, aluminum sample holder and covered with a glass cover plate; single crystals of PMDETA:NaTf were sealed in a quartz cuvette. Raman data of the solutions were recorded on a FT-Raman system (Bruker Equinox 55/FRA 106) with a CCD detector and Nd:YAG laser (1064 nm line). However, Raman data of the single crystals were recorded with a Jobin-Yvon T64000 system in the triple subtractive mode with a CCD detector using 532 nm line of a diode-pumped Nd:YVO<sub>4</sub> laser for excitation. All Raman data were collected in a 180° scattering geometry. The crystalline data were acquired using a laser power of

**Table 1: Structural data of the PMDETA:NaTf crystal.**

Parameters	
Crystal system	Monoclinic
Space group	P2 <sub>1</sub> /c
Temperature	173 (2) K
a (Å)	9.8001 (8)
b (Å)	29.867 (2)
c (Å)	17.9858 (14)
$\alpha$	90°
$\beta$	97.4740 (10)°
$\gamma$	90°
Volume (Å <sup>3</sup> )	5219.8 (7)
Z	6
Density (Mg/m <sup>3</sup> )	1.318
R1	0.0420
Crystal size (mm <sup>3</sup> )	0.34 x 0.18 x 0.16

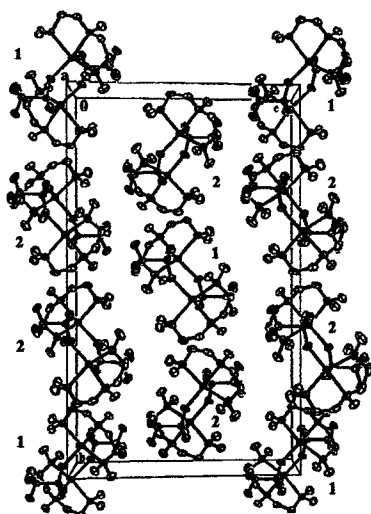


**Figure 1:** Packing diagram of the PMDETA:NaTf crystal.

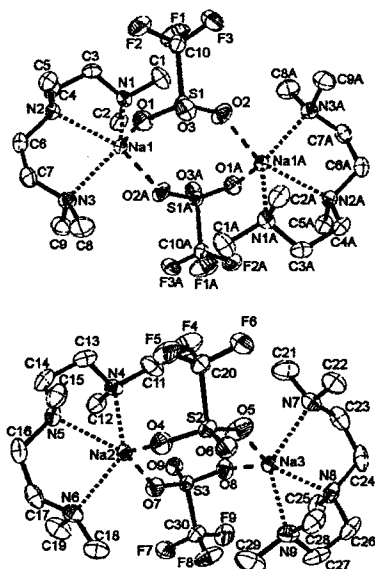


**Figure 2:** Dimer 1 (top) and 2 (bottom) structures in the PMDETA:NaTf crystal

300 mW (crystal data) and 200 mW (solution data) measured at the laser head.

### 3. Results and Discussion

**3.1 Crystal structure.** A crystal structure of PMDETA:LiTf could not be determined using X-ray diffraction because a single crystal of adequate size could not be isolated. The PMDETA:NaTf crystal forms a  $P2_1/c$  unit cell in the monoclinic space group (Figure 1). The asymmetric unit of crystalline PMDETA:NaTf consists of one and half (PMDETA:NaTf)<sub>2</sub> molecules such that there are two different kinds of dimers in the unit cell. Dimer (1)

**Table 2:** Selected bond lengths (Å) and angles (°) in the PMDETA:NaTf crystal.

	dimer (1)	dimer (2)
Na – N	2.5063 (14)	2.4758 (14)
	2.4812 (13)	2.5053 (14)
	2.4937 (15)	2.4587 (15)
		2.4792 (14)
		2.4773 (15)
Na – O	2.2903 (12)	2.3054 (13)
	2.2709(13)*	2.3074 (13)
		2.2620 (13)
		2.2809 (12)
<i>bond angle</i>		
N – Na – N	73.88 (5)	73.44 (5)
	73.81 (4)	74.17 (5)
	133.50 (5)	129.79 (5)
		73.93 (5)
		73.42 (5)
		131.58 (5)

has a center of symmetry whereas dimer (2) does not. In the unit cell, there are two dimer (1) and four dimer (2) types, as illustrated in Figure 1. In both dimers, the sodium ion is coordinated to two triflate oxygen and three nitrogen atoms (Figure 2). Structural data are summarized in Table 1; selected bond lengths and angles for the PMDETA:NaTf crystal are listed in Tables 2 and 3. There are only a few minor differences between the bond angles and lengths of the two dimers.

The conformational structures of the PMDETA oligomers can be characterized in terms of the C–N–C–C and N–C–C–N dihedral angles (gauche, g,  $60^\circ \pm 30^\circ$ ; gauche minus,  $\bar{g}$ ,  $-60^\circ \pm 30^\circ$ ; trans, t,  $\pm 180^\circ \pm 30^\circ$ ). An individual PMDETA molecule can have sixteen different conformations, because it has two N–C–C–N dihedral angles, a methyl group coordinated to the shared nitrogen atom, and two methyl groups attached to the terminal nitrogen atoms. The N–C–C–N dihedral angle is of most interest because it is directly affected by coordination of the cation to the nitrogen atoms. In the PMDETA:NaTf crystal (Table 3), dimer (1) has only one set of N–C–C–N dihedral angles ( $-62.3$ ,  $61.2^\circ$ ) because the PMDETA molecules are related by the inversion center. Dimer (2) has two different sets of dihedral angles for the PMDETA molecule ( $60.8$ ,  $-62.0^\circ$ ;  $61.4$ ,  $-58.9^\circ$ ). Overall, the N–C–C–N dihedral angles of the crystalline PMDETA:NaTf are g and  $\bar{g}$ . The conformation of both PMDETA:NaTf dimers is  $x_1 g x_1 - x_2 \bar{g} x_2$  ( $x_1 = t, g$ ;  $x_2 = t, \bar{g}$ ).

**Table 3: Dihedral angles (°) of the PMDETA:NaTf crystals with their corresponding conformations.**

Dimer 1		
bond sequence	Dihedral angle	conformation
C-N1-C-C	-170.15 (14)	t
C-N1-C-C	69.79 (17)	g
N1-C-C-N2	61.06 (18)	g
C-C-N2-C	77.17 (16)	g
C-C-N2-C	-159.29 (13)	t
C-N2-C-C	159.98 (13)	t
C-N2-C-C	-76.81 (16)	$\bar{g}$
N2-C-C-N3	-62.32 (18)	$\bar{g}$
C-C-N3-C	-73.94 (17)	$\bar{g}$
C-C-N3-C	164.38 (14)	t
Dimer 2		
C-N4-C-C	-172.86 (14)	t
C-N4-C-C	67.28 (19)	g
N4-C-C-N5	60.85 (19)	g
C-C-N5-C	83.39 (17)	g
C-C-N5-C	-153.26 (15)	t
C-N5-C-C	159.39 (14)	t
C-N5-C-C	-77.40 (17)	$\bar{g}$
N5-C-C-N6	-62.00 (19)	$\bar{g}$
C-C-N6-C	-75.59 (18)	$\bar{g}$
C-C-N6-C	162.25 (14)	t
C-N7-C-C	-166.61 (15)	t
C-N7-C-C	72.21 (19)	g
N7-C-C-N8	61.49 (19)	g
C-C-N8-C	75.55 (17)	g
C-C-N8-C	-160.94 (14)	t
C-N8-C-C	155.94 (15)	t
C-N8-C-C	-80.41 (19)	$\bar{g}$
N8-C-C-N9	-59.1 (2)	$\bar{g}$
C-C-N9-C	-67.89 (19)	$\bar{g}$
C-C-N9-C	171.83 (15)	t

**3.2 Thermal Analysis.** Differential scanning calorimetry (DSC) was used to characterize thermal transitions in the PMDETA:NaTf crystal. The DSC thermogram (data not shown) shows two endothermic phase transitions occurring at 104 and 237°C in the first heating cycle. In the cooling cycle, the only thermal transition observed is at 238°C. During the second heating cycle, there is only one transition occurring at 236°C. In addition, this peak becomes broader and smaller, indicating a decrease in the crystallinity of the sample. However, the temperatures at which PMDETA:NaTf melts (237°C) and recrystallizes (238°C) are reproducible upon cycling, within experimental error.

**Table 4: Band frequencies (cm<sup>-1</sup>) and assignments of PEO, LPEI, and LPMEI complexed to LiTf and NaTf.**

NaTf	"Free"	Contact Ion Pair	Aggregate I
PEO	753	756	761
LPEI	754	756–757	762
LPMEI	751–752	756	758–759
LiTf			
PEO	752–753	757	760–761
LPEI	752–753	755–757	759–760
LPMEI	752	757–758	761–762

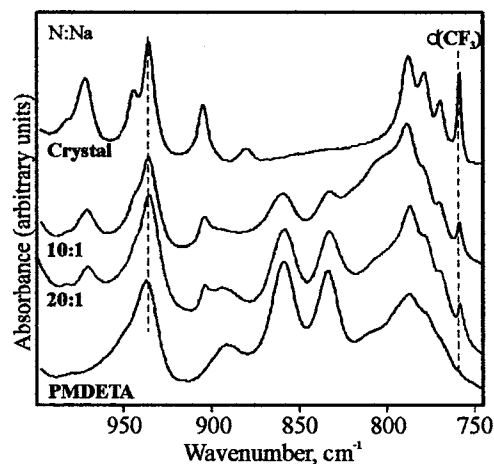


**Figure 3a: IR spectra from 750 to 1000 cm<sup>-1</sup> of PMDETA, PMDETA:NaTf solutions, and crystalline PMDETA:NaTf.**

**3.3 Vibrational Spectroscopy.** The PMDETA:LiTf and PMDETA:NaTf crystals have distinct spectral signatures, which are related to their local structures. Comparing crystalline spectral signatures to those of the amorphous phase can provide critical insight into the local structures present in solutions of PMDETA:LiTf and PMDETA:NaTf. This work will focus on the 750 to 1200 cm<sup>-1</sup> region where both PMDETA and triflate modes will be explored. In the 770 to 1000 cm<sup>-1</sup> region, the frequencies and intensities of the bands are particularly sensitive to conformations of the PMDETA backbone. Bands in this region have also been shown to provide information about backbone conformation in ethylene oxide-based systems<sup>3,25-30</sup>.

**3.3.1 Ionic Association Region.** The frequencies and intensities of the CF<sub>3</sub> symmetric deformation mode,  $\delta(\text{CF}_3)$ , provides information about ionically associated species. Spectral-structural correlations have been previously worked out for PEO<sup>7,26,30-35</sup>, LPEI<sup>36</sup>, and LPMEI<sup>21,37</sup> systems complexed with LiTf and NaTf, which are



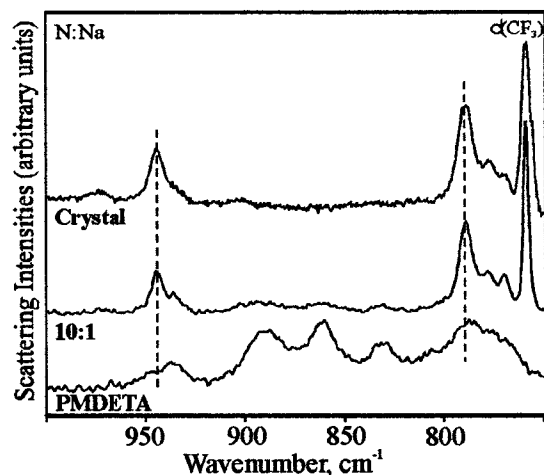


**Figure 3b:** Raman spectra from 750 to 1000  $\text{cm}^{-1}$  of PMDETA, PMDETA:NaTf solutions, and crystalline PMDETA:NaTf.

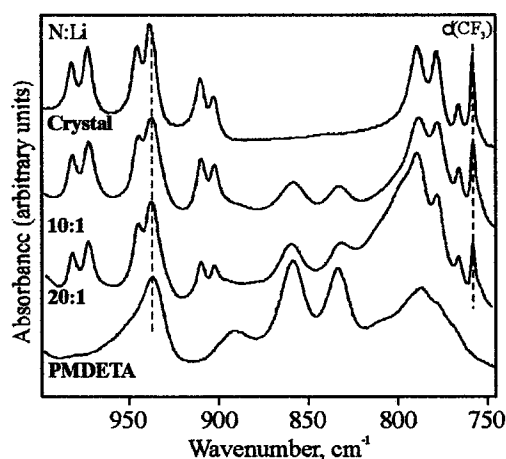


**Figure 4:** IR spectra from 750 to 1000  $\text{cm}^{-1}$  of PMDETA, PMDETA:LiTf solutions, and crystalline PMDETA:LiTf.

listed in Table 4. In the salt complexes of both LPEI and LPMEI, the relative amount of aggregate species increases with increasing salt composition.

In crystalline PMDETA:NaTf (Figures 3a & b), the  $\delta(\text{CF}_3)$  band occurs at  $759 \text{ cm}^{-1}$  (IR & Raman). This band is actually due to the vibrations of triflate ions coordinated by sodium ions such that the local geometry is best described as a  $[\text{Na}_2\text{Tf}]^+$  species. This frequency is somewhat low for an aggregate species compared to the reported values in LPEI:NaTf and PEO:NaTf systems. In crystalline PMDETA:LiTf (Figure 4), the  $\delta(\text{CF}_3)$  band occurs at  $758 \text{ cm}^{-1}$  (IR & Raman), which is the value observed in LPEI:LiTf systems. This band is assigned to the  $[\text{Li}_2\text{Tf}]^+$  species, based on similarities with the spectroscopic data in crystalline PMDETA:NaTf. The dominant species in both the PMDETA:LiTf and PMDETA:NaTf solu-

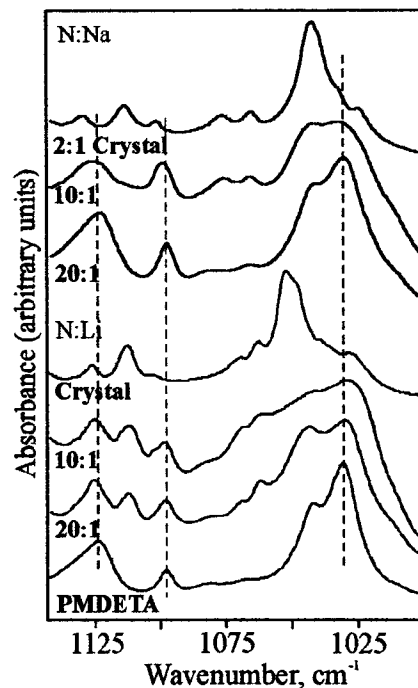


**Figure 5:** IR spectra from 1000 to 1200  $\text{cm}^{-1}$  of PMDETA, PMDETA:LiTf and PMDETA:NaTf solutions, and crystalline PMDETA:LiTf and PMDETA:NaTf.

tions are  $[\text{M}_2\text{Tf}]^+$  ( $\text{M} = \text{Li}, \text{Na}$ ).

The frequency of the  $\text{SO}_3$  symmetric stretch,  $\nu_s(\text{SO}_3)$ , is also affected by coordination of the triflate ion with the cation. Raman-active bands at 1032–1033, 1037–1042, and 1044–1056  $\text{cm}^{-1}$  correspond to “free” ions, contact ion pairs, and aggregate species, respectively, in ethylene oxide-based systems complexed with  $\text{LiTf}$ <sup>5,7,26,31,32</sup>. Similar results are reported in poly(ethylene oxide):NaTf systems; again there is a second aggregate species present at 1058  $\text{cm}^{-1}$ <sup>30,38</sup>. In LPEI and LPMEI systems, there are no reported frequencies for the  $\nu_s(\text{SO}_3)$  bands because there are polymer bands that occur at the same frequencies as the  $\nu_s(\text{SO}_3)$  bands.

In the absorbance spectra of crystalline PMDETA:NaTf (Figure 5), the  $\nu_s(\text{SO}_3)$  band occurs at  $\sim 1043 \text{ cm}^{-1}$  (IR); in crystalline PMDETA:LiTf, this band occurs at 1048 and 1052  $\text{cm}^{-1}$ . Studies of  $\nu_s(\text{SO}_3)$  are complicated by underlying PMDETA bands in the PMDETA:LiTf and PMDETA:NaTf spectra. However, the Raman spectra are relatively simple in this region. The  $\nu_s(\text{SO}_3)$  mode occurs at 1049  $\text{cm}^{-1}$  in the PMDETA:LiTf solutions (data not shown) and 1043  $\text{cm}^{-1}$  in crystalline PMDETA:NaTf (Figure 6). The aggregate species in crystalline PMDETA:NaTf is dominant in the corresponding

**Table 5: Selected IR and Raman vibrational frequencies (cm<sup>-1</sup>) of PMDETA, crystalline PMDETA:NaTf, and crystalline PMDETA:LiTf.**

IR							Raman			
<b>PMDETA</b>	770	779	787	791			769	777	786	
	~807	834	859	891			831	861	890	
			937	~944			936	944		
	1031	1042	1098	~1123			1071	1098	1123	~1128
<b>PMDETA NaTf</b>	770	779	788	880			770		778	789
	904		936	944	972	982	~934	944		
	1065	1072					1071			
	1102	1114	1124	1130						
<b>PMDETA LiTf</b>	766	779	790				766	775	779	790
	903	910	938	945	973	982	937	945		
	1063	1070		1098			1075			
	1103	1112	1126							

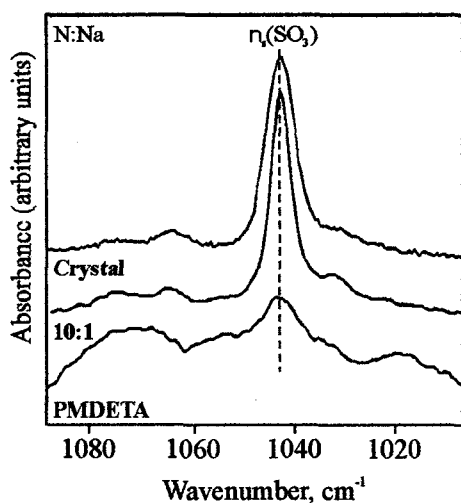


**Figure 6:** Raman spectra from 1000 to 1100 cm<sup>-1</sup> of PMDETA, PMDETA:NaTf solution, and crystalline PMDETA:NaTf.

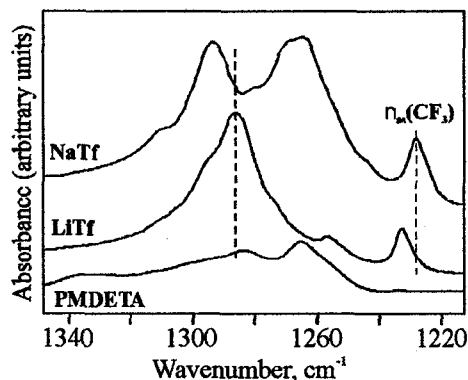


**Figure 7:** IR spectra from 1210 to 1350 cm<sup>-1</sup> of the PMDETA, crystalline PMDETA:LiTf, and crystalline PMDETA:NaTf.

solutions, even at low triflate compositions (20:1; data not shown).

Utilizing standard group theoretical methods<sup>39</sup>, a correlation field analysis of crystalline PMDETA:-NaTf shows that the irreducible representations of the  $\nu_s(\text{SO}_3)$  modes can be classified according to the irreducible representation of the  $P2_1/c$  unit cell group as

$$\text{DIMER 1: } \Gamma(\nu_{as}(\text{SO}_3)) = A_g + B_g + A_u + B_u \quad (1)$$

$$\text{DIMER 2: } \Gamma(\nu_{as}(\text{SO}_3)) = 2A_g + 2B_g + 2A_u + 2B_u \quad (2)$$

In principle, there should be six Raman active components ( $3A_g + 3B_g$ ) observed in which four components result from dimer (2). However, in the Raman spectra, only  $\nu_s(\text{SO}_3)$  band is observed (1043 cm<sup>-1</sup>), indicating that all the Raman active components occur at the same frequency. Therefore, there are rather small spectral differences between the two dimers in crystalline PMDETA:NaTf.

**3.3.2 Conformation Region.** Selected IR and Raman frequencies of PMDETA, crystalline PMDETA:NaTf, and crystalline PMDETA:LiTf are listed in Table 5. When NaTf or LiTf is added to PMDETA, major changes occur in the spectra, such as the disappearance of PMDETA bands, the appearance of new bands, and the narrowing of bandwidths. Most striking is the disappearance of the strong bands at 834 and 859 cm<sup>-1</sup> upon crystallization in both PMDETA:NaTf (Figure 3a) and PMDETA:LiTf (Figure 4), indicating a change in conformation. Similar results are evident in the Raman spectra. These solution IR and Raman bands are due to PMDETA molecules with at least one trans N-C-C-N dihedral angle, based on quantum

chemical calculations of PMDETA in the gas phase<sup>40</sup>.

In the 750–810  $\text{cm}^{-1}$  region, the IR and Raman bands become more intense with smaller bandwidths upon crystallization of PMDETA:LiTf and PMDETA:NaTf. In the 900–1000  $\text{cm}^{-1}$  region, the PMDETA band at 944  $\text{cm}^{-1}$  (IR & Raman) does not shift in frequency upon crystallization of PMDETA:NaTf and PMDETA:LiTf. The new IR bands that form in this region become more intense as the salt composition increases in both PMDETA:NaTf and PMDETA:LiTf.

There are some spectroscopic differences between crystalline PMDETA:LiTf (Figures 3a) and PMDETA:NaTf (Figures 3a & 4). The IR band at 766  $\text{cm}^{-1}$  in PMDETA:LiTf is 4  $\text{cm}^{-1}$  lower in frequency compared to this band in PMDETA:NaTf (770  $\text{cm}^{-1}$ ). These bands consist of predominantly  $\text{CH}_2$  rocking motion<sup>40</sup>. The two IR bands at 779 and 788  $\text{cm}^{-1}$  in PMDETA:LiTf and 779 and 790  $\text{cm}^{-1}$  in PMDETA:NaTf are associated with mixed  $\text{CH}_2$  rocking and C–N stretching motions<sup>40</sup>. There is a new PMDETA band at 880  $\text{cm}^{-1}$  (IR), which only occurs in the crystalline PMDETA:NaTf spectrum (Figure 3a). In crystalline PMDETA:LiTf, the two IR bands at 938 and 945  $\text{cm}^{-1}$  occur at lower frequencies in PMDETA:NaTf (936 & 944  $\text{cm}^{-1}$ ). These bands are assigned to mixed  $\text{CH}_2$  rocking, C–N stretching and C–C stretching motions<sup>40</sup>.

**3.3.3 1000 to 1350  $\text{cm}^{-1}$  region.** The PMDETA bands in the 1000 to 1050  $\text{cm}^{-1}$  region are hard to isolate due to the presence of  $\nu_{\text{as}}(\text{SO}_3)$  modes. In the Raman spectra (Figure 6), the PMDETA bands in this region are weak compared to the strong  $\nu_{\text{as}}(\text{SO}_3)$  band. In the 1050 to 1080  $\text{cm}^{-1}$  region, the IR bands in PMDETA:NaTf are 2  $\text{cm}^{-1}$  lower in frequency than in PMDETA:LiTf (Figure 5; Table 5). In both PMDETA:LiTf and PMDETA:NaTf crystals, the 1075  $\text{cm}^{-1}$  band shifts 2  $\text{cm}^{-1}$  higher in frequency upon crystallization. In the PMDETA:NaTf spectra, there is a new IR band at 1114  $\text{cm}^{-1}$ , which only forms in the crystalline phase. In both PMDETA:LiTf and PMDETA:NaTf, the PMDETA bands (IR) at 1098 and 1124  $\text{cm}^{-1}$  decreases in intensity upon crystallization.

The  $\text{CF}_3$  asymmetric stretching mode occurs at 1233  $\text{cm}^{-1}$  in crystalline PMDETA:LiTf and 1228  $\text{cm}^{-1}$  in crystalline PMDETA:NaTf (Figure 7). The frequencies of these bands do not change upon crystallization from solution (data not shown). The  $\text{SO}_3$  asymmetric stretch,  $\nu_{\text{as}}(\text{SO}_3)$ , of the triflate ion is also affected by coordination to the cations, as illustrated in Figure 7. The  $\nu_{\text{as}}(\text{SO}_3)$  bands in PMDETA:NaTf are separated compared to PMDETA:LiTf, indicating that the coordination of the sodium cation to the triflate anion is stronger. Therefore, the perturbation of the vibrational potential

energy environment is stronger in PMDETA:NaTf resulting in a separation of the  $\nu_{\text{as}}(\text{SO}_3)$  bands.

The apparent simplicity of the PMDETA:LiTf crystal spectrum (1286, 1294  $\text{cm}^{-1}$ ) in this region is deceptive. The two-fold degeneracy of the  $\nu_{\text{as}}(\text{SO}_3)$  mode in an isolated triflate ion is broken by the potential energy environment in the crystal. Formally, each of the resulting two components in a unit cell is then correlated through intermolecular interactions, resulting in a vibrational multiplet structure that can be analyzed by standard group theoretical methods<sup>39</sup>. However a crystal structure is not known for PMDETA:LiTf, therefore, a symmetry-based analysis cannot be accomplished.

The situation in the PMDETA:NaTf crystal is more complicated. A correlation field analysis shows that the irreducible representations of the  $\nu_{\text{as}}(\text{SO}_3)$  modes can be classified according to the irreducible representation of the  $\text{P2}_1/\text{c}$  unit cell group as

$$\text{DIMER 1: } \Gamma(\nu_{\text{as}}(\text{SO}_3)) = 2A_g + 2B_g + 2A_u + 2B_u \quad (3)$$

$$\text{DIMER 2: } \Gamma(\nu_{\text{as}}(\text{SO}_3)) = 4A_g + 4B_g + 4A_u + 4B_u \quad (4)$$

Because the sample was in the form of a microcrystalline powder, in principle all twelve infrared active components ( $6A_u + 6B_u$ ) could be observed in a transmission experiment. In the spectrum, prominent bands are observed at 1265, 1269, and 1293  $\text{cm}^{-1}$ , with a smaller, asymmetric band at 1279  $\text{cm}^{-1}$ . In addition, a very weak band occurs at 1309  $\text{cm}^{-1}$ . The inability to observe all twelve infrared active components may be due to small dipole moment derivatives of some factor group components, or very small correlation field splittings that leave certain factor group components at roughly the same frequency. Without an oriented single crystal and a complete set of polarized infrared reflection spectra, a detailed assignment of these five bands in terms of their symmetry species is not possible. In the  $\nu_{\text{as}}(\text{SO}_3)$  region, the spectra are also complicated by the underlying PMDETA bands, which make a small contribution to the spectra.

#### 4. Conclusions

Single crystals of PMDETA:NaTf have been isolated and characterized using X-ray diffraction, DSC, IR, and Raman techniques. Local structures similar to those in the crystal are present in the PMDETA:LiTf and PMDETA:NaTf solutions, even at a 20:1 composition, demonstrating that spectroscopic studies of the PMDETA:LiTf and PMDETA:NaTf crystals can provide insight into the local structures present in solutions of PMDETA:LiTf and PMDETA:NaTf. In addition,

spectroscopic data shows a significant change in conformation upon passing from solution to the crystalline phase. The X-ray diffraction data show that PMDETA has  $g-\bar{g}$  N-C-C-N dihedral angles in the crystalline phase; quantum chemical calculations suggest that PMDETA has a combination of  $g$ ,  $t$ , and  $\bar{g}$  N-C-C-N dihedral angles, in solution phase. The PMDETA bands in the 800 to 900  $\text{cm}^{-1}$  region could only be assigned based on quantum chemical calculations of PMDETA with a trans N-C-C-N dihedral angle.

In crystalline PMDETA:NaTf, the differences in the dimers' symmetries does not greatly affect their bond angles and lengths. In addition, these differences are not evident in the IR or Raman spectra, based on standard symmetry group analysis.

For crystalline PMDETA:NaTf, the  $\delta(\text{CF}_3)$  band (759  $\text{cm}^{-1}$ ) is due to the  $[\text{Na}_2\text{Tf}]^+$  aggregate species. The aggregate species in crystalline PMDETA:LiTf (758  $\text{cm}^{-1}$ ) is attributed to the  $[\text{Li}_2\text{Tf}]^+$  species, based on similarities in vibrational frequencies of the  $\delta(\text{CF}_3)$  band in crystalline PMDETA:NaTf. The ionic association in PMDETA:LiTf and PMDETA:NaTf solutions is similar to that in the PMDETA:LiTf and PMDETA:NaTf crystals, where in solutions even at a 20:1 composition, the primary ionic species is  $[\text{M}_2\text{Tf}]^+$  ( $\text{M} = \text{Li}, \text{Na}$ ). However, this ionically associated species vibrate at slightly lower frequencies (758-759  $\text{cm}^{-1}$ ) than in PEO-based electrolyte systems (761-763  $\text{cm}^{-1}$ ).

## 5. Acknowledgements

We thank Scott Boesch for the Hartree-Fock/density functional calculations of PMDETA, PMDETA:LiTf, and PMDETA:NaTf. This work was partially supported by funds from the National Science Foundation, Contract No. DMR-0072544.

## 6. References

- (1) Papke, B. L.; Ratner, M. A.; Shriver, D. F. *J. Electrochem. Soc.* **1982**, *129*, 1434-1438.
- (2) Armand, M. B.; Chabagno, J. M.; Duclot, M. J. Polyethers as Solid Electrolytes. In *Fast Ion Transport in Solids*; Vashista, P., Mundy, J. M., Shenoy, G. K., Eds.; Elsevier: Amsterdam, 1979; pp 131-136.
- (3) Huang, W.; Frech, R.; Johansson, P.; Lindgren, J. *Electrochim. Acta* **1995**, *40*, 2147-2151.
- (4) Bruce, P. G. *Faraday Discuss. Chem. Soc.* **1989**, *88*, 43-54.
- (5) Frech, R.; Huang, W.; Dissanayake, M. A. K. L. *Mat. Res. Soc. Symp. Proc.* **1995**, *369*, 523-534.
- (6) Kearley, G. J.; Johansson, P.; Delaplane, R. G.; Lindgren, J. *Solid State Ionics* **2002**, *147*, 237-242.
- (7) Rhodes, C. P.; Frech, R. *Macromolecules* **2001**, *34*, 2660-2666.
- (8) Rhodes, C. P.; Khan, M.; Frech, R.; Ruf, M. *J. Phys. Chem.* **submitted**.
- (9) Sutjianto, A.; Curtiss, L. A. *J. Phys. Chem. A* **1998**, *102*, 968-974.
- (10) Seneviratne, V.; Frech, R.; Furneaux, J.; Kahn, M. **manuscript in progress**.
- (11) Rhodes, C. Crystalline and Amorphous Phases in Polymer Electrolytes and Model Systems. Dissertation, University of Oklahoma, 2001.
- (12) Boesch, S. E.; York, S. S.; Frech, R.; Wheeler, R. A. *Phys. Chem. Comm.* **2001**, *1*.
- (13) York, S. S.; Boesch, S. E.; Wheeler, R. A.; Frech, R. *Macromolecules* **in press 2003**.
- (14) York, S. S.; Boesch, S. E.; Wheeler, R. A.; Frech, R. *Phys. Chem. Comm.* **2002**, 99-111.
- (15) Sanders, R. A.; Frech, R.; Kahn, M. *J. Phys. Chem. B* **submitted 2003**.
- (16) Saegusa, T.; Ikeda, H.; Fujii, H. *Macromolecules* **1972**, *5*, 108.
- (17) Chatani, Y.; Irie, T. *Polymer* **1988**, *29*, 2126-2129.
- (18) Tanaka, R.; Ueoka, I.; Takaki, Y.; Kataoka, K.; Saito, S. *Macromolecules* **1983**, *16*, 849-853.
- (19) Tanaka, R.; Fujita, T.; Nishibayashi, H.; Saito, S. *Solid State Ionics* **1993**, *60*, 119-123.
- (20) Tanaka, R.; Koike, M.; Tsutsui, T.; Tanaka, T. *J. Poly. Sci. : Poly. Letters ed.* **1978**, *16*, 13-19.
- (21) Sanders, R. A.; Snow, A. G.; Frech, R.; Glatzhofer, D. T. *Electrochim. Acta* **2003**, *48*, 2247-2253.
- (22) Sanders, R. A.; Frech, R.; Kahn, M. *J. Phys. Chem. B* **2003**, *107*, in press.
- (23) Sanders, R. A.; Boesch, S. E.; Snow, A. G.; Hu, L. R.; Frech, R.; Wheeler, R. A.; Glatzhofer, D. T. *Polym. Prepr.* **2003**, *44*, 996-997.
- (24) Sanders, R. A.; Boesch, S. A.; Snow, A. G.; Hu, L.; Frech, R.; Wheeler, R. A.; Glatzhofer, D. T. **manuscript in progress**.
- (25) Matsuura, H.; Fukuhara, K. *J. Poly. Sci. B* **1986**, *24*, 1383-1400.
- (26) Frech, R.; Huang, W. *Solid State Ionics* **1994**, *72*, 103-107.
- (27) Frech, R.; Huang, W. *Macromolecules* **1995**, *28*, 1246-1251.
- (28) Goutev, N.; Ohno, K.; Matsuura, H. *J. Phys. Chem. A* **2000**, *104*, 9226-9232.
- (29) Murcko, M. A.; DiPaola, R. A. *J. Am. Chem. Soc.* **1992**, *114*, 10010-10018.
- (30) Rhodes, C. P.; Frech, R. *Solid State Ionics* **1999**, *121*, 91-99.
- (31) Schantz, S.; Sandahl, J.; Borjesson, L.; Torell, L. M.; Stevens, J. R. *Solid State Ionics* **1988**, *28-30*, 1047-1053.

- (32) Huang, W.; Frech, R.; Wheeler, R. A. *J. Phys. Chem.* **1994**, *98*, 100-110.
- (33) Frech, R.; Chintapalli, S.; Bruce, P. G.; Vincent, C. A. *Macromolecules* **1999**, *32*, 808-813.
- (34) Seneviratne, V.; Furneaux, J. E.; Frech, R. *Macromolecules* **2002**, *35*, 6392-6396.
- (35) Frech, R.; Rhodes, C. P.; York, S. S. *Mat. Res. Soc. Symp. Proc.* **1999**, *548*, 335-345.
- (36) York, S.; Frech, R.; Snow, A.; Glatzhofer, D. *Electrochim. Acta* **2001**, *46*, 1533-1537.
- (37) Sanders, R. A.; Frech, R. *Curve-fitting analysis of LPMEI:LiTf and LPMEI:NaTf in the 735 - 840  $\text{cm}^{-1}$  region using commercially available software (Thermo Galactic, Grams/AI 7.00). The spectral bands were fitted using a mixed Gaussian-Lorentzian product function and a straight baseline. unreported results.*
- (38) Kakihana, M.; Schantz, S.; Torell, L. M. *Solid State Ionics* **1990**, *40/41*, 641-644.
- (39) Fately, W. G.; Dollish, F. R.; McDevitt, N. T.; Bentley, F. F. *Infrared and Raman Selection Rules for Molecular and Lattice Vibrations: The Correlation Method.*; Wiley-Interscience: New York, 1972.
- (40) Boesch, S.; Wheeler, R. *Calculations (for vibrational mode assignments) of PMDETA, PMDETA:LiTf and PMDETA:NaTf were performed using B3LYP, a hybrid Hartree-Fock/density functional method, with a 6-31G(d) basis set. unreported results.*

#### **IV. LPMEI complexed with LiTf and NaTf**



PERGAMON

Available online at [www.sciencedirect.com](http://www.sciencedirect.com)

SCIENCE @ DIRECT®

Electrochimica Acta 48 (2003) 2247–2253

Reprint with Permission from Elsevier

ELECTROCHIMICA

Acta

[www.elsevier.com/locate/electacta](http://www.elsevier.com/locate/electacta)

## A spectroscopic and conductivity comparison study of linear poly(*N*-methylethylenimine) with lithium triflate and sodium triflate

Rebecca A. Sanders, Albert G. Snow, Roger Frech\*, Daniel T. Glatzhofer

Department of Chemistry and Biochemistry, University of Oklahoma, 620 Parrington Oval, Norman, OK 73019, USA

Received 19 May 2002

### Abstract

Linear poly(ethylenimine) (LPEI) is an NH-containing analog of poly(ethylene oxide) (PEO). Various groups (e.g. CH<sub>3</sub>) can be attached to the nitrogen atoms in order to decrease the crystallinity and eliminate hydrogen bonding of the host polymer. This paper focuses on linear poly(*N*-methylethylenimine), LPMEI, with dissolved lithium triflate (LiTf) and sodium triflate (NaTf). These electrolytes were investigated using infrared spectroscopy, differential scanning calorimetry (DSC), and impedance measurements of the conductivity. A spectroscopic comparison of LPMEI containing LiTf and NaTf over a composition range of 5:1 to 20:1 (nitrogen:cation) shows that contact ion pairs are the predominant species in both systems except for the 5:1 NaTf sample, where the “free” triflate ions are the predominant species. Furthermore, there is an increase in the degree of ionic association with increasing salt concentration in the LiTf systems. The effect of salt concentration on the glass transition temperature (*T*<sub>g</sub>) of the polymer host was examined using DSC. In LPMEI, *T*<sub>g</sub> occurs at −91 °C and increases to 3 °C at a 5:1 (N:Li) composition. Conductivity measurements of the LPMEI:LiTf system over a composition range of 5:1 to 20:1 are compared with the LPEI:LiTf systems for temperatures between 25 and 60 °C. In addition, X-ray powder diffraction (XRD) show a significant presence of crystalline domains in the LPMEI:NaTf samples.

© 2003 Elsevier Science Ltd. All rights reserved.

**Keywords:** Linear poly(*N*-methylethylenimine); Vibrational spectroscopy; Ionic association; Conductivity; Glass transitions

### 1. Introduction

Polymer electrolytes based on poly(ethylene oxide), PEO, are a widely researched area because of their applications in lithium rechargeable battery technology [1]. The most commonly studied salts in PEO polymer electrolytes are LiCF<sub>3</sub>SO<sub>3</sub>, LiN(CF<sub>3</sub>SO<sub>2</sub>)<sub>2</sub>, LiSbF<sub>6</sub>, LiBF<sub>4</sub>, and LiClO<sub>4</sub>. To achieve a better understanding of the mechanism of ionic transport, research efforts have been focused on cation–anion interactions [2] and cation–polymer interactions [3], both of which play critical roles in ion transport. Both cation–anion and cation–polymer interactions presumably affect the ionic mobilities; in addition, the former are expected to also play a major role in determining the number of effective charge carriers. Cation–anion interactions lead to the

formation of associated ionic species while cation–polymer interactions are manifested in changes on the polymer backbone conformation. Thus local structures (ionically associated species and local backbone conformation) may be used to directly study the nature of those important interactions and provide essential insight needed to understand the mechanism of ionic transport [4]. It is believed that ion conduction occurs more readily in the amorphous phase; however, Gadjourova et al. report that the crystalline phase is more conductive than the amorphous phase in the compound P(EO)<sub>6</sub>:LiSbF<sub>6</sub> [5]. Since PEO is a highly crystalline material, PEO-based electrolytes are generally poor ionic conductors. Consequently, other polymer hosts are being explored to achieve higher ionic conductivity.

Linear poly(ethylenimine) or LPEI is structurally analogous to PEO, however, LPEI is more synthetically versatile because various groups can be attached to the nitrogen atom. Pure LPEI is highly crystalline [6] and makes a poor host for the formation of polymer

\* Corresponding author. Tel.: +1-405-325-3831; fax: +1-405-325-6111.

E-mail address: [rfrech@ou.edu](mailto:rfrech@ou.edu) (R. Frech).

electrolytes with high ionic conductivity. By adding various side chains (e.g.  $-\text{CH}_3$ ) to LPEI, the crystallinity can be decreased. Linear poly(*N*-methylethylenimine) or LPMEI, a methyl-substituted derivative of LPEI, is completely amorphous at room temperature, unlike LPEI, which melts at 58 °C [7–9]. The ionic conduction and  $T_g$  of LPEI and LPMEI with  $\text{LiClO}_4$  and  $\text{LiCF}_3\text{SO}_3$  have been previously reported by Tanaka and Nishibayashi [10]. This paper will investigate LPMEI with  $\text{LiCF}_3\text{SO}_3$  and  $\text{NaCF}_3\text{SO}_3$  using Fourier transform infrared spectroscopy (FT-IR), differential scanning calorimetry (DSC), X-ray powder diffraction (XRD), and complex impedance.

## 2. Experimental

### 2.1. Synthesis of LPMEI

LPMEI was synthesized from LPEI (avg. MW ca. 86000) that had been prepared using methods previously reported [11]. All other materials were used as received from Aldrich. LPEI (5.02 g, 0.116 moles) was added to 50 ml of distilled water, then heated. After the LPEI dissolved, formic acid (88%, 200 ml) and formalin (37%, 125 ml) were added to the solution. The solution was heated to reflux the solvent for 24 h and, after cooling, 150 ml of concentrated HCl was added. The solvents were removed under reduced pressure to provide the ternary ammonium hydrochloride salt. The salt was dissolved in distilled water (200 ml), and run through an ion exchange column (Dowex 2X8 ion-exchange resin, hydroxide salt). The neutralized polymer/water solution was placed under reduced pressure and solvents removed. The resulting polymer was dissolved in benzene, and any excess water was removed by azeotropic distillation using a Dean-Stark trap. The resulting solution was centrifuged to remove any remaining impurities. The solvent was removed under reduced pressure [12]. The resulting viscous polymer was characterized by nuclear magnetic resonance (NMR) and FT-IR. These NMR and FT-IR data were consistent with literature values [9,12]. The LPMEI was a golden dark brown viscous liquid with an average molecular weight of ca. 115000, derived from the molecular weight of LPEI assuming no polymer degradation.

### 2.2. Preparation of polymer electrolytes

Anhydrous acetonitrile (99.8%), lithium trifluoromethane sulfonate,  $\text{LiCF}_3\text{SO}_3$ , and sodium trifluoromethane sulfonate,  $\text{NaCF}_3\text{SO}_3$ , were obtained from Aldrich. These salts will be abbreviated as LiTf and NaTf, respectively. Dry acetonitrile was used as received. Both the LiTf and NaTf were heated under

vacuum at 120 °C for 48 h. All chemicals were stored and used in a dry nitrogen glove box (VAC,  $\leq 1$  ppm  $\text{H}_2\text{O}$ ) at room temperature. To prepare the LPMEI:LiTf solutions of a desired composition, the appropriate amount of LiTf was added to 0.175 g of LPMEI. All of the LPMEI, LPMEI:LiTf, and LPMEI:NaTf samples were dissolved in dry acetonitrile to prepare a homogeneous solution. The LPMEI:LiTf solutions were stirred for approximately 2 h before casting as films. Similar methods were used to make the LPMEI:NaTf solutions. The compositions of the samples are reported as a nitrogen to cation ratio (N:M<sup>+</sup>). LPMEI:LiTf samples were prepared at 5:1, 10:1, 15:1, and 20:1 compositions, and 5:1, 10:1, 15:1, and 20:1 compositions were used for LPMEI:NaTf.

### 2.3. FT-IR spectroscopy

All of the samples were prepared for FT-IR measurements by casting the solutions onto zinc selenide windows and drying under a nitrogen purge for 24 h. To insure solvent removal, the samples were placed under vacuum for 24 h. The homogeneous thin films were translucent with a faint golden-brown coloration. IR data were collected on a Bruker IFS66V FT-IR spectrometer (KBr beam splitter) under vacuum (8 mbar) at a  $1\text{ cm}^{-1}$  spectral resolution. Curve-fitting analysis was performed on bands in the  $735\text{--}840\text{ cm}^{-1}$  region using commercially available software (Thermo Galactic, GRAMS/32 5.22). The spectral bands were fitted using a mixed Gaussian–Lorentzian product function and a straight baseline.

### 2.4. Differential scanning calorimetry

Samples were cast onto Teflon, dried in a nitrogen environment for 24 h, and placed under vacuum for 24 h. As the LiTf content increased, the samples became more rigid. Solid domains were observed in the 10:1 and 5:1 LPMEI:NaTf samples, which were very brittle. After drying, a 10–15 mg sample was sealed in a 40  $\mu\text{l}$  aluminum pan. Thermal data were collected on a Mettler DSC 820 calorimeter with commercially available software from Mettler Toledo (STAR<sup>®</sup> v.6.10) under a dry nitrogen purge. Each sample was heated to 60 °C for 30 min followed by two cooling and heating cycles between 60 and  $-140\text{ °C}$  ( $5\text{ °C min}^{-1}$ ). However, to obtain the melting point of the 5:1, 10:1, 15:1, and 20:1 LPMEI:NaTf samples, DSC data were acquired by cycling the samples between 25 and 150 °C at a heating and cooling rate of  $5\text{ °C min}^{-1}$ .

### 2.5. X-ray powder diffraction

The NaTf and 5:1 LPMEI:NaTf (brittle film) were ground into a fine powder-like material and pressed on



to a microscope slide. The LPMEI, 20:1, 15:1, and 10:1 LPMEI:NaTf samples were cast onto a microscope slide then dried under nitrogen (24 h) and vacuum (24 h). Powder X-ray diffractograms were recorded using a Scintag XTRA diffractometer with CuK $\alpha$  radiation over the range  $8 \leq 2\theta \leq 50^\circ$  in 2 $\theta$  steps of  $0.100^\circ$  with a scan rate of  $2.5^\circ \text{ min}^{-1}$ . All X-ray data were recorded at room temperature.

## 2.6. Complex impedance

Each LPMEI:LiTf sample was cast directly onto a 12.5 mm stainless steel electrode in a nitrogen atmosphere. The solvent was allowed to evaporate for 24 h in the glove box and 24 h under vacuum. The film thickness was measured using a micrometer built into the conductivity cell. Conductivity measurements were made over the frequency range 0.005–10000 kHz using a Hewlett–Packard 4192A LF impedance analyzer with LABVIEW™ 5.1 software (National Instruments). Conductivity data for the LPMEI:NaTf samples were not collected due to experimental difficulties in acquiring data. These difficulties are related to interfacial contact problems between the electrodes and the electrolyte.

The conductivity data for all LPMEI:LiTf compositions were measured using a heating cycle ranging from 25 to 60 °C in 10 °C increments. For the LPEI:LiTf samples, the data were collected between 20 and 70 °C in 10 °C increments [13]. The impedance plots were curve-fitted using commercially available software (Solartron Instruments LTD, LEVM 7.1v).

## 3. Discussion

### 3.1. Ionic association

The CF<sub>3</sub> symmetric deformation [ $\delta(\text{CF}_3)$ ] spectral region contains distinct bands due to several ionically associated species: “free” ions, contact ion pairs [LiTf], and the aggregate species [Li<sub>2</sub>Tf]<sup>+</sup> [14–17]. In Fig. 1, the  $\delta(\text{CF}_3)$  band at  $757 \text{ cm}^{-1}$  appears broader in the LPMEI:LiTf spectra than in the LPMEI:NaTf spectra. The lower frequency asymmetric wing of the band in the LiTf system becomes a shoulder in the NaTf system. The breadth and structure of the band suggest that there is more than one ionic species present. By deconvoluting the  $\delta(\text{CF}_3)$  region, the band frequencies and integrated intensities of each ionic species present can be determined (Table 1). In LPMEI:LiTf complexes the ionic association increases with LiTf concentration. As salt concentration increases, the formation of the aggregate species increases while the proportion of “free” ions and contact ion pairs decreases. Similar trends are seen in the LPMEI:NaTf complexes except that there is no unambiguous evidence of aggregate formation and the

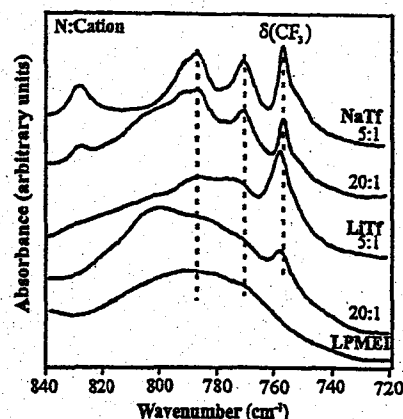


Fig. 1. IR spectra of LPMEI with a 5:1 and 20:1 nitrogen:cation ratio of LiTf and NaTf in the 735–835  $\text{cm}^{-1}$  region.

Table 1

A comparison of the band center frequency in the  $\delta(\text{CF}_3)$  region for LPMEI–LiTf and LPMEI–NaTf at varying nitrogen:cation ratios

Composition (N:Li)	Band center frequency (% relative intensity) ( $\text{cm}^{-1}$ )		
	Aggregate	Contact ion pairs	“Free”
<b>LiTf</b>			
20:1		757 (64)	752 (36)
15:1	762 (12)	758 (61)	752 (27)
10:1	762 (14)	758 (60)	752 (26)
5:1	761 (20)	758 (56)	752 (24)
<b>NaTf</b>			
20:1		756 (73)	751 (27)
15:1		756 (62)	751 (38)
10:1		756 (54)	751 (46)
5:1		756 (48)	752 (52)

proportion of “free” ions increases with salt composition. In the LPMEI:NaTf complexes, the degree of ionic association does not increase with increasing NaTf concentration as in the LPMEI:LiTf complexes. This may be due to the LPMEI:NaTf complexes forming crystalline domains at high NaTf concentrations. This will be discussed in a later section.

The SO<sub>3</sub> asymmetric stretch,  $\nu_{\text{as}}(\text{SO}_3)$  of the Tf<sup>−</sup> ion is affected by the coordination to the lithium ions, as illustrated in Fig. 2. The two  $\nu_{\text{as}}(\text{SO}_3)$  bands (1290, 1261  $\text{cm}^{-1}$  in LPMEI:NaTf) have larger intensities, smaller bandwidths, and a smaller frequency separation in the LPMEI:NaTf samples than in the LPMEI:LiTf samples. The greater frequency separation of the bands in the LiTf complexes indicates stronger coordination of the Tf<sup>−</sup> with the lithium ion(s). In addition, this separation appears to slightly increase at higher LiTf content, a trend that is not observed in LPMEI:NaTf.

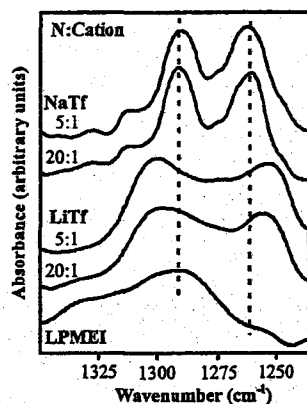


Fig. 2. IR spectra of the  $\nu_{as}(\text{SO}_3)$  region of LPMEI with a 5:1 and 20:1 nitrogen:cation ratio of LiTf and NaTf.

### 3.2. Structural changes in the polymer

A number of dramatic changes in the host LPMEI bands occur with the addition of salt. There is a broad band in the pure LPMEI spectrum between 760 and 820  $\text{cm}^{-1}$  (Fig. 1). The breadth and very poorly resolved band structure suggest that this feature actually consist of several broad, overlapping bands. Based on a comparison with the  $N,N,N',N'$ -tetramethylethylenediamine  $[(\text{CH}_3)_2\text{NCH}_2\text{CH}_2\text{N}(\text{CH}_3)_2]$  spectrum and its computational analysis [18], bands in this region are assigned to a complex mixture of C–C and C–N stretching,  $\text{CH}_2$  wagging,  $\text{CH}_2$  twisting, and  $\text{CH}_2$  rocking motions. The addition of LiTf increases the intensity of a somewhat less broad feature between roughly 760 and 790  $\text{cm}^{-1}$ . However, the addition of NaTf results in two very distinct bands of medium intensity at 770 and 787  $\text{cm}^{-1}$ , with the appearance of a third weaker band at 828  $\text{cm}^{-1}$ .

There are also structural changes in the LPMEI spectra in the 1090 to 1190  $\text{cm}^{-1}$  region (Fig. 3) upon the addition of salt. The modes in this region are comprised mainly of  $\text{CH}_3$  wagging, C–C stretching, and  $\text{CH}_2$  twisting motions [18]. In both LPMEI:LiTf and LPMEI:NaTf complexes, the polymer band at 1118  $\text{cm}^{-1}$  shifts to a higher frequency and diminishes in intensity with increasing salt concentration until the band intensity almost completely disappears at the highest salt concentrations studied. The band at 1157  $\text{cm}^{-1}$  in the LPMEI:NaTf spectra is identified as the asymmetric  $\text{CF}_3$  stretch,  $\nu_{as}(\text{CF}_3)$ . This band occurs 3  $\text{cm}^{-1}$  lower in LPMEI:NaTf (1157  $\text{cm}^{-1}$ ) than in LPMEI:LiTf (1160  $\text{cm}^{-1}$ ). It should also be noted that the bandwidth is greater in LPMEI:LiTf than in the LPMEI:NaTf, indicating a more locally disordered sample.

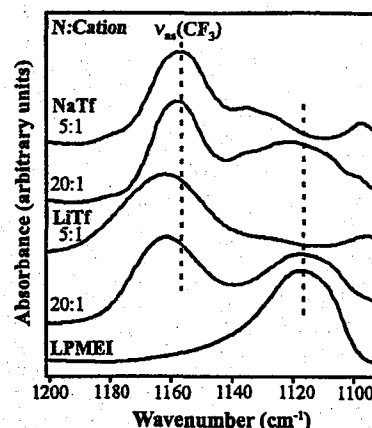


Fig. 3. IR spectra of LPMEI with a 5:1 and 20:1 nitrogen:cation ratio of LiTf and NaTf in the 1090–1190  $\text{cm}^{-1}$  region.

### 3.3. Glass transitions and melting points

Table 2 summarizes the glass transition temperatures ( $T_g$ ) and melting points ( $T_m$ ) of LPMEI with various compositions of LiTf and NaTf. With a  $T_g$  of  $-91^\circ\text{C}$ , LPMEI is characterized as an amorphous material at room temperature. In the LPMEI:LiTf system,  $T_g$  increases with increasing LiTf concentration, because the polymer becomes more structurally ordered due to the coordination of the backbone to the lithium ions. However, the  $T_g$  in the LPMEI:NaTf system does not follow the same trend. Even at a 10:1 NaTf composition, the  $T_g$  does not change, although the LPMEI:NaTf systems are more structurally ordered than the LiTf polymer complexes. A  $T_g$  is not observed in the 5:1 LPMEI:NaTf sample because the crystalline domains are much larger than the amorphous regions.

Table 2  
Glass transition temperatures ( $T_g$ ) and melting temperatures ( $T_m$ ) of LPMEI, LPMEI–LiTf, and LPMEI–NaTf with varying nitrogen:cations ratios

Composition (N:Li)	$T_g$ ( $^\circ\text{C}$ )	Composition (N:Na)	$T_g$ ( $^\circ\text{C}$ )	$T_m$ ( $^\circ\text{C}$ )
LPMEI	–91			
20:1	–63	20:1	–90	119
15:1	–53	15:1	–89	119
10:1	–48	10:1*	–88	128,
				133
5:1	3	5:1*	–	125,
				141

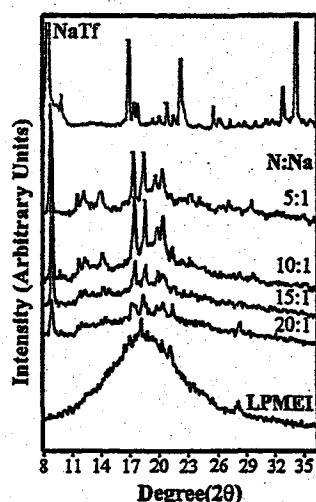


Fig. 4. XRD data of NaTf and LPMEI with varying concentrations of NaTf.

All LPMEI:NaTf samples exhibit a melting temperature, which ranges from 119 (20:1) to 141 °C (5:1). The melting temperature increases with increasing salt concentration, correlating with an increase in the degree of sample crystallinity. Upon cycling the samples, the  $T_m$  is relatively unchanged within experimental error. The melting transition of the 10:1 and 5:1 LPMEI:NaTf samples is not sharply defined. In particular, there appear to be two superimposed thermal events in the 5:1 sample, with onsets at 125 and 141 °C, respectively. However, these are only seen in freshly prepared samples and disappear upon cycling between 50 and 150 °C, leaving a sharp melting transition with an onset at 134 °C for the 5:1 LPMEI:NaTf sample.

The LPMEI:NaTf complexes consist of two distinct phases, amorphous and crystalline, based on both  $T_g$  and  $T_m$  data. The crystalline phases present in the LPMEI:NaTf complexes were verified by XRD as shown in Fig. 4.

#### 3.4. X-ray diffraction patterns

The diffractograms of all the LPMEI:NaTf samples reveal both a crystalline and an amorphous phase (Fig. 4). In the 20:1 composition, the amorphous phase dominates the sample so that only a few of the crystalline peaks are present. At the higher salt concentrations, new peaks appear and increase in intensity as the crystalline phase grows. Fig. 4 shows that the diffractograms from the LPMEI:NaTf samples are due to the formation of a new crystalline complex of salt and

polymer, rather than pure NaTf salting out at higher salt concentrations.

#### 3.5. Ionic conductivity

Fig. 5 represents temperature-dependent ionic conductivity data of LPMEI:LiTf and LPEI:LiTf at several compositions. The lines in the figure are present only as a visual aid. In the LPMEI:LiTf systems, the 20:1 composition exhibits the highest ionic conductivity at all temperatures measured. This composition also has the highest relative concentration of contact ion pairs as estimated from the intensity data of Table 1. As the LiTf concentration increases, the ionic conductivity decreases at all temperatures measured.

It is interesting to compare ionic conductivities in LPMEI:LiTf and LPEI:LiTf. The LPMEI:LiTf complexes exhibit higher ionic conductivity values than the LPEI:LiTf complexes at the same salt compositions (Fig. 5). Fig. 6 shows the conductivity data of varying compositions of LPMEI:LiTf and LPEI:LiTf at 30 and 60 °C. The 30 and 60 °C data have different scales. In the LPEI:LiTf system at 30 °C, the 5:1 composition is more conductive than the 20:1 composition at low temperatures, which is opposite of the behavior in the LPMEI:LiTf system. At high LiTf compositions, the hydrogen bonds in LPEI are disrupted, leading to a more disordered system and higher ionic conduction. However, at a 5:1 LiTf composition LPMEI:LiTf is less conductive than LPEI:LiTf at 30 °C. This pattern seen in the conductivity data at 30 °C is different at 60 °C, which is above the melt of LPEI. The conductivity of both systems follows the same trend as LiTf concentration increases.

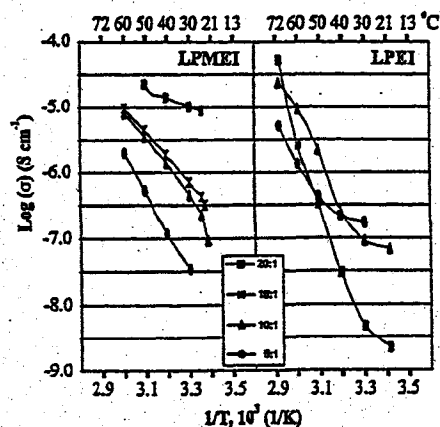


Fig. 5. Temperature dependent conductivity data of LPMEI and LPEI with varying concentrations of LiTf.

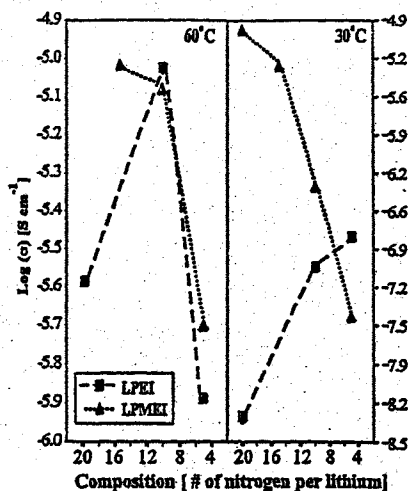


Fig. 6. A comparison of ionic conductivity values at 30 and 60 °C of LPEI and LPMEI with LiTf at varying nitrogen:lithium ratios.

#### 4. Conclusions

A comparative vibrational spectroscopic study shows that the LPMEI:LiTf complexes are homogeneous and highly disordered, whereas the LPMEI:NaTf samples contain a crystalline phase and an amorphous phase. The differences in the morphology of LPMEI:LiTf and LPMEI:NaTf is also evident in the DSC and XRD data. The  $T_g$  of LPMEI changes to a higher temperature when the concentration of LiTf increases. In the LPEI:NaTf samples, the  $T_g$  of LPMEI does not change significantly with increasing salt concentrations. In the most concentrated LPMEI:NaTf sample, a  $T_g$  is not detected, suggesting the presence of large crystalline domains. The presence of such domains is confirmed using XRD.

The formation of a new crystalline compound in the LPMEI:NaTf system was verified by the DSC and XRD data. A crystalline compound in the related LPEI:NaTf system was reported by Harris et al. [19], who suggest a 4:1 stoichiometry.

The LPMEI:LiTf samples are more conductive at lower LiTf concentrations, where the samples are comprised of mostly contact ion pairs. Further, the LPMEI:LiTf complexes have higher conductivities than the LPEI:LiTf complexes except at high LiTf concentrations. The changes in the LPMEI:LiTf conductivity values with increasing salt concentration are opposite from what occurs in the LPEI:LiTf samples below the melt of LPEI. Since LPMEI is amorphous, the conductivity decreases with increasing LiTf concentrations because the polymer host becomes a more locally ordered system. However, in the crystalline LPEI, the addition of LiTf disrupts the hydrogen bonding, therefore, the samples are more disordered at higher salt

concentrations. Above the melting temperature of LPEI, the conductivity data of LPMEI:LiTf and LPEI:LiTf behave similarly. The LPMEI:LiTf conductivity data do not agree with the results of Tanaka and Nishibayashi, who reported that the LPEI:LiTf complexes had higher ionic conductivity values than LPMEI:LiTf complexes at the same composition [10]. Further, the overall conductivity values reported here are higher than their values.

The ionic association of triflate ion in LPMEI:LiTf and LPMEI:NaTf is determined from spectral band fitting analysis using structure-spectral correlations previously obtained from studies of PEO:LiTf complexes [15,17]. In LPMEI:LiTf complexes, the degree of ionic association increases with increasing LiTf concentration as expected. The LPMEI:NaTf complexes contain relatively more "free" ions at higher salt concentrations than LPMEI:LiTf complexes.

#### Acknowledgements

We acknowledge Chris Burba and Varuni Seneviratne for their assistance with the X-ray powder diffraction. In addition, Shawna York is acknowledged for her collection of conductivity data for LPEI:LiTf. This work was partially supported by funds from the National Science Foundation, Contract Number DMR-0072544.

#### References

- [1] M. Gauthier, A. Bélanger, B. Kapfer, G. Vassort, M. Armand, *Polymer Electrolyte Reviews*, vol. 2, Elsevier, London, 1989, p. 285.
- [2] B.L. Papke, M.A. Ratner, D.F. Shriver, *J. Electrochem. Soc.* 129 (1982) 1434–1438.
- [3] M.B. Armand, J.M. Chabagno, M.J. Duclot, *Polyethers as Solid Electrolytes, Fast Ion Transport in Solids*, Elsevier, Amsterdam, 1979.
- [4] P.G. Bruce, *Faraday Discuss. Chem. Soc.* 88 (1989) 43–54.
- [5] Z. Gadjourova, Y.G. Andreev, D.P. Tunstall, P.G. Bruce, *Nature* 412 (2001) 520–523.
- [6] Y. Chatani, T. Kobatake, H. Tadokoro, R. Tanaka, *Macromolecules* 15 (1982) 170–176.
- [7] T. Sangusa, H. Ikeda, H. Fujii, *Macromolecules* 5 (1972) 108.
- [8] Y. Chatani, T. Irie, *Polymer* 29 (1988) 2126–2129.
- [9] R. Tanaka, I. Ueoka, Y. Takaki, K. Kataoka, S. Saito, *Macromolecules* 16 (1983) 849–853.
- [10] R. Tanaka, T. Fujita, H. Nishibayashi, S. Saito, *Solid State Ionics* 60 (1993) 119–123.
- [11] S. York, R. Frech, A. Snow, D. Glatzhofer, *Electrochim. Acta* 46 (2001) 1533–1537.
- [12] R. Tanaka, M. Koike, T. Tsutsui, T. Tanaka, *J. Polym. Sci. Polym. Lett. Ed.* 16 (1978) 13–19.
- [13] S.R. Starkey-York, *Local structures and conductivity in polyethylenimine and polyphosphazene polymer electrolytes*, Dissertation, Chemistry and Biochemistry, University of Oklahoma, 2002.

- [14] S. Schantz, J. Sandahl, L. Borjesson, L.M. Torell, J.R. Stevens, *Solid State Ionics* 28–30 (1988) 1047–1053.
- [15] R. Frech, W. Huang, *Solid State Ionics* 72 (1994) 103–107.
- [16] W. Huang, R. Frech, R.A. Wheeler, *J. Phys. Chem.* 98 (1994) 100–110.
- [17] R. Frech, W. Huang, M.A.K.L. Dissanayake, *Mater. Res. Soc. Symp. Proc.* 369 (1995) 523–534.
- [18] R.A. Sanders, S. Boesch, R. Frech, R. Wheeler, Calculation of *N,N',N''*-tetramethylethylenediamine (TMEDA):lithium triflate ( $\text{CF}_3\text{SO}_3$ ) systems were performed using B3LYP, a hybrid Hartree–Fock density functional method, with a basis set of 6-31G(d), in preparation.
- [19] C.S. Harris, D.F. Shriver, M.A. Ratner, *Macromolecules* 19 (1986) 987–989.

## **V. LPMEI modeled by PMDETA**

**N,N,N',N',N''-  
PENTAMETHYLDIETHYLENETRIAMINE  
(PMDETA) AS A MODEL COMPOUND FOR  
LINEAR POLY(N-METHYLETHYLENIMINE),  
LPMEI**

Rebecca A. Sanders<sup>1</sup>, Scott E. Boesch<sup>1</sup>, Albert G. Snow<sup>2</sup>,  
Lieyu (Richard) Hu<sup>1</sup>, Roger Frech<sup>1</sup>, Ralph A. Wheeler<sup>1</sup>,  
and Daniel T. Glatzhofer<sup>1</sup>

<sup>1</sup>Department of Chemistry & Biochemistry, University of  
Oklahoma

620 Parrington Oval, Norman, OK 73019

<sup>2</sup>Department of Chemistry, Wichita State University  
Wichita, KS 67260

### Introduction

Polymer electrolytes based on poly(ethylene oxide), PEO ( $\text{[OCH}_2\text{CH}_2\text{]}_n$ ), are a widely researched area because of their applications in lithium rechargeable battery technology<sup>1</sup>. PEO has been investigated as a polymer-based electrolyte using various salts such as  $\text{LiCF}_3\text{SO}_3$ ,  $\text{LiN}(\text{CF}_3\text{SO}_2)_2$ ,  $\text{LiSbF}_6$ ,  $\text{LiBF}_4$ , and  $\text{LiClO}_4$ <sup>1</sup>. However, some of the attention in the field of polymer electrolytes has been directed towards linear poly(ethylenimine), LPEI ( $\text{[NHCH}_2\text{CH}_2\text{]}_n$ ), which is structurally analogous to PEO. LPEI is more synthetically versatile than PEO, because various groups can be attached to the nitrogen atom such as  $-\text{CH}_3$ <sup>2</sup>,  $-\text{CH}_2\text{CH}_3$ ,  $-\text{CH}_2\text{CH}_2\text{CN}$ <sup>3</sup>, and  $-\text{CH}_2\text{CH}_2\text{OCH}_2\text{CH}_2\text{OCH}_3$ <sup>4</sup>. Pure LPEI is highly crystalline<sup>5</sup> and makes a poor host for the formation of polymer electrolytes with high ionic conductivity. However, by attaching various side chains to LPEI, the crystallinity can be decreased. Linear poly(N-methylethylenimine), LPMEI, is a methyl-substituted derivative of LPEI and is completely amorphous at room temperature, unlike LPEI, which melts at  $58^\circ\text{C}$ <sup>6-8</sup>. Since these polymer-based electrolytes are complex systems, model compounds are necessary to achieve a fundamental understanding of these systems. Using small molecules as model compounds makes it feasible to calculate their vibrational modes and frequencies, which can be correlated to the corresponding polymer-based electrolyte. This paper will investigate N,N,N',N',N''-pentamethyldiethylenetriamine (PMDETA),  $\text{CH}_3\text{N}(\text{CH}_2\text{CH}_2\text{N}(\text{CH}_3)_2)_2$ , complexed with  $\text{LiCF}_3\text{SO}_3$  (LiTf) as a possible model compound for LPMEI,  $\text{[NCH}_2\text{CH}_2\text{CH}_2\text{]}_n$ , using hybrid Hartree-Fock/ density functional calculations and Fourier transform infrared spectroscopy (FTIR).

### Experimental

**Synthesis of LPMEI.** High molecular weight LPMEI (ca. 115,000 MW), a dark golden-brown viscous oil, has been synthesized using a previously reported method<sup>9</sup>. Low molecular weight LPMEI (ca. 550 MW) is a light-golden brown liquid that was synthesized using similar methods with the following changes. Low molecular weight LPEI (ca. 423 MW) was purchased from Aldrich. Excess water was removed from the product under reduced pressure instead of by azeotropic distillation from a benzene solution using a Dean-Stark trap. The resulting polymer also did not have to be centrifuged to remove particulates. The resulting viscous polymer was characterized by nuclear magnetic resonance (NMR) and

FTIR. The LPMEI (ca. 550 MW) contains small amounts of branching based on the NMR data.

**Sample Preparation.** PMDETA, anhydrous acetonitrile, and LiTf were obtained from Aldrich. PMDETA was distilled over sodium metal. The anhydrous acetonitrile was used as received. LiTf was heated under vacuum at  $120^\circ\text{C}$  for 48 hours. The chemicals were stored and used in a dry nitrogen glovebox (VAC, 1ppm  $\text{H}_2\text{O}$ ) at room temperature. To prepare the PMDETA:LiTf solutions, LiTf was dissolved into PMDETA at various concentrations and stirred for at least three hours.

The sample preparation for high molecular weight LPMEI:LiTf has been previously reported<sup>9</sup>. For low molecular weight LPMEI:LiTf, solutions were prepared by adding the appropriate amount of LiTf to 0.100 g of LPMEI. The samples were dissolved in anhydrous acetonitrile to prepare a homogeneous solution. All of the LPMEI:LiTf solutions were stirred for approximately three hours before they were cast into films. The compositions of the solutions are reported as a nitrogen to lithium molar ratio (N:Li).

**FTIR Spectroscopy.** For FTIR measurements, the PMDETA and PMDETA:LiTf solutions were placed between zinc selenide windows in a sealed sample holder. The FTIR method for the high molecular weight LPMEI has been previously reported<sup>9</sup>. All of the low molecular weight LPMEI and LPMEI:LiTf solutions were cast onto the zinc selenide windows and dried under a nitrogen purge for 24 hours. To ensure solvent removal, the LPMEI and LPMEI:LiTf samples were placed under vacuum for 24 hours. FTIR data were recorded on a Bruker IFS66V with a KBr beam splitter over a range of  $500 - 4000 \text{ cm}^{-1}$  ( $1 \text{ cm}^{-1}$  resolution). The spectra of the PMDETA solutions were measured under a dry air purge; the LPMEI samples data were collected under vacuum (8 mbar).

**Computational methods.** Calculations were performed on single molecules of PMDETA and PMDETA:LiTf in the gas phase using the B3LYP hybrid Hartree-Fock/density functional method with the 6-31G(d) basis set. The calculated frequencies above  $1000 \text{ cm}^{-1}$  are scaled by a multiplicative factor of 0.9614, and below  $1000 \text{ cm}^{-1}$  are scaled by a multiplicative factor of 1.0013.

### 3. Results & Discussion

**Computational Analysis.** Calculations of PMDETA and the PMDETA:LiTf complex show that the N-C-C-N dihedral angle is in the gauche conformation. For the PMDETA:LiTf, the lithium is coordinated to the three nitrogen atoms in the PMDETA and two oxygen atoms of the triflate ion. The calculated vibrational frequencies and mode descriptions were assigned to the experimental bands based on the calculated IR intensities and frequencies.

**Table 1: Experimental and calculated scaled IR frequencies ( $\text{cm}^{-1}$ ) of PMDETA and PMDETA:LiTf along with their corresponding mode descriptions. (v = stretch,  $\omega$  = wag, and  $\rho$  = rock)**

PMDETA		PMDETA:LiTf			Modes Description
Cal.	Exp.	20:1 Exp.	10:1 Exp.	2:1 Cal.	
		910	910	916	$\rho(\text{CH}_2)$ ; $\nu(\text{C-N})$ $\nu(\text{C-C})$
960 $\rho(\text{CH}_2)$	937	937	937	953	$\rho(\text{CH}_2)$ ; $\nu(\text{C-N})$ $\nu(\text{C-C})$
972 $\rho(\text{CH}_2)$	944	945	945	963	$\rho(\text{CH}_2)$ ; $\nu(\text{C-N})$ $\nu(\text{C-C})$
		981	981	1007	$\omega(\text{CH}_3)$ ; $\rho(\text{CH}_2)$ ; $\nu(\text{C-N})$

Selected calculated vibrational mode descriptions, calculated IR frequencies, and experimental IR frequencies are described in Table 1 (PMDETA and PMDETA:LiTf). Some of the calculated vibrational frequencies and modes change when one LiTf molecule is added to PMDETA. For instance, the 960 and 972  $\text{cm}^{-1}$  bands calculated in PMDETA shift to 953 and 963  $\text{cm}^{-1}$  when LiTf is introduced into the system. Furthermore, the nature of these modes change from a predominant  $\text{CH}_2$  rocking motion to mixed  $\text{CH}_2$  rocking, C-C stretching, and C-N stretching motions resulting from interactions with LiTf.

**Spectroscopic Analysis.** Spectral correlations are made between PMDETA and high molecular weight LPMEI using the low molecular weight LPMEI spectrum. The low molecular weight LPMEI spectrum acts as an intermediate in the spectral correlation, because it exhibits bands similar to both PMDETA and high molecular weight LPMEI. Vibrational modes assignments of the high molecular weight LPMEI can be made based on the calculated vibrational assignments of the PMDETA data. The spectral correlation described here will be confined to the conformation region (800 – 1000  $\text{cm}^{-1}$ ). This region is sensitive to interaction between the cation and polymer host, which reflect conformational changes in the backbone<sup>10</sup>.

In the conformation region (800 – 1000  $\text{cm}^{-1}$ ), the major differences between PMDETA and high molecular weight LPMEI occur in the 810 – 890  $\text{cm}^{-1}$  region (Figure 1). The bands at 833 and 859  $\text{cm}^{-1}$  in PMDETA decrease in intensity and shift to higher frequencies in the low (842, 859  $\text{cm}^{-1}$ ) and high (850, 868  $\text{cm}^{-1}$ ) molecular weight LPMEI. In addition, the bandwidths of these bands increase as the molecular weight of LPMEI increases. These changes in the bandwidth, intensities, and frequencies are due to the differences in their chain length. The PMDETA bands in this region cannot be assigned to a specific vibrational motion, because there are no calculated frequencies between 810 to 915  $\text{cm}^{-1}$ . However, vibrational mode assignments of PMDETA in this region may be possible if the PMDETA molecule is configured in a conformation other than the gauche conformation.

In the 870 – 1000  $\text{cm}^{-1}$  region, the PMDETA spectra are comparable to both the low and high molecular weight LPMEI spectra. Both the 892 and 939  $\text{cm}^{-1}$  bands are not as affected by the chain length. The PMDETA band at 937  $\text{cm}^{-1}$  has a similar bandwidth and intensity as the corresponding low (938  $\text{cm}^{-1}$ ) and high (939  $\text{cm}^{-1}$ ) molecular weight LPMEI. This band in the PMDETA spectrum is assigned to the  $\text{CH}_2$  rocking motion. There is an underlying band around 944  $\text{cm}^{-1}$  in PMDETA, low molecular weight LPMEI, and high molecular weight LPMEI based on the asymmetry of this band. In PMDETA, this underlying band is also assigned to the  $\text{CH}_2$  rocking motion. With the addition of LiTf, the underlying band in the PMDETA (945  $\text{cm}^{-1}$ ) and low molecular weight LPMEI (949  $\text{cm}^{-1}$ ) spectra increases in intensity. Furthermore, the PMDETA:LiTf spectrum has four new bands occurring at 902, 910, 972, and 981  $\text{cm}^{-1}$ . The band at 910  $\text{cm}^{-1}$  is assigned to the  $\text{CH}_2$  rocking, C-N stretching, and C-C stretching motions whereas the 981  $\text{cm}^{-1}$  band is assigned to the  $\text{CH}_3$  wagging,  $\text{CH}_2$  rocking, and C-N stretching motions. The four new PMDETA bands correlate to the LPMEI bands at 901 and 983  $\text{cm}^{-1}$  in the high molecular weight, and to 901 and 984  $\text{cm}^{-1}$  in the low molecular weight. The band at 901  $\text{cm}^{-1}$  in both low and high molecular weight LPMEI has a broad bandwidth,

which is due to an underlying band that appears at about 910  $\text{cm}^{-1}$  upon the addition of LiTf.

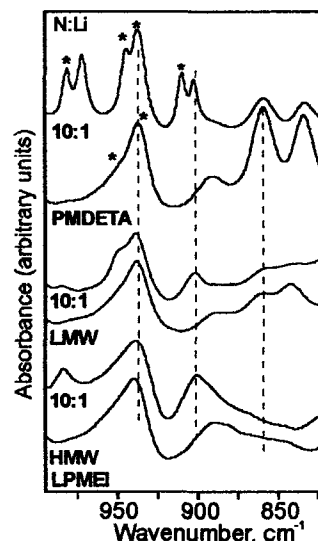


Figure 1: FTIR spectra of PMDETA, low molecular weight LPMEI (LMW), and high molecular weight LPMEI (HMW) with a 10:1 nitrogen to lithium ratio of LiTf in the 810 – 1000  $\text{cm}^{-1}$  region. The asterisk (\*) indicates the PMDETA bands in which the vibrational mode assignments can be correlated to LPMEI.

Spectral correlations of PMDETA to LPMEI and their interaction with LiTf can also be made in other regions. In addition, PMDETA with  $\text{NaCF}_3\text{SO}_3$  (NaTf) has similar band frequencies and intensities to the corresponding LPMEI:NaTf samples. The spectral correlations between PMDETA:NaTf and LPMEI:NaTf will also be investigated.

## Conclusions

PMDETA is a useful model for LPMEI based on a comparison of their spectral bandwidths, intensities, and frequencies. Not only does PMDETA model the vibrational frequencies of LPMEI, but it also models the interactions of the lithium ions with the polymer host in the conformation region. Therefore, vibrational mode assignments of LPMEI can be made using calculated PMDETA mode assignments in this region.

The low molecular weight LPMEI (ca. 550 MW) acts as a useful intermediate transition in the spectral correlations of PMDETA and high molecular weight LPMEI (ca. 115,000 MW). This is due to the striking similarities in the spectral signatures of low molecular weight LPMEI to both PMDETA and high molecular weight LPMEI.

## Acknowledgments.

This work was partially supported by funds from the National Science Foundation, Contract No. DMR-0072544 and supercomputer time from NSF/NRAC award no. MCA96-N019.

## References

- (1) Gauthier, M.; Bélanger, A.; Kapfer, B.; Vassort, G.; Armand, M. *Polymer Electrolyte Reviews*; Elsevier: London, 1989; Vol. 2.
- (2) Tanaka, R.; Koike, M.; Tsutsui, T.; Tanaka, T. *J. Poly. Sci.: Poly. Letters ed.* 1978, 16, 13-19.



- (3) Erickson, M.; Glatzhofer, D. T.; Frech, R. *Electrochimica Acta* **2002**, Accepted.
- (4) Snow, A. G.; Sanders, R. A.; Frech, R.; Glatzhofer, D. T. *Electrochimica Acta* **2002**, Accepted.
- (5) Chatani, Y.; Kobatake, T.; Tadokoro, H.; Tanaka, Y. *Macromolecules* **1982**, *15*, 170-176.
- (6) Saugusa, T.; Ikeda, H.; Fujii, H. *Macromolecules* **1972**, *5*, 108.
- (7) Chatani, Y.; Irie, T. *Polymer* **1988**, *29*, 2126-2129.
- (8) Tanaka, R.; Ueoka, I.; Takaki, Y.; Kataoka, K.; Saito, S. *Macromolecules* **1983**, *16*, 849-853.
- (9) Sanders, R. A.; Snow, A. G.; Frech, R.; Glatzhofer, D. T. *Electrochimica Acta* **2002**, Accepted.
- (10) Matsuura, H.; Fukuhara, K. *J. Polym. Sci. B* **1986**, *24*, 1383-1400.

## **APENDIX B – Manuscripts Not Included**

---

- I. Rebecca A. Sanders, Scott E. Boesch, Albert G. Snow, Lieyu (Richard) Hu, Roger Frech, Ralph A. Wheeler, and Daniel T. Glatzhofer. “Spectroscopic Investigation of Linear Poly(N-methylethylenimine), LPMEI, using a Model Compound: N,N,N',N',N''-Pentamethyldiethylenetriamine (PMDETA) with Lithium Triflate ( $\text{LiCF}_3\text{SO}_3$ ) and Sodium Triflate ( $\text{NaCF}_3\text{SO}_3$ ).” *Manuscript in progress*.
  
- II. Albert G. Snow, Rebecca A. Sanders, Roger Frech, and Daniel T. Glatzhofer. “Synthesis and Spectroscopic Studies of Linear Poly(N-(2-(2-methoxyethoxy)ethyl)ethylenimine), a PEI/PEO Hybrid, and its Interactions with Lithium Triflate”. *Electrochimica Acta* 48 (14-16) 2003,p2065-2069.